TECHNICAL REPORT STANDARD TITLE PAGE

1. Report No.	2. Government Accession No.	3. Recipient's Catalog No.
FHWATX-77-23-1		

4. Title and Subtitle	5. Report Date
PREDICTION OF TEMPERATURE AND STRESSES IN HIGHWAY BRIDGES BY A NUMERICAL PROCEDURE USING DAILY WEATHER REPORTS	February 1977
	6. Performing Organization Code
7. Author(s)	8. Performing Orgonization Report No.
Thaksin Thepchatri, C. Philip Johnson, and Hudson Matlock	Research Report Number 23-1
9. Performing Orgonization Name and Address	10. Work Unit No.
Center for Highway Research The University of Texas at Austin Austin, Texas 78712	11. Contract or Grant No. Research Study 3-5-74-23
	13. Type of Report and Period Covered
12. Sponsoring Agency Name and Address	Interim
Texas State Department of Highways and Public Transportation; Transportation Planning Division P. O. Box 5051 Austin, Texas 78763	14. Sponsoring Agency Code

15. Supplementary Notes

Work done in cooperation with the Department of Transportation, Federal Highway Administration. Research Study Title: "Temperature Induced Stresses in Highway Bridges by Finite Element Analysis and Field Tests"

16. Abstract

This research focused on the development of computational procedures for the prediction of the transient bridge temperature distribution due to daily variations of the environment such as solar radiation, ambient air temperature, and wind speed. The temperature distribution is assumed to be constant along the centerline of the bridge but can vary arbitrarily over its cross section. The finite element method was used for the two-dimensional heat flow analysis. Temperature stresses, however, are computed from elastic beam theory.

In this work a computer program, TSAP, which included the heat flow and thermal stress analysis in a complete system was developed. The environmental data required for input are the solar radiation intensity, ambient air temperature and wind speed. Daily solar radiation intensity is available through the U.S. Weather Bureau at selected locations while air temperature and wind speed can be obtained from local newspapers. This program provides a versatile and economical method for predicting bridge temperature distributions and the ensuing thermal stresses caused by daily environmental changes. Various types of highway bridge cross-sections can be considered. In this work, three bridge types are considered: (1) a post-tensioned concrete slab bridge, (2) a composite precast pretensioned bridge, and (3) a composite steel bridge. Specific attention was given to the extreme summer and winter climatic conditions representative of the city of Austin, Texas.

17. Key Words	18. Distribution Statement
prediction, temperature, stresses, bridges, procedure, weather, model, finite element, elastic beam theory	No restrictions. This document is available to the public through the National Technical Information Service, Springfield, Virginia 22161.

19. Security Classif. (of this report)	20. Security Classif. (of this page)	21. No. of Pages	22. Price
Unclassified	Unclassified	165	

Form DOT F 1700.7 (8-69)

PREDICTION OF TEMPERATURE AND STRESSES IN HIGHWAY BRIDGES BY A NUMERICAL PROCEDURE USING DAILY WEATHER REPORTS

by

Thaksin Thepchatri
C. Philip Johnson
Hudson Matlock

Research Report Number 23-1

Temperature Induced Stresses in Highway Bridges
by Finite Element Analysis and Field Tests

Research Project 3-5-74-23

conducted for

Texas
State Department of Highways and Public Transportation

in cooperation with the
U. S. Department of Transportation
Federal Highway Administration

by the

CENTER FOR HIGHWAY RESEARCH
THE UNIVERSITY OF TEXAS AT AUSTIN

February 1977

The contents of this report reflect the views of the authors, who are responsible for the facts and the accuracy of the data presented herein. The contents do not necessarily reflect the official views or policies of the Federal Highway Administration. This report does not constitute a standard, specification, or regulation.

PREFACE

Computational procedures for predicting temperature and stresses in highway bridges due to daily environmental changes are presented. A two-dimensional finite model is used for predicting the temperature distribution while elastic beam theory is used for predicting the bridge stresses. The environmental data required in the analysis are available from daily weather reports.

Program TSAP, which included the subject procedures in a complete system, was used to predict bridge temperature and stress distributions caused by the climatic conditions representative of the city of Austin, Texas. Several individuals have made contributions in this research. With regard to this project special thanks are due to John Panak, Kenneth M. Will, and Atalay Yargicoglu. In addition, thanks are due to Nancy L. Pierce and the members of the staff of the Center for Highway Research for their assistance in producing this report.

ABSTRACT

This research focused on the development of computational procedures for the prediction of the transient bridge temperature distribution due to daily variations of the environment such as solar radiation, ambient air temperature, and wind speed. The temperature distribution is assumed to be constant along the center-line of the bridge but can vary arbitrarily over its cross section. The finite element method was used for the two-dimensional heat flow analysis. Temperature stresses, however, are computed from elastic beam theory.

In this work a computer program, TSAP, which included the heat flow and thermal stress analysis in a complete system was developed. The environmental data required for input are the solar radiation intensity, ambient air temperature and wind speed. Daily solar radiation intensity is available through the U.S. Weather Bureau at selected locations while air temperature and wind speed can be obtained from local newspapers. This program provides a versatile and economical method for predicting bridge temperature distributions and the ensuing thermal stresses caused by daily environmental changes. Various types of highway bridge cross-sections can be considered. In this work, three bridge types are considered: 1) a post-tensioned concrete slab bridge, 2) a composite precast pretensioned bridge, and 3) a composite steel bridge. Specific attention was given to the extreme summer and winter climatic conditions representative of the city of Austin, Texas.

SUMMARY

A computational procedure for the prediction of temperature induced stresses in highway bridges due to daily changes in temperature has been developed. The procedure has been implemented into a computer program, TSAP, which is able to predict both the temperature distribution and the temperature induced stresses for a variety of bridge types. This work is of particular significance because the important environmental data required in the analysis (such as solar radiation, ambient air temperature and wind speed) are available from daily weather reports. A two-dimensional finite model is used for predicting the temperature distribution while ordinary beam theory is used for predicting the bridge movements and stresses due to temperature changes. Outgoing (long-wave) radiation, which has not been considered in the past, was included in the finite element temperature model, thus allowing for a continuous temperature prediction over a given period of days and nights.

This research indicates that the amplitude and form of the temperature gradient are mainly functions of the intensity of the solar radiation, ambient air temperature and wind speed. The most extreme environmental conditions for Austin, Texas, were found to take place on a clear night followed by a clear day with a large range of air temperature. The shape and depth of the bridge cross-section and its material thermal properties such as absorptivity, emissivity, and conductivity, are also significant factors. For example, due to the low thermal conductivity of concrete, the nonlinearity of the temperature distribution in deep concrete structures was found to be considerable greater than that experienced in composite steel bridges. In addition to the nonlinear form of the temperature gradient, temperature stresses also arise from the form of statical indeterminancy of the bridge. This study indicates that temperature induced stresses in any statically indeterminate bridge will be bounded by the stresses computed from a one- and two-span case.

Results for three bridge types subjected to environmental conditions representative of Austin, Texas, are presented. In general, it was found that thermal deflections are small. Thermal stresses, however, appear to be significant. For the weather conditions considered, temperature induced tensile stresses in a prestressed concrete slab bridge and a precast prestressed I-Beam were found to be in the order of 60 to 80 percent respectively of the cracking stress of concrete suggested by the AASHTO Specifications. Compressive stresses as high as 40 percent of the allowable compressive strength were predicted in a prismatic thick slab having a depth of 17 inches. For a composite steel-concrete bridge, on the other hand, temperature stresses were approximately 10 percent of the design dead and live load stresses.

IMPLEMENTATION

As a result of this research a computer program, TSAP (Temperature and Stress Analysis Program), has been developed to form a complete system for predicting temperature behaviors of highway bridges due to daily changes of temperature. Based on the favorable comparisons between the predicted and measured results, the proposed method offers an excellent opportunity to determine bridge types and environmental conditions for which temperature effects may be severe.

A user's guide, the program listing, and example problems will be contained in the final report of project No. 3-5-74-23. This program has been recently adapted to the computer facilities of the Texas State Department of Highways and Public Transportation. Since the method used is based on a two-dimensional model for predicting the temperature distribution and ordinary beam theory for the stress analysis, the program is relatively easy to use. Environmental data is available through regular Weather Bureau Reports while material thermal properties may be obtained from one of the handbooks on concrete engineering. In this study three types of highway bridges subjected to climatic changes found in Austin, Texas, were considered. These bridges were analyzed for several environmental conditions representative of both summer and winter conditions.

This study has demonstrated the feasibility and validity of analytically predicting the structural response of bridge superstructures subjected to daily atmospheric variations. Typical magnitudes of temperature induced stresses for three bridge types have been established. Since solar radiation levels vary considerably with altitude, air pollution and latitude, additional studies were undertaken for other locations in the State of Texas. The results of that study will be summarized in the final report mentioned above. The adaptation of TSAP to the Highway Department computer facilities will allow the department engineers to directly determine the temperature induced stresses for other bridge types in different locations in the State of Texas.

TABLE OF CONTENTS

LIST OF TABLES

LIST OF FIGURES

CHAPTER 1. INTRODUCTION

1.1 General

It has been recognized for a long time that bridge superstructures exposed to environmental conditions exhibit considerable structural response. Temperature effects in bridges are affected by both daily and seasonal temperature changes. For a statically determinate structure, the seasonal change will not lead to temperature induced stresses. This temperature change, however, causes large overall expansion and contraction. Daily fluctuations of temperature, on the other hand, result in temperature gradients through the depth of the bridge which in turn induce high internal stresses.

Although current bridge specifications (41)* have provisions concerning thermal movements in highway bridges, they do not have specific statements in regard to temperature induced stresses. It is well known that no induced stresses are produced in a single span statically determinate bridge if the temperature distribution has either a uniform or linear form. However, experiences from field measurements in various types of bridges (20, 48,58) indicate that temperature distributions over the depth of the bridge are nonlinear. The nonlinear temperature distribution is a source of induced stresses even if the bridge is statically determinate. For indeterminate structures, the structural response under temperature differentials is believed to be more severe. This is true since additional internal stresses are induced due to the flexural restraint caused by interior supports. Hence, in general, the temperature stresses are attributed to two principal factors: 1) the nonlinear form of the temperature gradient through the depth of the bridge, and 2) to the form of statical indeterminacy of the bridge.

---

* Numbers in parentheses refer to references in the Bibliography.

Research which has been performed on the subject to date indicates that the amplitude and form of the temperature gradient are mainly functions of the intensity of the solar radiation, ambient air temperature and wind speed. The shape and depth of the bridge cross-section and its material properties are also the significant factors. For example, due to the low thermal conductivity of concrete, the nonlinearity of the temperature distribution in concrete structures is found to be considerably greater than that experienced in steel structures. Consequently, high stresses can be induced in deep concrete bridges. These stresses, under particular condition, are additive to stresses caused by dead load and live loads; thus increasing the magnitude of the final stresses. Cracks in an exposed building structure due to high temperature stresses were reported by Meenan (38). He found that temperature differentials could cause small vertical cracks in the beam web in the vicinity of the intermediate support. The structure was a two-span, continuous post-tensioned concrete beam.

Temperature induced stresses are generally ignored in the design process. Thermal movements together with creep and shrinkage, on the other hand, are considered in the design by means of expansion joints (17). A survey of bridge specifications by Zuk (59) has shown that Germany, Austria, Sweden and Japan are the only countries with a thermal induced stress provision in their specifications. During the past two decades, temperature effects in highway bridges have been studied by several researchers in an effort to assess the magnitudes of temperature stresses caused by environmental changes. In the following, some of the pertinent developments will be presented.

1.2 Literature Review

Narouka, Hirai and Yamaguti (40) performed temperature tests on the interior of a composite steel bridge in Japan in 1955. The results of the tests showed that temperature distributions over the thickness of the concrete slab were nonlinear. The maximum temperature gradient in the slab was about 16°F. The maximum temperature differential between the top and bottom flanges of the steel girder, on the other hand, was only 5°F.

In 1957, Barber (1) presented a formula to estimate the maximum pavement surface temperature. The model took into account the relationship between pavement temperature, air temperature, wind speed, solar radiation intensity and the thermal properties of the pavement materials.

Zuk (57) in 1961 developed a rigorous method for computing thermal stresses and deflections in a statically determinate composite bridge. Equations were given explicitly for estimating stresses and strains due to various linear thermal gradients over the bridge cross section.

In 1963, Liu and Zuk (35) extended Zuk's earlier work (57) to study temperature effects in simply supported prestressed concrete bridges. The model included the change of prestressing force caused by temperature change in tendon. In this study, it was assumed that the tendon had the same temperature as the surrounding concrete. Results of the study showed that the deflections were less than 0.04 percent of the span length, and the changes in prestressing force varied from -3 percent to 5 percent of initial prestress. Temperature induced stresses were computed to be about 200 psi in compression and about 100 psi in tension. Interface shears and moments concentrated at the ends of the beam, however, were found to be as high as 30 kips and 123 in-kips, respectively.

In 1965, Zuk (58) modified Barber's equation (1) in an effort to predict the maximum bridge surface temperatures for the Virginia area. He also presented an equation for calculating the maximum temperature differential between the top and bottom temperatures of a composite steel bridge. Good correlations were reported between the computed and the measured values. For example, the predicted maximum surface temperature was 102°F, compared to the measured value of 98°F. Similarly, the computed maximum differential temperature was 24°F, compared to the measured temperature of 23°F. It was confirmed from these field tests that the temperature distributions over the concrete slab deck were nonlinear. For the interior steel beams, on the other hand, the temperature distributions were either linear or uniform.

Also in 1965, Zuk (59) suggested a simple empirical equation to be used as a design check of thermal stresses in simply supported composite steel bridges. The formula was based on a series of field experiments of various bridges. It related the temperature stress at the bottom of the

slab and the depth of the bridge.

Capps (10) in 1968 made measurements of temperature distributions and movements in a steel box structure in England. A method of predicting the steel temperatures, using ambient air temperature and solar radiation intensity was also developed. It was found that the change of temperature caused large movement in the tested bridge.

In 1969, Zuk (60) suggested a method for estimating the bridge movements. By observing the thermal behaviors in four bridges for approximately one year, he found that there existed a relationship between the air temperature and the bridge movement. As a guide for design, end movements were assumed to be approximately twice the product of coefficient of thermal expansion of the material, the moving length of the structure, and the change in air temperature.

Wah and Kirksey (48) in 1969 reported a thorough study of thermal behavior in a bridge. The test bridge was a simply supported structure. Its cross section consisted of 14 pan-type reinforced concrete beams as supporting girders. The study included a theoretical treatment, an experimental model, and field tests. Equations were developed to calculate the thermal stresses and deflections in a beam-slab bridge. Field tests were performed on two summer days and one winter night. A significant discrepancy was found between the measured and the calculated deflections which was attributed to the deviation of the bridge from the theoretical model and the inability to accurately represent the temperature distributions for the analysis. Tensile stresses as high as 1500 psi were reported at the top surface of the slab. These stresses according to the authors (48) were computed from the measured strains.

A three-span continuous reinforced concrete bridge was field tested by Krishnamurthy (34) in 1971. Measured surface temperatures were used in computing temperature distributions inside the bridge cross section. Changes in reaction caused by temperature differentials were predicted and compared with the measured values. The comparisons were reported to be unsatisfactory, which has been attributed to the following factors: 1) loss of structural integrity and/or symmetry of the bridge, 2) malfunctions and/or inadequacy of reaction measuring equipment, and 3) inaccuracies arising from the reaction measurement procedure.

Emerson (20) in 1973 described a method of calculating the distribution of temperature in highway bridges. An iterative method, based on the one-dimensional linear flow of heat was successfully used to predict the temperature distributions in concrete slab bridges. The model related the bridge temperature to the significant environmental variables, i.e., the solar radiation, the ambient air temperature and the wind speed. Temperatures predicted by this model were shown to compare favorably with experimental results. For steel bridges, on the other hand, equations were developed based on experimental data.

In 1974, Berwanger (4) modified the thermal stress theory presented by Zuk (57) to account for symmetrically and unsymmetrically reinforced concrete slabs subjected to uniform and nonlinear temperature change. Consideration was given for both a simple span and a continuous composite steel bridge. Temperature induced stresses computed from assumed 45°F temperature gradients, linear in concrete slab and uniform in steel beam, were found to be of sufficient magnitude to warrant further investigations.

Will (49) has recently developed a finite element program for predicting bridge response under temperature changes. For each element, the temperature may be linear in the plane and may have a quartic distribution over its thickness. The method has been shown to be effective in predicting bridge thermal behaviors. The three-dimensional structural response including the effects of skew boundaries can be studied from this program. Selected bridges were also field tested and good correlations between the predicted and measured values have been obtained.

1.3 Objective and Scope of the Study

The objective of this study is to develop a versatile, yet economical, method for predicting bridge temperature distributions and the corresponding temperature induced stresses caused by daily environmental changes. The proposed method is capable of solving temperature problems for various types of highway bridge cross sections and different conditions of the environment. A computer program which included the heat flow and the thermal stress analysis in a complete system was developed. The necessary environmental data required for input are the solar radiation intensity, ambient air temperature and wind speed. The daily solar radiation intensity is available

through the U.S. Weather Bureau (14) at selected locations in the nation. The air temperature and wind speed, on the other hand, can be obtained from local newspapers.

To accomplish the goal of the study, the scope consisted of the following works. Theoretical models based on one- and two-dimensional heat flow theory were developed in order to predict surface temperatures as well as the complete distribution of temperature over the bridge cross section. The outgoing (long-wave) radiation, which has not been considered in the past, was included in these temperature models. Therefore, the method presented has the superiority in that the temperature can be predicted continuously over a given period of days and nights. In addition, due to the shape of the bridge section, for example the section of Fig 1.1b, the two-dimensional temperature model was developed in order to take into account the temperature distribution which is nonlinear both vertically and horizontally. A stress model employing one-dimensional beam theory was also developed. It should be noted, however, that this stress model can simulate the overall bridge thermal behavior subjected to an arbitrary two-dimensional temperature distribution over the cross section.

Based on the favorable comparisons between the predicted and the measured results, the proposed approach thus offers an excellent opportunity to determine bridge types and environmental conditions for which temperature effects are severe. However, only limited types of highway bridges subjected to climatic changes found in Austin, Texas were considered in this dissertation. These bridges as shown in Fig 1.1 are: 1) a post-tensioned concrete slab bridge, 2) a composite precast pretensioned bridge, and 3) a composite steel bridge. Analyses of several environmental conditions representative of summer and winter conditions were carried out and the results of the investigations were discussed. In these analyses, past records of the solar radiation levels and the daily air temperature distributions during the years 1967-1971 were used. Temperature effects in both statically determinate and indeterminate bridges were also studied. The major findings and the suggestions for future researchers based on the findings of this work are presented at the end of this report.

It is also of importance to note that the study concerns primarily the stresses induced by temperature differential over the depth of highway

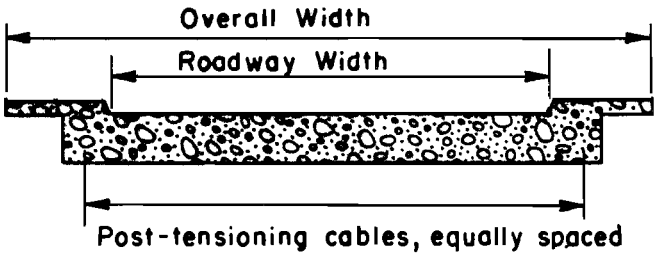

a) Post-tensioned concrete slab bridge

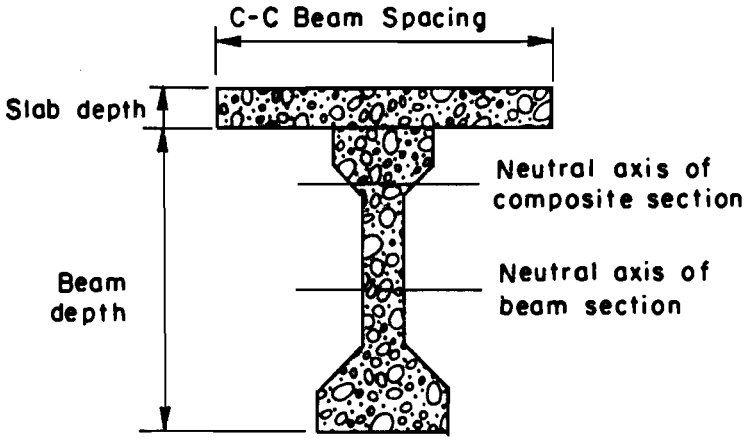

b) Composite precast pretensioned bridge

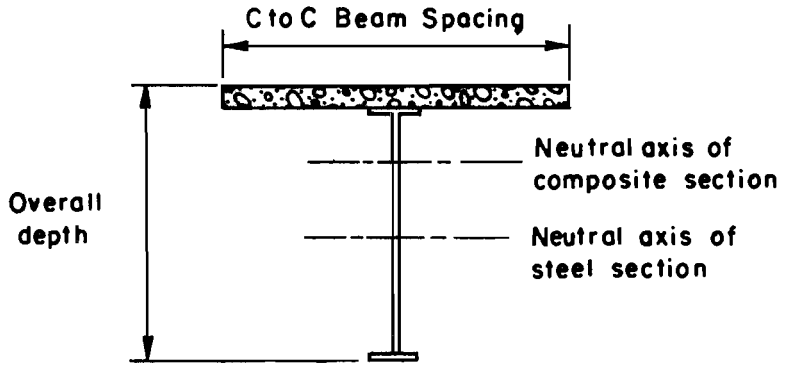

c) Composite steel bridge

Fig 1.1. Typical highway bridge cross sections.

bridges. Combining effects caused from dead load and live loads plus impact are therefore ignored.

CHAPTER 2. THE NEED AND THE APPROACH

2.1 The Need

The problem of thermal effects in various types of highway bridges has been of major interest to bridge design engineers for many years. Past research which has been done in this area indicated that a temperature difference between the top and bottom of a bridge can result in high temperature induced stresses (4,58). However, there still exist uncertainties concerning the magnitudes and effects of these stresses caused by daily variations of the environment. Consequently, in current design practice, temperature stresses are generally ignored, although the Specification (41), section 1.2.15, states that provision shall be made for stresses or movements resulting from variations in temperature.

Ekberg and Emanuel (17) reported that temperature effects have been considered more frequently for steel bridges than for concrete bridges. This is perhaps attributed to the lack of both theoretical and experimental work on the thermal behavior in concrete structures. As concrete bridges become more frequently designed to behave continuously under live load, the temperature effects become more significant than those designed with simple spans. In addition, for deep concrete sections which are commonly found in long span bridges, the temperature distributions over the depth will be highly nonlinear thus resulting in high internal stresses. For example, Van (45) found that under certain conditions thermal stresses could cause serious crackings in reinforced concrete structures, and that daily amplitudes of stresses of the order of 200 to 600 psi could result in the exposed concrete structures. Matlock and co-workers (37) found that relatively mild temperature variations caused structural changes of the same order, and sometimes greater than those of the live load produced by the test trucks. The test bridge was a skew, three-span post-tensioned slab structure. Similar concerns have also been expressed and the problems investigated by other researchers are cited in section 1.2.

As mentioned in Chapter 1 the magnitude of temperature induced stresses principally depends on the nonlinear form of the temperature gradient over

the depth of the section; thus in order to predict reliable stresses actual bridge temperatures must be obtained. Although Emerson (20) has recently been able to determine bridge temperatures using recorded weather data the method is limited only to the unidirectional heat flow. The shape of the section will, by no doubt, influence the temperature distributions inside the bridge. For structures with a complicated cross section, the temperatures will be nonlinear both vertically and horizontally, thus requiring the development of two-dimensional heat flow theory. The capability of the procedure in predicting temperature through a full 24 hour period or over a period of several days also needed to be considered.

Of equal importance is the stress analysis procedure for determining thermal induced stresses. The stress model thus developed will then be used in combination with the temperature model to form a complete system for predicting temperature effects in various types of highway bridges. The result of this research will provide bridge design engineers a simple but rational approach to the problem of estimating the effects of environmental changes on bridge superstructures.

2.2 The Approach

As noted in the preceding chapter, the purpose of this work is to assess the magnitude of temperature induced stresses in highway bridges; induced stresses caused by other factors, such as creep and shrinkage are, therefore, beyond the scope of this study. Also, the influence of temperature upon creep is not considered. The problem of the determination of thermal effects in bridges thus falls into two stages. The first stage involves the calculation of temperature distributions throughout the structural member as a function of time subjected to daily climatic conditions. The second stage involves the determination of the corresponding instantaneous induced stresses.

In the analysis of the temperature distribtuion over the bridge cross section, it is assumed that all thermal properties of the member are time-independent. The distribution of temperature within the member at a given time can be calculated by solving the heat-conduction equation. To solve this equation, however, it is necessary that the temperature on the boundary

and the initial condition be specified. The initial condition, in this context, refers to the starting time at which the bridge is assumed to attain a thermal equilibrium with the environment. At this time the bridge temperature is uniform and equal to the surrounding air temperature. The boundary conditions, on the other hand, depend on the variations of the environment. They can be estimated by considering the law of heat exchange between the surface and its environment. Environmental variables such as solar radiation, ambient air temperature and wind speed have been shown to be the most significant factors (1,58).

The purely analytical solution of the above heat flow theory is possible only in a few simplified cases. In this research, two numerical approaches followed from Emerson (20) and Brisbane (9) will be employed. The first is a one-dimensional model based on finite differences. The other is a two-dimensional model using finite elements. Both methods are modified to have a capability of determining temperatures through a full 24 hour period or over a period of several days. This is achieved by taking into account the outgoing radiation which has not been considered in the past.

The analysis of thermal stresses follows the assumptions that the state of strain is linear under nonuniform temperature distributions, and that the heat flow process is unaffected by a deformation. The stress model used in this study is the simplest one. The one-dimensional beam theory is employed in conjunction with the principle of superposition. All materials are assumed to behave elastically. Structural stiffness is computed based on the uncracked section. In brief, the temperature induced stresses are computed as follows. The bridge is considered to be completely restrained against any movement, thus creating a set of built-in stresses. This condition also induces a set of end forces which are applied back at the ends since the bridge is free from external end forces. This causes another set of stresses which vary linearly over the depth. The final stresses are then obtained by superimposing the above two sets of stresses. In the following chapters, the detail of the development of the mathematical models and their applications will be presented.

CHAPTER 3. ENVIRONMENTAL VARIABLES INFLUENCING BRIDGE TEMPERATURE AND HEAT FLOW CONDITIONS

3.1 Introduction

It is true that there are a large number of factors, in addition to dead and live loads, which affect the structural response of highway bridges. Factors such as creep, shrinkage, temperature, humidity and settlement are known to have the most significant effect. Temperature, however, is believed to cause primary movements and induced stresses following subsidence of creep and shrinkage (3,19,50). In order to study temperature effects in highway bridges, the bridge temperature distribution must be known. It is found in this research that daily bridge temperature distributions can be predicted analytically if daily variations of solar radiation intensity, ambient air temperature and wind speed are given. In this chapter, the significance of these environmental variables on bridge temperature variations will be discussed. Also presented in this chapter are the heat exchange processes which exchange heat between bridge surfaces and the environment, and the heat conduction process which conducts heat from exterior surfaces to the interior body of the bridge.

3.2 Environmental Variables

Temperature behavior in highway bridges is caused by both short-term (daily) and long-term (seasonal) environmental changes. Seasonal environmental fluctuations from winter to summer, or vice versa, will cause large overall expansion and contraction. If the bridge is free to expand longitudinally the seasonal change will not lead to temperature induced stresses. However, daily changes of the environment result in a temperature gradient over the bridge cross section that causes temperature induced stresses. The magnitude of these stresses depends on the nonlinear form of the temperature gradient and the flexural indeterminacy of the bridge. Past research in this area indicates that the most significant environmental variables which influence the temperature distribution are solar radiation, ambient air temperature

and wind speed. The significance of these variables will be discussed below.

3.2.1 Solar Radiation

Solar radiation, also known as insolation (incoming solar radiation), is the principal cause of temperature changes over the depth of highway bridges. Solar radiation is maximum on a clear day. The sun's rays which are absorbed directly by the top surface cause the top surface to be heated more rapidly than the interior region thus resulting in a temperature gradient over the bridge cross section. Studies have shown that surface temperatures increase as the intensity of the solar radiation absorbed by the surface increases. The amount of solar radiation actually received by the surface depends on its orientation with respect to the sun's rays. The intensity is maximum if the surface is perpendicular to the rays and is zero if the rays become parallel to the surface. Therefore, the solar radiation intensity received by a horizontal surface varies from zero just before sunrise to maximum at about noon and decreases to zero right after sunset. It is found, however, that the maximum surface temperature generally takes place around 2 p.m. This lag of surface temperature is attributed to the influence of the daily air temperature variation which normally reaches its maximum value at 4 p.m. The significance of the variation of air temperature on bridge temperature distributions will be discussed in section 3.2.2.

In order to predict daily bridge temperature distributions, the variation of the insolation intensity during the day must be known. This can be accomplished by field measurements. Several types of pyranometers, such as the Eppley pyranometer have been developed for this purpose. Another approach is to use data published in the U.S. Weather Bureau Reports. Solar radiation intensities measured at different weather stations over the nation are recorded every day. Unfortunately, these data are recorded as the daily integral, i.e., the total radiation received in a day. Since it is desirable to use data which has been recorded to predict the bridge temperature distributions, several approximate procedures have been proposed to estimate the variation of solar radiation intensity during the day using the daily radiation data. The pertinent procedures are described below.

It has been confirmed from field measurements that the variation of daily solar radiation intensity on a horizontal surface is approximately

sinusoidal. For example, Monteith (39) has shown that a sine curve representation will give good results at times of high radiation intensities, i.e., at about noon. Later, Gloyne (22) suggested a $(\text{sine})^2$ curve. His method has been shown to give better results at times of relatively low intensities as well as high intensities of radiation. The variation of solar radiation with time as presented by Gloyne is

$$I(t) = \frac{2S}{T} \text{Sin}^2 \alpha \qquad (3.1)$$

where $I(t)$ = insolation intensities at time t, $\text{btu/ft}^2\text{/hr}$,

S = total insolation in a day, btu/ft^2,

T = length of day time, hr,

and $\alpha = \frac{\pi t}{T}$.

Field measurements on solar radiation intensity also indicate that the amount of insolation received each day varies with the time of year and latitude. Local conditions, such as atmospheric contamination, humidity and elevation above sea level, affect the total solar energy received by a surface. Hence, Eq 3.1 may yield good estimates at some locations but may fail at others. So, in order for the above equation to be valid, it must be checked with respect to the location of particular interest. For this reason, comparisons were made between the results using Eq 3.1 and the measured values (42) at the location of 30°N latitude. This location is approximately the same as that for the city of Austin, Texas. Values of the total insolation in a day (S) were taken from the U.S. Weather Bureau Reports. They represent the average of the maximum values as recorded during the years 1967-1971. These averaged values are given in Table 3.1. Correlations of the predicted values using Eq 3.1 with measured values (42) for three typical months are shown in Fig 3.1. It can be seen that the predicted values underestimate the solar radiation intensities at the end of the day. Also, at noon predicted values are overestimated. Hence, a modified model is developed in this work, the purpose of which is to get a better estimate of solar radiation intensities. Using the data presented in Ref 42, a new improved model, which is basically based on the Gloyne's model, was obtained by trial

TABLE 3.1 AVERAGE MAXIMUM TOTAL INSOLATION IN A DAY ON THE HORIZONTAL SURFACE (1967-1971) AND LENGTH OF DAYTIME (LATITUDE 30°N)

Month	Insolation (btu/ft^2)	Time(CST)		Length of Daytime(hr.)
		Sunrise(A.M.)	Sunset(P.M.)	
JAN	1500	7:30	6:00	10.5
FEB	1960	7:15	6:15	11.0
MAR	2289	6:30	6:30	12.0
APR	2460	6:00	7:00	13.0
MAY	2610	5:30	7:00	13.5
JUN	2631	5:30	7:30	14.0
JUL	2550	5:30	7:30	14.0
AUG	2380	6:00	7:00	13.0
SEP	2289	6:30	6:30	12.0
OCT	1925	6:30	6:00	11.5
NOV	1570	7:00	5:30	10.5
DEC	1329	7:30	5:30	10.0

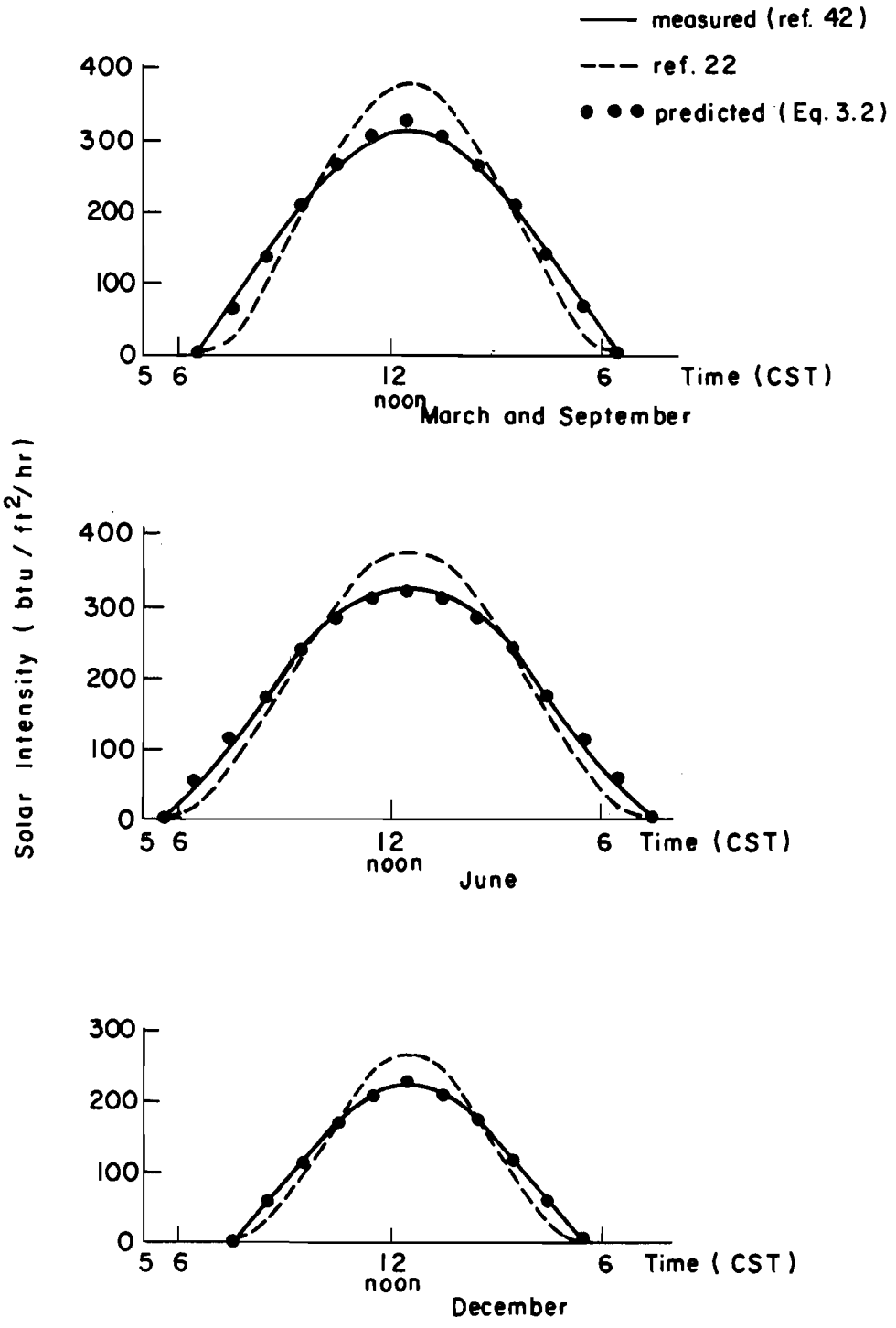

Fig 3.1. Hourly distributions of solar radiation intensity for a clear day (Latitude 30°N).

and error. Finally, the proposed empirical equation is

$$I(t) = \frac{1.7S}{T}\left(\frac{\sin^2\alpha + 2\sin\alpha}{3}\right) \tag{3.2}$$

Good correlations between the predicted values using equation 3.2 and the measured values are shown in Fig 3.1. Although only three different months are used in this comparison, it is believed that the method applies for other months of the year. From Table 3.1, it can be seen that the highest solar radiation intensity occurs in June. In December, the radiation is the minimum due to the reduced angle of incidence of the sun's rays, their longer path through atmosphere and the shorter period of sunlight.

3.2.2 Air Temperature

Air temperature varies enormously with locations on earth and with the seasons of the year. The manner in which daily air temperature varies with time must be known in order to predict temperature effects in bridge. The maximum and the minimum value of air temperatures in a day are regularly recorded at almost all weather stations in the nation. The hourly temperature distribution, however, can only be obtained from local weather reports.

On clear days with little change in atmospheric conditions, the air temperature generally follows two cycles. The normal minimum temperature is reached at or shortly before sunrise, followed by a steady increase in temperature due to the sun's heating effect. This increase continues until the peak temperature is reached during the afternoon, usually around 4 to 5 p.m. Then the temperature decreases until the minimum reading is reached again the next morning. This cyclic form of temperature variation can be changed by the presence of clouds, rain and snow, etc. Clouds, for example, form a blanket so that much of the sun's radiation fails to reach the earth, this results in lowering air temperature during the day. At night, back radiation from the clouds cause a slight increase in air temperature. Plots of hourly air temperature variation on a clear day for typical summer and winter months are shown in Fig 3.2. These data were obtained from local newspapers (Austin, Texas) during the year 1967-1971. It can be seen that the trend of all curves follows the discussion mentioned above.

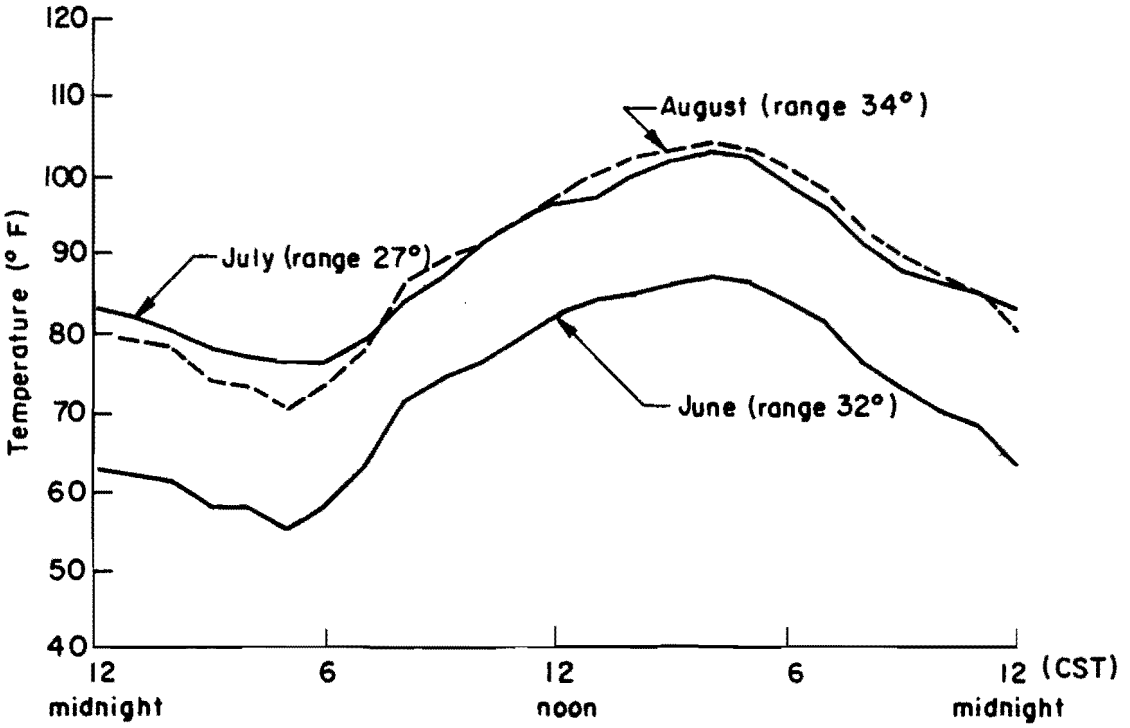

a) Summer

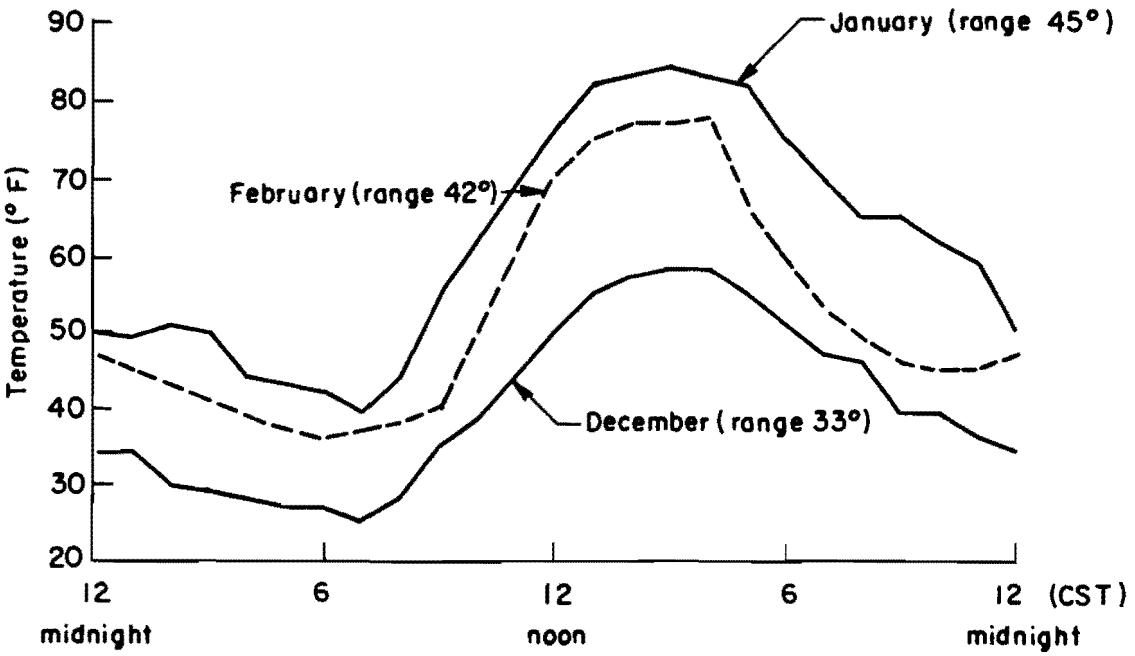

b) Winter

Fig 3.2. Hourly distributions of air temperature (Austin,Texas).

It is worth noting that the times of high and low ambient air temperature do not coincide with the times of maximum and minimum solar radiation intensity. This is true for both the daily and the yearly conditions. The month of August is generally considered as the hottest month of the year, January the coldest; yet the greatest intensity of radiation occurs in June and the lowest in December. On a daily basis, the maximum air temperature normally occurs at 4 p.m., yet the maximum solar radiation intensity occurs at noon. Table 3.2 summarizes temperature data as recorded in Austin, Texas. Normal and extreme air temperature are tabulated for each month of the year. Figure 3.3 depicts the annual air temperature variation.

Studies done in this research have shown that during a period of clear days and nights, variations of bridge temperature distribution over the concrete cross section are small at about 2 hours after sunrise. At this time, it is possible to assume a thermal equilibrium state in which the bridge temperature is the same as that of surrounding air temperature. In this study, it was also found that the range of air temperature from a minimum value to a maximum value during a given day affects the bridge temperature distribution. A large range of air temperature will cause a large temperature differential over the bridge depth which in turn causes high temperature induced stresses. Figure 3.2 depicts variations of air temperature which yield maximum ranges of air temperature as recorded in Austin, Texas. It is of interest to note that the range of air temperature is higher in winter than in summer. In January, the range is 45°F while 34°F is found in August.

3.2.3 Wind Speed

Wind is known to cause an exchange of heat between surfaces of the bridge and the environment. The speed of the wind has an effect in increasing and lowering surface temperatures. From this research study, it is found that maximum temperature gradients over the bridge depth are reached on a still day. On a sunny afternoon, wind decreases temperatures on the top surface and increases temperatures at the bottom. This effect, of course, results in lowering the temperature gradient during the day. At night, maximum reversed temperature gradients are also decreased by the presence of the wind.

TABLE 3.2 NORMALS, MEANS AND EXTREMES (REF 13)
LATITUDE 30° 18'N, LONGITUDE 97° 42'N
ELEVATION (GROUND) 597 FEET

Austin, Texas

Month	Temperature							Wind			
	Normal			Extremes				Mean Hourly Speed	Fastest Mile		
	Daily Max.	Daily Min.	Monthly (Av.)	Record Highest	Year	Record Lowest	Year		Speed	Direction	Year
JAN	60.3	40.5	50.4	86	1963	12	1963	9.9	47	N	1962
FEB	64.0	43.5	53.8	87	1962	22	1967	10.2	57	N	1947
MAR	70.6	48.7	59.7	96	1967	23	1962	10.9	44	W	1957
APR	78.0	57.3	67.7	98	1963	39	1962	10.9	44	NE	1957
MAY	85.2	64.9	75.1	99	1967	52	1968	10.2	47	NE	1946
JUN	92.0	71.7	81.9	100	1967	55	1964	9.6	49	SE	1956
JUL	95.1	73.9	84.5	103	1964	64	1968	8.7	43	S	1953
AUG	95.6	73.7	84.7	105	1962	61	1967	8.3	47	N	1959
SEP	89.7	68.5	79.1	102	1963	47	1967	8.0	45	NE	1961
OCT	81.9	59.5	70.7	95	1963	39	1966	8.1	47	NW	1967
NOV	69.6	47.9	58.8	89	1963	31	1966	9.1	48	NW	1951
DEC	62.8	42.6	52.7	84	1966	21	1966	9.2	49	NW	1956

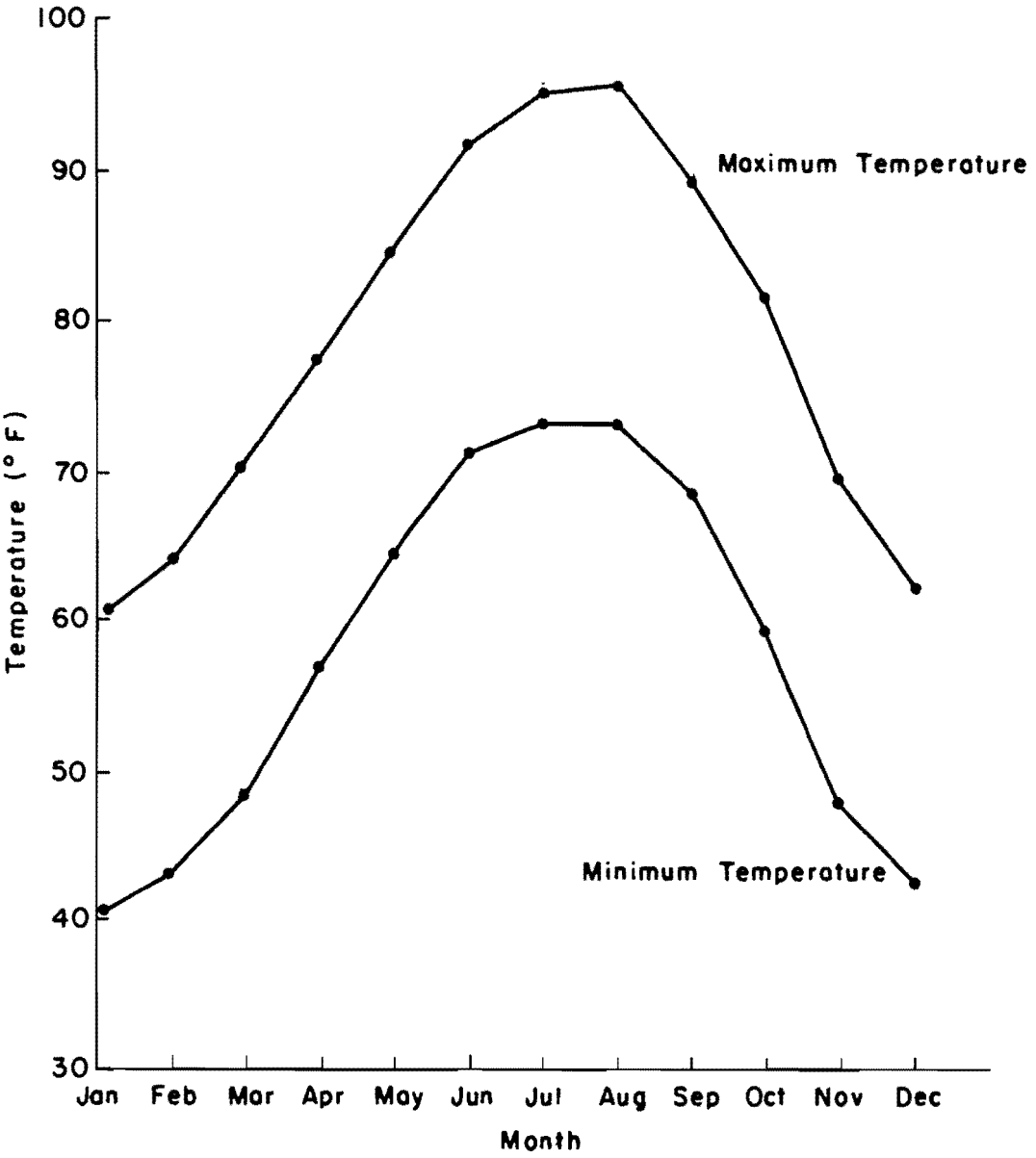

Fig 3.3. Average maximum and minimum air temperatures (Austin,Texas).

Wind speed is recorded by all weather stations. Table 3.2 gives the average wind speed for each month of the year as recorded in Austin, Texas.

3.3 Heat Flow Conditions

The prediction of time varying bridge temperature distributions involves the solution of the heat flow equations governing the flow of heat at the bridge boundaries and within the bridge. In general, heat is transferred between the bridge boundaries and the environment by radiation and convection. Heat, on the other hand, is transferred within the bridge boundaries by conduction. In order to estimate the temperatures in highway bridges the relationship between atmospheric conditions and the heat transfer from the bridge boundaries to the atmosphere must be known. The development of this relationship will be established below.

3.3.1 Heat Flow by Radiation

Radiation is the primary mode of heat transfer which results in warming and cooling bridge surfaces. The top surface gains heat by absorbing solar radiation during the day and loses heat by emitting out-going radiation at night. The amount of heat exchange between the environment and the bridge boundaries depends on the absorptivity and emissivity of the surface, the surface temperature, the surrounding air temperature and the presence of clouds. Values of absorptivity of a plain concrete surface depends on its surface color. In general, its values lie between 0.5 to 0.8. Concrete with asphaltic surface has higher absorptivity and published values are between 0.85 to 0.98. The emissivity, on the other hand, is independent of the surface color. Its values lie between 0.85 to 0.95. For steel, the absorptivity varies from 0.65 to 0.80 and the emissivity is between 0.85 to 0.95.

The heat transferred by radiation is caused by both short-wave and long-wave radiation. Heat energy absorbed by the surface from the short-wave radiation can be estimated from

$$Q_s = rI \tag{3.3}$$

TABLE 3.3 VALUES OF EMISSIVITY AND ABSORPTIVITY (REF 27)

Surface	Emissivity 50-100 F	Absorptivity for Solar Radiation
Black non-metallic surfaces such as asphalt, carbon, slate, paint, paper	0.90 to 0.98	0.85 to 0.98
Red brick and tile, concrete and stone, rusty steel and iron, dark paints (red, brown, green, etc.)	0.85 to 0.95	0.65 to 0.80
Yellow and buff brick and stone, firebrick, fireclay	0.85 to 0.95	0.50 to 0.70
White or light-cream brick, tile, paint or paper, plaster, white-wash	0.85 to 0.95	0.30 to 0.50
Dull brass, copper, or aluminum; galvanized steel; polished iron	0.20 to 0.30	0.40 to 0.65

where Q_s = heat gain by short-wave radiation, btu/ft^2/hr,

r = absorptivity of the surface,

and I = solar radiation intensity, btu/ft^2/hr,

Values of I on a cloudless day can be obtained either by field measurement or by using Eq 3.2. If Eq 3.2 is used the total insolation in a day (S) must be known.

The study of heat exchange which results from the long-wave radiation follows from the Stefan-Boltzmann law. This law states that all bodies will emit radiant electromagnetic energy at a rate which is found to be proportional to the fourth power of the absolute temperature of the body. The rate at which the energy is emitted is given by

$$Q_e = e\sigma\theta^4 \tag{3.4}$$

where Q_e = emitting energy, btu/ft^2/hr,

e = emissivity,

σ = Stefan-Boltzmann constant,

= 0.174×10^{-8}, btu/ft^2/hr/°R^4,

and θ = absolute temperature , °R (Rankine).

Note that °R = °F + 459.67.

It can be shown (12) theoretically that heat loss by long-wave radiation from bridge surfaces to the environment can be approximated by

$$Q_L = e\sigma(\theta_s^4 - \theta_a^4) \tag{3.5}$$

where Q_L = heat loss by long-wave radiation, btu/ft^2/hr,

θ_s = surface temperature, °R,

θ_a = air temperature, °R .

It has been confirmed from field measurements (51) that Eq 3.5 yields a reasonable estimate of radiation loss between the earth's surface and the

environment under cloudy sky condition. Equation 3.5, however, is found to underestimate the net heat loss from the surface when the sky is clear. This is due to the fact that the clouds, which can be regarded as a black body, absorbs solar radiation during the day and emits it back to the earth during the night. According to Swinbank (43), the incoming long-wave radiation, R , can be estimated from

$$R = \epsilon \theta_a^6 \tag{3.6}$$

where R = incoming long-wave radiation under clear sky, $btu/ft^2/hr$,

ϵ = a constant, approximately 0.496×10^{14} , $btu/ft^2/hr/°R^6$,

and θ_a = air temperature, $°R$.

Equation 3.6 has been shown to represent the data from a number of sites with a high accuracy. Therefore, net radiation loss at the top surface of a bridge is given by

$$Q_{LC} = e \sigma \theta_s^4 - \epsilon e \theta_a^6 \tag{3.7}$$

where Q_{LC} = net heat loss by long-wave radiation under clear sky condition, $btu/ft^2/hr$.

3.3.2 Heat Flow by Convection

The two types of heat exchange by convection between bridge boundaries and the environment are termed free and forced convection. In the absence of the wind, heat is transferred from the heated surface by air motion caused by density differences within the air. This process is known as free convection. It is known that heat loss by forced convection is greater than by free or natural convection.

Experiments done by Griffiths and Davis (25) show that heat loss by free convection is proportional to the 5/4 power of the temperature difference between two surfaces. However, it has been shown from field measurements (51) that heat loss by convection at bridge surfaces can be approximately

estimated by assuming heat loss to be proportional to the first power of the temperature difference. Such results are shown in Fig 3.4. Therefore, in general, heat loss by convection from a dry surface is given by (51)

$$Q_c = h_c (T_s - T_a) \tag{3.8}$$

where Q_c = heat loss by convection, btu/ft^2/hr,

T_s = surface temperature, °F,

T_a = air temperature, °F,

h_c = convection film coefficient,

= $0.665 + 0.133\,u$, btu/ft^2/hr/°F,

u = wind speed, mph .

The effect of the wind on the loss of heat by convection is recognized in the film coefficient, h_c .

3.3.3 Heat Flow by Conduction

Heat is transferred within the bridge boundaries by conduction. For a known time-dependent boundary temperature, the interior temperature distribution is governed by the well-known transient heat-conduction equation,

$$\frac{\partial T}{\partial t} = \frac{k}{\rho c}\left(\frac{\partial^2 T}{\partial x^2} + \frac{\partial^2 T}{\partial y^2} + \frac{\partial^2 T}{\partial z^2}\right) \tag{3.9}$$

where T = temperature of mass as a function of t, x, y and z, °F,

t = time, hr,

x, y, z = directions in Cartesian coordinates, ft,

k = thermal conductivity, btu/hr/ft/°F,

ρ = density, lb/ft^3,

and c = specific heat, btu/lb/°F .

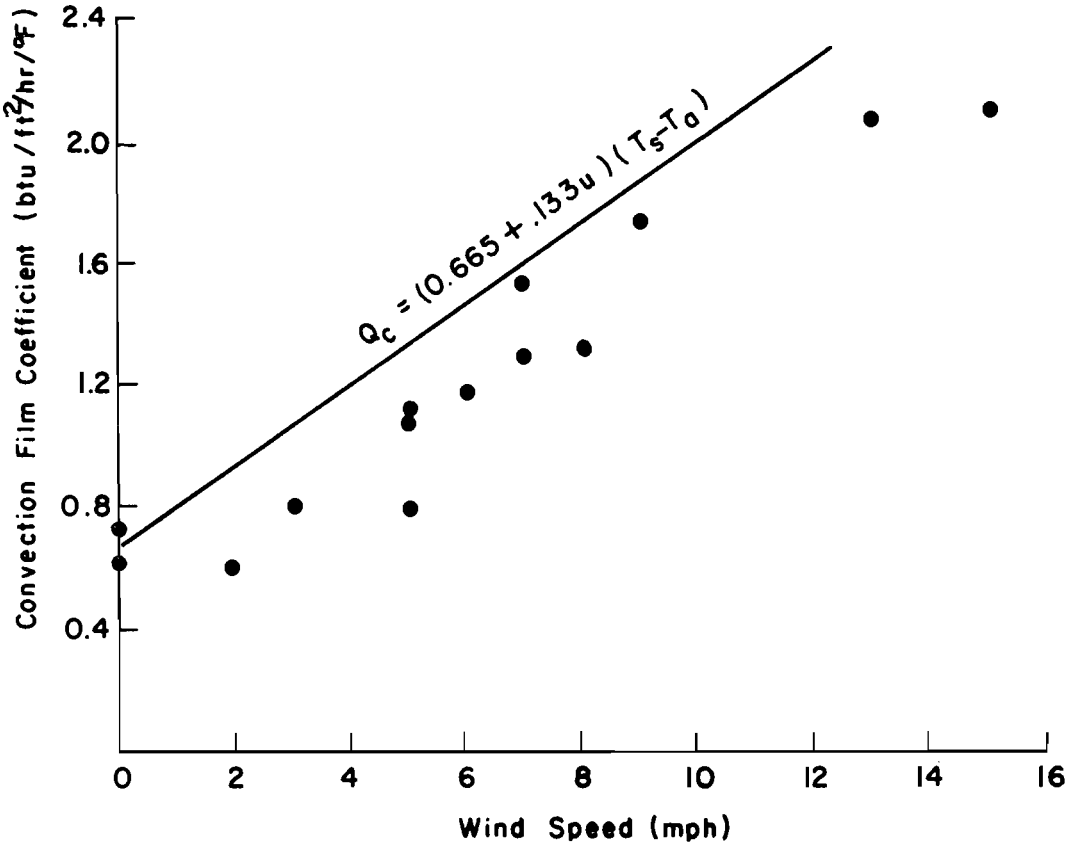

Fig 3.4. Variation of convective film coefficient with wind speed (Ref 51).

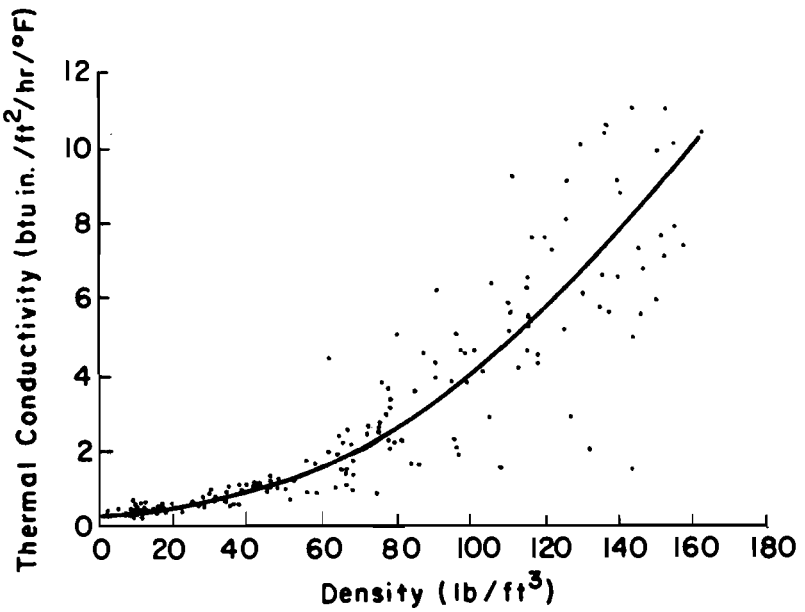

Fig 3.5. Variation of thermal conductivity with density (Ref 5).

The thermal conductivity, k , is a specific characteristic of the material. It indicates the capacity of a material for transferring heat. Experiments (5) have shown that its magnitude increases as the density of the material increases. Results of such experiments are depicted in Fig 3.5. Normally, the average thermal conductivity of concrete and steel are 0.75 and 26.6 btu/hr/ft/°F respectively. Whether the material is wet or dry affects the thermal conductivity. It has been shown that a wet concrete has higher thermal conductivity than a dry concrete.

Shapes of temperature distribution over the bridge depth depend mainly on its conduction property. A steel beam, for example, because of its high thermal conductivity, will quickly reach the temperature of the surrounding air temperature. However, this is not true for a concrete beam. Nonlinear temperature distribution is usually found in concrete structures as a result of its low thermal conductivity.

CHAPTER 4. MATHEMATICAL MODELS

4.1 Introduction

The three basic mechanisms of heat transfer, conduction, convection and radiation were discussed separately in the preceding chapter. It should be noted, however, that the actual flow of heat is a result of all three mechanisms of heat transfer acting simultaneously. In general, convection and radiation will govern the flow of heat at the boundaries while conduction governs the heat flow within the body. Temperature induced stresses in highway bridges can be computed only if the temperature distribution over the cross section is known. The purpose of this chapter is, therefore, to couple these basic mechanisms of heat transfer in an effort to arrive at a systematic way of predicting the bridge temperature as a function of time. Once the temperature distribution throughout the bridge cross section at any time is known, a one-dimensional structural model is used to calculate the temperature induced stresses. The proposed mathematical model, thus, includes the heat transfer and the thermal stress analysis in one complete system.

4.2 Bridge Temperature Prediction

The development of mathematical formulations used in predicting the temperature distributions for both one and two-dimensional heat flow will be discussed. Correlations of the predicted and the measured temperatures will be presented in the next chapter.

4.2.1 One-Dimensional Model for Predicting the Temperature Distribution

The determination of time varying temperature gradients within the bridge deck may be approximated by assuming that the heat transfers through a slab having a finite thickness and infinite lateral dimensions. In this approach edge effects are neglected and the heat transfer will depend on only one space variable in the direction of the slab thickness.

For a known time-dependent boundary temperature distribution, the interior temperatures in a homogeneous isotropic body with no internal heat source is governed by the Fourier equation

$$\frac{\partial T}{\partial t} = K\left(\frac{\partial^2 T}{\partial x^2} + \frac{\partial^2 T}{\partial y^2} + \frac{\partial^2 T}{\partial z^2}\right) \tag{4.1}$$

where x, y, z = directions in Cartesian coordinates, ft,

t = time, hr,

T = temperature at any point (x, y, z) at time t, °F,

K = diffusivity, ft^2/hr.

The diffusivity, K, is a property of the material, and the time rate of temperature change will depend on its numerical value. The diffusivity is defined by

$$K = \frac{k}{c\rho} \tag{4.2}$$

where k = thermal conductivity, btu/hr/ft/°F,

c = specific heat, btu/lb/°F,

ρ = density, lb/ft^3.

For one-dimensional heat flow, Eq 4.1 reduces to

$$\frac{dT}{dt} = K\frac{d^2 T}{dx^2} \tag{4.3}$$

Hence, the original equation is greatly simplified as the temperature becomes a function of t and x only. To solve Eq 4.3 it is necessary that the initial and the boundary conditions are specified. For a bridge exposed to atmospheric variations, the initial condition is usually referred to as the time at which the temperature distribution throughout the bridge is uniform.

The boundary conditions are the known surface temperatures. These temperatures can be predicted by considering the heat exchange process which takes place at bridge surfaces. Heat is transferred from the environment to bridge surfaces by convection and radiation.

At the top surface, heat balance can be expressed as

Heat absorbed from short wave radiation	=	Heat lost by convection + Heat lost by long wave radiation + Heat lost by conduction.

Under clear sky condition, the above equation is then represented by a sum of Eqs 3.8, 3.7, and Eq 4.3 at initial conditions:

$$rI = h_c(T_s - T_a) + (e\sigma\theta_s^4 - e\epsilon\theta_a^6) - k\left(\frac{\partial T}{\partial x}\right)_{x=0} \qquad (4.4)$$

where r = absorptivity of the surface,

e = emissivity of the surface,

I = total incoming solar radiation intensity,

h_c = convection film coefficient of the top surface,

k = thermal conductivity of the material,

T_s = top surface temperature,

T_a = top air temperature,

θ_s = top surface temperature, °R,

θ_a = top air temperature, °R,

σ = Stefan-Boltzmann constant, $= 0.174 \times 10^{-8}$ btu/ft^2/hr/°R^4 ,

ϵ = coefficient of incoming long wave radiation, and

$\frac{\partial T}{\partial x}$ = temperature gradient in the x-direction .

At the bottom surface, the heat balance equation is

Heat gained by conduction	=	Heat lost by convection + Heat lost by long wave radiation.

or

$$- k\left(\frac{\partial T}{\partial x}\right)_{x=L} = h_c (T_s - T_a) + e\sigma(\theta_s^4 - \theta_a^4) \qquad (4.5)$$

where L = thickness of the bridge deck,

h_c = convection film coefficient of the bottom surface,

T_s = bottom surface temperature,

T_a = bottom air temperature,

θ_s = bottom surface temperature, $^\circ R$,

θ_a = bottom air temperature, $^\circ R$, and

Equations 4.3, 4.4 and 4.5 are thus the necessary equations to predict the transient temperature distribution over the bridge deck. Although material thermal properties are assumed to be temperature independent, the presence of the nonlinear boundary conditions complicates the problem. The analytical solution is difficult to obtain. Thus, a numerical analysis procedure employing the finite difference method was selected.

To obtain a numerical solution, it is first necessary to transform the differential equations into their equivalent finite-differencing forms. The slab under consideration is first divided into equal space intervals Δx , each layer designated by node $i-1$, i , $i+1$, etc., as shown in Fig 4.1. Details of developing the numerical forms are outlined by Kreith (33) and will not be discussed here. Finally Eq 4.3, which used to determine temperature at interior points, becomes

$$T_i' = T_i + \frac{K\Delta t}{\Delta x^2}\left(T_{i-1} - 2T_i + T_{i+1}\right) \qquad (4.6)$$

where T_i' = temperature at node i at the end of time increment,

T_i = temperature at node i at the beginning of time increment,

K = diffusivity,

Δt = time increment, and

Δx = space increment .

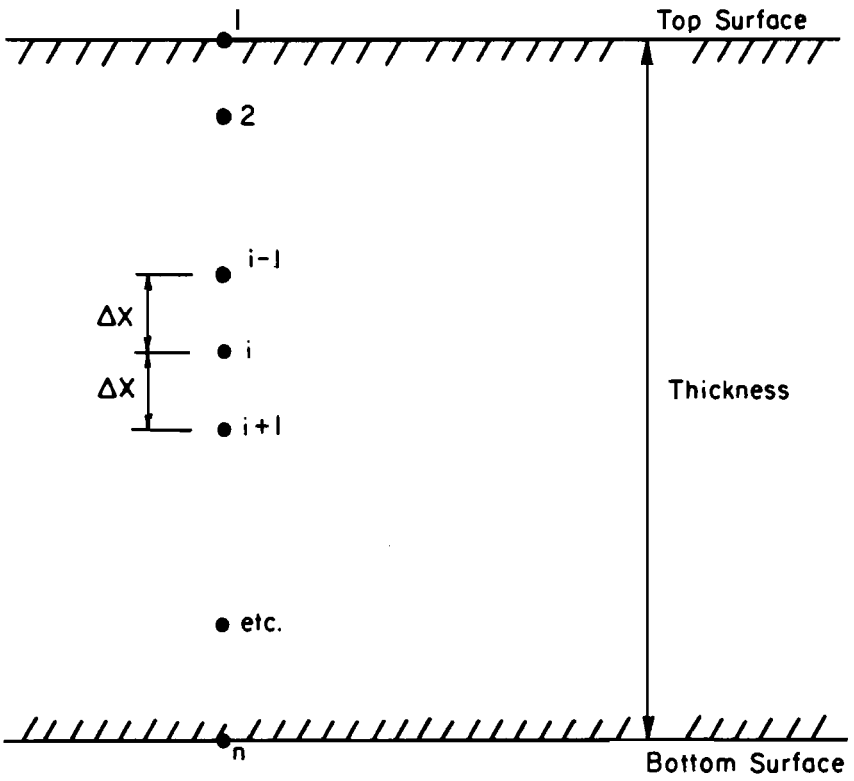

Fig 4.1. A typical slab cross section showing nodal point numbering.

Equation 4.6 allows one to compute the temperature at the interior points at the end of each time increment if temperature distribution at the beginning of the time increment is known. The surface temperature is computed by using Eqs 4.4 and 4.5. At the top surface, the differencing scheme is

$$rI = h_c (T_i - T_a) + (e\sigma\theta_i^4 - e\epsilon\theta_a^6) - \frac{k}{2\Delta x}(T_{i+1} - T_{i-1}) \qquad (4.7)$$

where $i=1$. Hence, T_{i-1} no longer exists. Substituting T_{i-1} from Eq 4.6 into Eq 4.7 yields

$$T_1' = T_1 + \frac{K\Delta t}{\Delta x^2}\left(\alpha_1 T_1 + 2T_2 + \beta_1 T_a + \gamma_1\right) \qquad (4.8)$$

where $\alpha_1 = -2 - 2\frac{\Delta x h_c}{k}$,

$\beta_1 = 2\frac{\Delta x h_c}{k}$, and

$\gamma_1 = 2\frac{\Delta x}{k}(rI - e\sigma\theta_1^4 + e\epsilon\theta_a^6)$.

Similarly, at the bottom surface, Eq 4.5 is rewritten as

$$\frac{k}{2\Delta x}(T_{n-1} - T_{n+1}) = h_c(T_n - T_a) + e\sigma(\theta_n^4 - \theta_a^4) \qquad (4.9)$$

By substituting for T_{n+1} from Eq 4.6 into Eq 4.9, yields

$$T_n' = T_n + \frac{K\Delta t}{\Delta x^2}(\alpha_2 T_n + 2T_{n-1} + \beta_2 T_a + \gamma_2) \qquad (4.10)$$

where $\alpha_2 = -2 - 2\frac{\Delta x h_c}{k}$

$\beta_2 = 2\frac{\Delta x h_c}{k}$

$$\gamma_2 = 2\frac{\Delta x}{k}(e\sigma\theta_a^4 - e\sigma\theta_n^4)$$

Thus, Eqs 4.8 and 4.10 give, respectively, temperatures at the top and bottom surface of the bridge deck in terms of environmental variables and temperature history within the slab. Values of I and T_a used in these two equations will be the average at the beginning and at the end of the time increment being considered. Equations 4.6, 4.8 and 4.10 are summarized in Fig 4.2 which describes the incremental equations used to calculate temperatures through the deck.

In order to perform the analysis the time and the space increments must be selected. The resulting accuracy of the solution depends on the size of the mesh chosen, with smaller subdivisions giving better accuracy. Due to the stability criteria of the finite difference solution, however, the selection of Δx and Δt should not be made independently. It can be shown that limitations on the selection of the spatial and time increment are governed by Eq 4.6. To illustrate this more clearly, Eq 4.6 is rewritten as

$$T_i' = \left(1 - 2\frac{K\Delta t}{\Delta x^2}\right) T_i + \frac{K\Delta t}{\Delta x^2}(T_{i-1} + T_{i+1}) \tag{4.11}$$

In the above equation it is evident that the coefficient, $\left(1 - 2\frac{K\Delta t}{\Delta x^2}\right)$, must at all times be positive to avoid oscillation, i.e., if all nodes have initially zero values of temperature except at node i where $T_i > 0$, the condition for T_i' to be positive is when $\frac{K\Delta t}{\Delta x^2} \leq \frac{1}{2}$. It has been proved (31) that the error of the solution is a minimum when $\frac{K\Delta t}{\Delta x^2} = \frac{1}{6}$. Therefore, for a selected time increment, Δt, a reasonable magnitude of the spatial increment, Δx, can be determined.

Equations 4.8 and 4.10 also impose limitations on the choice of Δx and Δt. Equation 4.8 is rewritten as

$$T_1' = \left(1 + \frac{K\Delta t}{\Delta x^2}\alpha_1\right) T_1 + \frac{K\Delta t}{\Delta x^2}(2T_2 + \beta_1 T_a + \gamma_1) \tag{4.12}$$

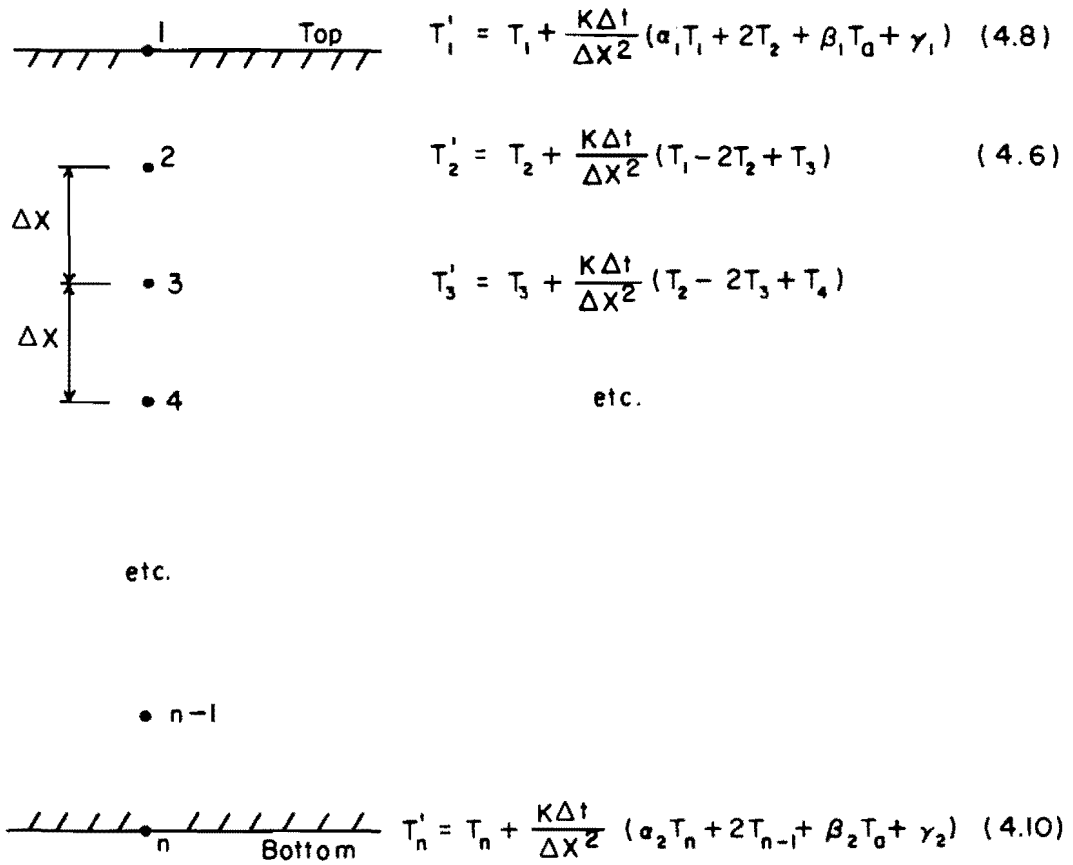

Fig 4.2. A typical slab cross section showing equations used in calculating temperatures.

Therefore, in accordance with the previous discussion the following condition must be satisfied

$$\frac{K\Delta t}{\Delta x^2} \leq \frac{1}{2}\left(1 + \frac{\Delta x h_c}{k}\right) \tag{4.13}$$

Since the above equation involves the varying values of h_c, the inequality must be checked at each time interval to ensure the numerical stability.

In summary, the method discussed above involves the following steps: at the initial time;

1. Obtain material thermal properties; conductivity, specific heat, etc.,
2. Establish time and space increment, Δt and Δx respectively,
3. Establish initial temperature distribution over the depth of the slab,

and for each time increment, Δt ;

4. Input environmental variables; air temperature, insolation intensity and wind speed,
5. Compute top and bottom surface temperature,
6. Compute all interior nodal temperatures, and
7. Repeat for the next time increment.

4.2.2 Two-Dimensional Model for Predicting the Temperature Distribution

In the preceding section, the temperature and the heat flow in one spatial dimension and the method of analysis were discussed. When the bridge has an irregular shape of cross section, the one-dimensional treatment may no longer be satisfactory. For example, studies have shown, in Chapter 5, that the temperature distribution over the cross section of a pan-type bridge is nonlinear in both the vertical and transverse direction. Good correlations between the measured and predicted temperature distributions are obtained when heat is considered to flow two dimensionally. Also, in Chapter 7,

studies of temperature effects in a composite precast pretensioned bridge show that although most of the slab portions experience one-dimensional heat flow from the top to the bottom, the flow of heat in the I-beam is in two dimensions. Moreover, the orientation of the bridge which is not in the east-west direction also necessitates the development of a two-dimensional heat flow model, which enables one to take into account the side heating effects.

In this section, a method of predicting the temperature distribution in a bridge which has constant temperature variations along its length but which may have arbitrary temperature distribution in the cross-sectional plane will be presented. Again, the classical approach to the exact solution will not be considered due to the difficulties in treating the geometry and the boundary conditions. Although there are several approximate methods available for the solution to this type of problem, the finite element method was selected for this work. The advantages of the finite element method are that complex bodies composed of different materials are easily represented. In addition, the method allows temperature or heat flow boundary conditions to be specified at any nodal point in the body. It can also be shown mathematically, that the method converges to the exact solution as the number of elements is increased.

In the finite element method it is necessary to find a functional such that the minimization of this functional will give functions which satisfy the field equations and boundary conditions of the problem of interest. Many functionals have been used by many researchers in solving the uncoupled field problem. Wilson and Nickell (53) used a functional proposed by Gurtin (26) to solve transient heat flow problems. A residual approach based on Galerkin's principle was used by Zienkiewicz and Parekh (56). Another functional was also presented by Brisbane, Becker and Parr (9) for thermoelastic stress analysis. It should be pointed out that whichever functional is used, the final forms for the finite element equations will essentially be the same. Instead of following the formal mathematical method, Wilson (52) used another approach. He showed that a physical interpretation of the heat transfer process in a solid body could also be used to formulate equilibrium equations needed in the finite element method.

Since the functional given in Ref 9 is relatively easy to handle, it will be used in formulating the mathematical model to predict bridge temperatures. The functional, with no internal heat source, is defined as

$$\pi(U,\dot{U}) = \int_v \left\{ \frac{1}{2} \underset{\sim}{\nabla} U \cdot \underset{\approx}{k} \underset{\sim}{\nabla} U + \rho c U \dot{U} \right\} dv - \int_s \underset{\sim}{n} \cdot \underset{\sim}{q} U \, ds \tag{4.14}$$

where v = volume of the domain,

s = surface of the domain's boundary,

$\underset{\approx}{k} = \underset{\approx}{k}(x^i)$ = conductivity tensor for an anisotropic material,

$c = c(x^i)$ = specific heat,

$\rho = \rho(x^i)$ = density,

$\underset{\sim}{q} = \underset{\sim}{q}(x^i)$ = heat flux vector across a boundary,

$\underset{\sim}{n} = \underset{\sim}{n}(x^i)$ = unit normal vector,

$U = U(x^i,t)$ = temperature,

$\dot{U} = \dot{U}(x^i,t)$ = time derivative of temperature,

$\underset{\sim}{\nabla} U$ = gradient of U, and

x^i = coordinates.

If temperature U is assumed to take a certain variation over the element and that it can be defined by the nodal point temperature, $\underset{\sim}{u}$, the functional above becomes $\pi(\underset{\sim}{u}, \dot{\underset{\sim}{u}})$. The equilibrium and the boundary equations can then be obtained by the virtue of the principle of minimum potential energy, i.e., by

$$\frac{\partial \pi}{\partial \underset{\sim}{u}} (\underset{\sim}{u}, \dot{\underset{\sim}{u}}) = 0 \tag{4.15}$$

Let $$U = \underset{\sim}{N} \underset{\sim}{u} \tag{4.16}$$

then $$\dot{U} = \underset{\sim}{N} \dot{\underset{\sim}{u}}$$

and $$\underset{\sim}{\nabla} U = \underset{\sim}{\nabla} \underset{\sim}{N} \underset{\sim}{u} = \underset{\approx}{D} \underset{\sim}{u} \tag{4.18}$$

Substituting above values into Eq 4.14, the result in the matrix form is

$$\pi(\underset{\sim}{u}, \dot{\underset{\sim}{u}}) = \int_v \left\{ \frac{1}{2} \underset{\sim}{u}^T \underset{\approx}{D}^T \underset{\approx}{k} \underset{\approx}{D} \underset{\sim}{u} + \rho c \underset{\sim}{u}^T \underset{\sim}{N}^T \underset{\sim}{N} \dot{\underset{\sim}{u}} \right\} dv - \int_s \underset{\sim}{u}^T \underset{\sim}{N}^T \underset{\sim}{n}^T \underset{\sim}{q} \, ds \qquad (4.19)$$

Applying Eq 4.15 to the above equation, then

$$\int_v \left\{ \underset{\approx}{D}^T \underset{\approx}{k} \underset{\approx}{D} \underset{\sim}{u} + \rho c \underset{\sim}{N}^T \underset{\sim}{N} \dot{\underset{\sim}{u}} \right\} dv - \int_s \underset{\sim}{N}^T \underset{\sim}{n}^T \underset{\sim}{q} \, ds = 0 \qquad (4.20)$$

In applying Eq 4.20 to highway bridge structures the heat flux $\underset{\sim}{q}$ will be the combination of a convective heat flux, $\underset{\sim}{Q}_c$, over S_1 and a radiation heat flux, $\underset{\sim}{Q}_r$, over S_2. These vectors are expressed, from Chapter 3, as

$$\underset{\sim}{Q}_c = h_c (U - U_a) \qquad (4.21)$$

under clear sky

$$\underset{\sim}{Q}_r = \underset{\sim}{Q}_s - \underset{\sim}{Q}_{LC} \qquad (4.22)$$

The convective vector, $\underset{\sim}{Q}_c$, can be treated exactly in the finite element formulation. However, this is not the case for the radiation term because $\underset{\sim}{Q}_{LC}$ contains the nonlinear temperature field. According to Eq 3.7

$$\underset{\sim}{Q}_{LC} = e\sigma (U + 460)^4 - 0.496 \times 10^{-14} (U_a + 460)^6 \, e \qquad (4.23)$$

To simplify the problem, the temperature of the previous time is used for U in Eq 4.23. In doing this, the time increment must be kept small to minimize the error. In fact, in the finite difference formulation discussed in section 4.2.1, previous values of temperature were used explicitly without considering this as the source of error.

Equation 4.20 can then be rewritten as

$$0 = \int_v \left\{ \underset{\approx}{D}^T \underset{\approx}{k} \underset{\approx}{D} \underset{\sim}{u} + \rho c \underset{\sim}{N}^T \underset{\sim}{N} \dot{\underset{\sim}{u}} \right\} dv + \int_{s_1} h_c \underset{\sim}{N}^T (\underset{\sim}{N} \underset{\sim}{u} - U_a) \, ds - \int_{s_2} \underset{\sim}{N}^T \underset{\sim}{n}^T \underset{\sim}{Q}_r \, ds \qquad (4.24)$$

or $$\underset{\approx}{C}\,\dot{\underset{\sim}{u}} + (\underset{\approx}{B} + \underset{\approx}{H})\,\underset{\sim}{u} = \underset{\sim}{q^*} + \underset{\sim}{h^*} \tag{4.25}$$

where $$\underset{\approx}{C} = \rho c \int_v \underset{\sim}{N}^T \underset{\sim}{N}\, dv \tag{4.26}$$

$$\underset{\approx}{B} = \int_v \underset{\approx}{D}^T \underset{\approx}{k}\, \underset{\approx}{D}\, dv \tag{4.27}$$

$$\underset{\approx}{H} = h_c \int_{s_1} \underset{\sim}{N}^T \underset{\sim}{N}\, ds \tag{4.28}$$

$$\underset{\sim}{q^*} = \int_{s_2} \underset{\sim}{N}^T \underset{\sim}{n}^T \underset{\sim}{Q_r}\, ds \tag{4.29}$$

and $$\underset{\sim}{h^*} = h_c U_a \int_{s_1} \underset{\sim}{N}^T\, ds \tag{4.30}$$

Coefficients for the matrices and vectors from Eqs 4.26 through 4.30 can be computed if the shape of the element and the form of temperature distribution over the element are specified. The triangular element with linear temperature field over the element is used here, see Fig 4.3. Matrices of the above equations are given explicitly in Appendix A. For a quadrilateral element, coefficients are formed from four triangular elements as shown in Fig 4.4. The unknown temperature at node 5 is eliminated from the equations by the method of static condensation.

Coefficients of the matrix $\underset{\approx}{C}$ given in Appendix A follow from the assumption that the heat capacity is lumped at the nodal points. This lumped method results in a diagonal heat capacity matrix, thus requiring less computation effort. The loss of accuracy of the solution due to this approximation, however, has been shown to be small (53).

For convenience, Eq 4.25 will be rewritten as

$$\underset{\approx}{C}\,\dot{\underset{\sim}{u}}_t + \underset{\approx}{K}\,\underset{\sim}{u}_t = \underset{\sim}{F} \tag{4.31}$$

where $$\underset{\approx}{K} = \underset{\approx}{B} + \underset{\approx}{H} \tag{4.32}$$

and $$\underset{\approx}{F} = \underset{\sim}{q^*} + \underset{\sim}{h^*} \tag{4.33}$$

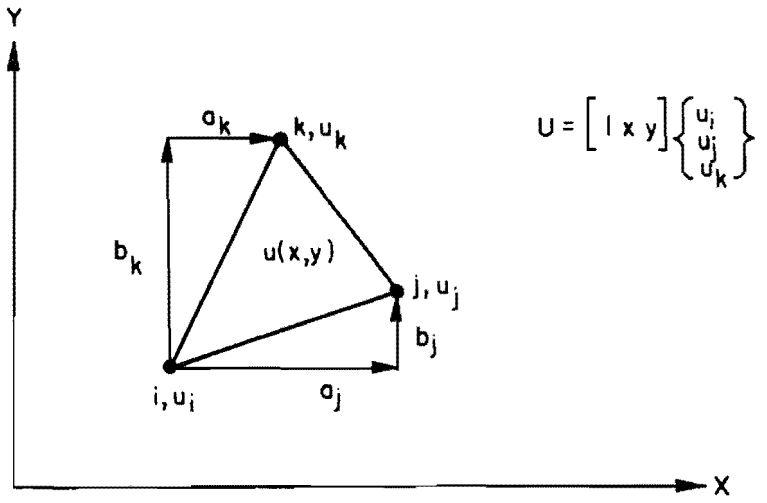

Fig 4.3. A typical triangular element.

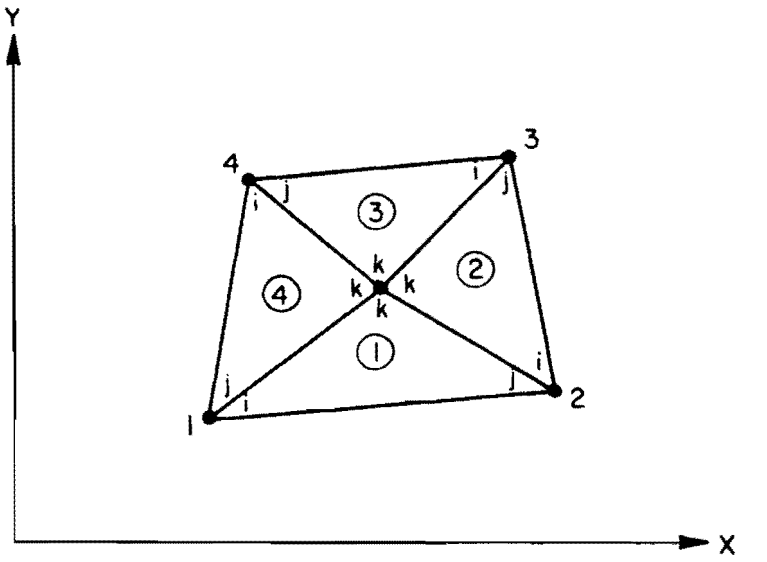

Fig 4.4. A typical quadrilateral element.

If the temperature at each node is assumed to vary linearly within the time increment, the rate of change in temperature is then constant and is given by

$$\dot{u}_t = \frac{u_t - u_{t-\Delta t}}{\Delta t} \tag{4.34}$$

where Δt = time increment

Substituting Eq 4.34 into Eq 4.31 and regrouping terms, yield

$$\underset{\approx}{K}^* \underset{\sim}{u}_t = \underset{\sim}{F}^* \tag{4.35}$$

where $$K^* = \underset{\approx}{K} + \frac{1}{\Delta t} \underset{\approx}{C} \tag{4.36}$$

and $$\underset{\sim}{F}^* = \underset{\sim}{F}_t + \frac{1}{\Delta t} \underset{\approx}{C} \underset{\sim}{u}_{t-\Delta t} \tag{4.37}$$

Equation 4.35 is now a system of linear equations and can be solved for the new temperature. If time increment and wind speed are constant for all time steps, the $\underset{\approx}{K}^*$ will then be independent of the time variable. In such a case, K^* needs to be triangularized only once resulting in computational efficiency for the subsequent time increments.

In summary, the method involves the following steps of calculation. At the initial time,

1. Calculate $\underset{\approx}{C}$ and $\underset{\approx}{K}$,
2. Modify for temperature boundary conditions,
3. Form $\underset{\approx}{K}^*$,
4. Triangularize $\underset{\approx}{K}^*$,

and for each time increment, Δt ,

5. Calculate $\underset{\sim}{F}$,

   where $\underset{\sim}{Q}_s$ is the average value at time t and $(t-\Delta t)$,

$\underset{\sim}{Q}_{LC}$ is the value at time $(t-\Delta t)$,

$\underset{\sim}{h^*}$ is the average value at time t and $(t-\Delta t)$,

6. Calculate $\underset{\sim}{F^*}$,
7. Solve equation $\underset{\approx}{K^*}\ \underset{\sim}{u}_t = \underset{\sim}{F^*}$, and
8. Repeat for next time increment.

4.3 Thermal Stress Analysis

After temperature throughout the bridge structure is known, temperature stresses can then be computed. These stresses, however, are only approximate because of the difficulty in determining the elastic modulus of concrete and its coefficient of thermal expansion. Besides, the unknown degree of edge restraints and the unexpected unsymmetrical geometry of the bridge also affect the resultant stress. The theory of the stress analysis, therefore, inevitably involves certain idealizations of the structure and material properties. In this work, temperature induced stresses are computed based on one-dimensional elastic beam theory and includes the following assumptions:

1. Temperature variation is constant along the length of the bridge but can vary in any manner over the cross section of the bridge,
2. Thermal strains vary linearly with temperature changes,
3. The principle of superposition is valid,
4. An isoptropic material,
5. Material properties are temperature independent, and
6. Plane sections remain plane after deformation.

In addition, the upcoming discussion will follow the classical thermoelasticity theory as developed by Duhamel and Neumann. This theory assumes that, although the state of strain of an elastic solid is affected by a nonuniform temperature distribution, the heat conduction process is unaffected by a deformation (7). This assumption is, of course, an approximation in the transient thermal problem. In order to understand the effects of temperature, a typical beam section away from the ends is represented by a set of

springs and straight rods as depicted in Fig 4.5a. Each spring has a spring constant E, i.e., the modulus of elasticity of the material. Originally, at zero reference temperature, all springs have the same length and are free from stress. If each spring is then subjected to the temperature rise as shown in Fig 4.5b, all springs will expand unequally and the system will seek a new equilibrium configuration. By removing the right connecting rod, each spring will expand freely and with zero stress. According to the second assumption mentioned above, thermal strain in each spring is

$$\epsilon_i' = \alpha T_i \qquad i = 1,5 \tag{4.38}$$

where ϵ_i' = thermal strain in the i^{th} spring,

α = coefficient of thermal expansion, and

T_i = temperature rise in the i^{th} spring.

The position of the system at this stage is shown in Fig 4.5c which violates the assumption that the plane section remains plane after deformation. To restore the original position, an appropriate compressive force is applied to each spring, thus resulting the compressive stress of

$$\sigma_i' = - E \alpha T_i \qquad i = 1,5 \tag{4.39}$$

where σ_i' = thermal stress in the i^{th} spring, and

E = spring constant.

For sections throughout the beam to maintain the same condition, it is necessary to distribute the compressive force of the magnitude (Eq 4.39) at the ends of the beam only. However, if the beam is free from external forces, the longitudinal stress must vanish on the ends. To eliminate the end forces, tensile stress of the magnitude $E \alpha T_i$ is applied to each spring at the ends of the beam. According to Saint Venant's principle, stresses and deformations at sections away from the ends can be estimated by the use of statically equivalent forces. Under these forces, the resulting strain distribution

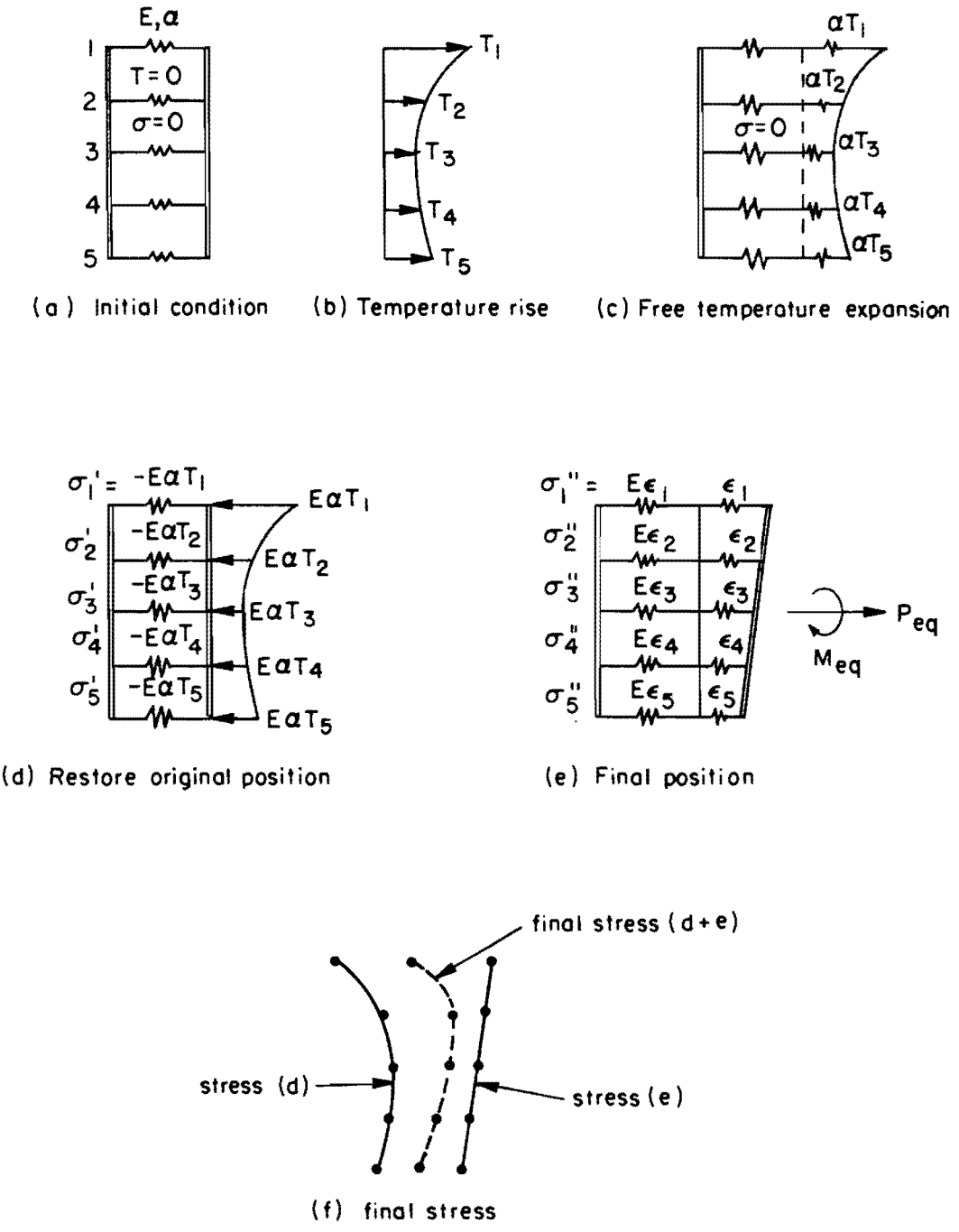

Fig 4.5. Spring system analogy to the thermal stress calculation.

will be linear over the depth and the final position of the spring system satisfies the assumption of plane sections remaining plane after deformation, Fig 4.5e. Stress in each spring is

$$\sigma_i'' = E \epsilon_i'' \qquad i = 1,5 \qquad (4.40)$$

where σ_i'' = stress in the i^{th} spring due to the statically equivalent forces,

and ϵ_i'' = strain in the i^{th} spring due to the statically equivalent forces.

Temperature induced stress in each spring is thus obtained by superimposing stresses of Fig 4.5d and Fig 4.5e. Final stress in each spring is, Fig 4.5f,

$$\sigma_i = \sigma_i' + \sigma_i'' \qquad i = 1,5 \qquad (4.41)$$

where σ_i = thermal induces stress in the i^{th} spring.

It should be pointed out that the application of Eq 4.41 is valid for sections at some distance from the ends of the beam. At the ends of the beam the resultant stresses must approach zero. Also, the deformed shape resulting from the temperature differential can be obtained by considering the system subjected to statically equivalent forces applied at both ends.

4.3.1 Thermal Stress Analysis using the One-Dimensional Temperature Distribution Model

The prediction of temperature distribution using this mathematical model was discussed in section 4.2.1. In calculating thermally induced stresses, consider a unit width of slab cross section subjected to temperature distribution as shown in Fig 4.6. The equivalent force and moment about the neutral axis x are

$$P_{eq} = \int_{-d/2}^{d/2} E \alpha T(y)\, dy \qquad (4.42)$$

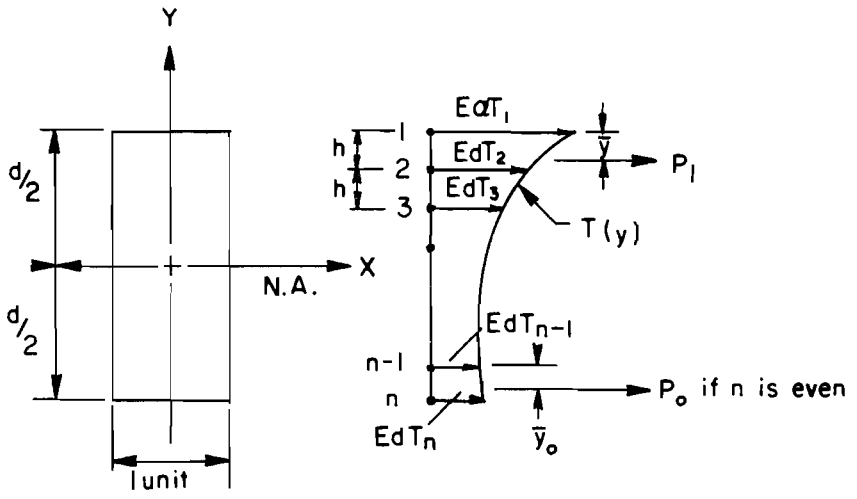

Fig 4.6. One-dimensional model showing the method of calculating temperature forces.

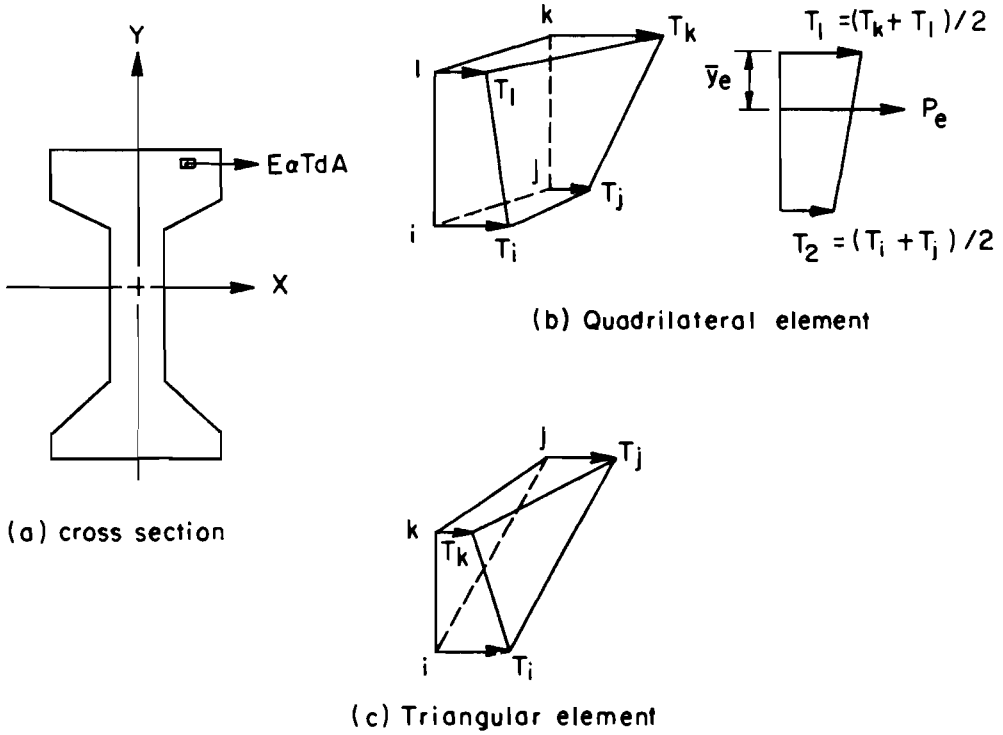

Fig 4.7. Two-dimensional model showing the method of calculating temperature forces.

and $$M^{x}_{eq} = \int_{-d/2}^{d/2} E\alpha\, T(y)\, y\, dy \tag{4.43}$$

The close form of integral calculus cannot be used directly since the shape of the temperature distribution is not available. As temperatures are predicted only at nodal points, the numerical integration procedure employing Simpson's and trapezoidal rule are used. By fitting a parabola through three successive points, the force and the location of the centroid under this parabolic temperature distribution are

$$P_i = E\alpha \frac{h}{3}(T_{2i-1} + 4T_{2i} + T_{2i+1}) \tag{4.44}$$

and $$\bar{y}_i = \frac{h(4T_{2i} + 2T_{2i+1})}{(T_{2i-1} + 4T_{2i} + T_{2i+1})} \tag{4.45}$$

On the other hand, if the temperature is assumed to be linear over two successive points, the following is obtained

$$P_o = \frac{E\alpha h}{2}(T_{n-1} + T_n) \tag{4.46}$$

$$\bar{y}_o = \frac{h(2T_n + T_{n-1})}{3(T_n + T_{n-1})} \tag{4.47}$$

Finally, Eqs 4.42 and 4.43 are written numerically as if n is odd

$$P_{eq} = \sum_{i=1}^{(n-1)/2} P_i \tag{4.48}$$

$$M^{x}_{eq} = \sum_{i=1}^{(n-1)/2} P_i \left[\frac{d}{2} - \left\{\bar{y}_i + (i-1)\,2h\right\}\right] \tag{4.49}$$

if n is even

$$P_{eq} = \sum_{i=1}^{(n-2)/2} P_i + P_o \tag{4.50}$$

and $$M^x_{eq} = \sum_{i=1}^{(n-2)/2} P_i \left[\frac{d}{2} - \left\{ \bar{y}_i + (i-1)\, 2h \right\} \right] - P_o \left\{ \frac{d}{2} - (h - \bar{y}_o) \right\} \tag{4.51}$$

Temperature induced stress at a point having distance y from the neutral axis is, therefore,

$$\sigma_i = \frac{P_{eq}}{d} + 12 \frac{M^x_{eq}\, y_i}{d^3} - E \alpha T_i \tag{4.52}$$

4.3.2 Thermal Stress Analysis using the Two-Dimensional Temperature Distribution Model

The prediction of temperature distribution using this mathematical model was discussed in section 4.2.2. In determining temperature induced stresses, equivalent end force and moments are computed numerically. For a linear temperature distribution over the element, Fig 4.7, the equivalent end force of element e is

$$P_e = A_e E_e \alpha_e T_{av} \tag{4.53}$$

where $T_{av} = \frac{1}{4} (T_i + T_j + T_k + T_\ell)$ for a quadrilateral

and $T_{av} = \frac{1}{3} (T_i + T_j + T_k)$ for a triangle.

A_e, E_e and α_e are the area, modulus of elasticity and coefficient of thermal expansion of element e respectively. If y_e and x_e denote the distance from the location of force P_e to the principal x-axis and y-axis respectively, the equivalent end moments of element e are given by

$$M^x_e = P_e y_e \; ; \quad M^y_e = P_e x_e \tag{4.54}$$

If the bridge section is divided into n number of elements, the total equivalent force and moments will be, respectively,

$$P_{eq} = \sum_{e=1}^{n} P_e \quad ; \quad M_{eq}^{x} = \sum_{e=1}^{n} P_e y_e \quad ; \quad M_{eq}^{y} = \sum_{e=1}^{n} P_e x_e \tag{4.55}$$

Finally, temperature induced stress at point i having coordinate (x_i, y_i) is

$$\sigma_i = \frac{P_{eq}}{A} + \frac{y_i}{I_x} M_{eq}^{x} + \frac{x_i}{I_y} M_{eq}^{y} - E_i \alpha_i T_i \tag{4.56}$$

4.3.3 Applications of the Method to Different Types of Bridge Geometry

It is important to note that the foregoing discussion is applicable only when the structural deformations, flexural and axial displacements, caused by equivalent forces are permitted to take place freely. When the boundary conditions are such that these deformations are prevented, additional stresses associated with the restraining forces must be considered.

A simply supported bridge is shown in Fig 4.8a. The thermal stress distribution at a section which is far away from the ends, under free movement condition, can be obtained directly by using Eq 4.41. However, if the bridge is supported on friction bearings, free movement is now prevented and friction forces are developed. Stresses caused by these friction forces must then be superimposed to the above stresses to yield the final stresses. Similarly, in the case of a continuous bridge, Fig 4.8b, the free vertical displacement is not allowed. Thermal induced stresses at section 1-1, however, can be calculated by substituting M_{1-1} for M_{eq} in Eq 4.52. Another example is when the bridge has varying thicknesses along the length, Fig 4.8c. In this case, the bridge is first divided into a number of prismatic beam members. It can be seen that the method approximates the geometry of the bridge in the region of the varying thickness. For each beam element the equivalent forces are computed. At nodal points where adjacent elements have different

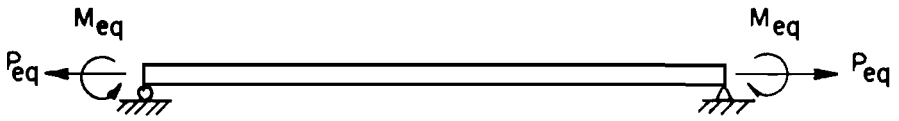

(a) One-span bridge

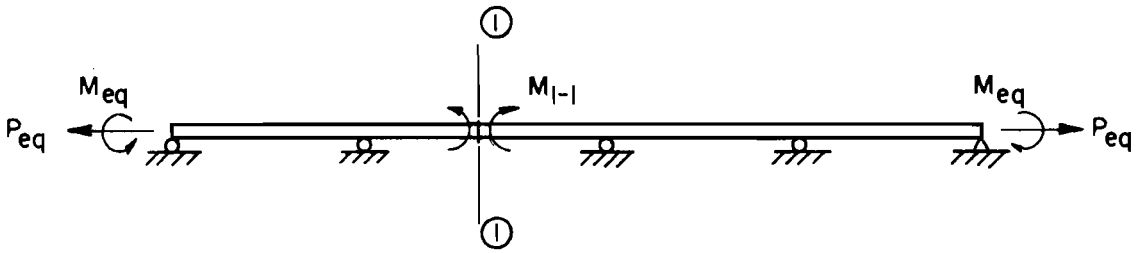

(b) Four-span bridge

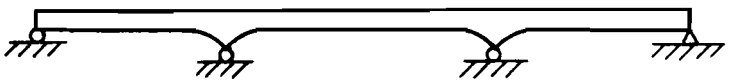

(c) Non-prismatic three-span bridge

Fig 4.8. Elevation views of highway bridges.

thicknesses, there will be unbalanced forces and moments. Stresses caused by equivalent forces can then be obtained by using the stiffness method. Final stresses are then computed using Eq 4.41.

CHAPTER 5. VERIFICATIONS OF THE MATHEMATICAL MODELS

5.1 Introduction

The purpose of this chapter is to correlate existing measured bridge temperature distributions with the results computed from theoretical considerations developed in Chapter 4. Both one- and two-dimensional heat transfer models will be verified to validate the method used. Although the analyses involved approximations of the bridge cross-section, and the lack of actual information on the material properties, the agreement in the gross trends and the orders of magnitude is considered to be satisfactory. Two types of highway bridge as shown in Fig 5.1 and Fig 5.4 were used for this purpose.

5.2 Temperature Prediction by the One-Dimensional Model

The selected bridge was a three-span concrete slab structure located in Houston, Texas. The slab thickness varies from 17 inches to a maximum of 34 inches at the central support. Partial plan and elevation views of the bridge are shown in Fig 5.1. A field test was performed on 24 August 1974. The solar radiation intensity, ambient air temperature and wind speed were recorded. Surface temperatures were also measured at selected points. The locations of the points are depicted in Fig 5.1. Details of the field test can be found in Ref 49.

The test day was considered to be partly clear and partly cloudy. As is shown in Fig 5.2, the variation of the measured solar radiation intensity experienced a great deal of fluctuations. Although the maximum value is approximately 90 percent of the maximum intensity recorded on a clear day, the daily total radiation is only about 50 percent of that for a clear day. The distribution of the measured air temperature is also shown in Fig 5.2. The range of the temperature from the minimum to the maximum value was observed to be only 10°F. The field test was terminated at approximately 4:30 p.m. due to a heavy rain.

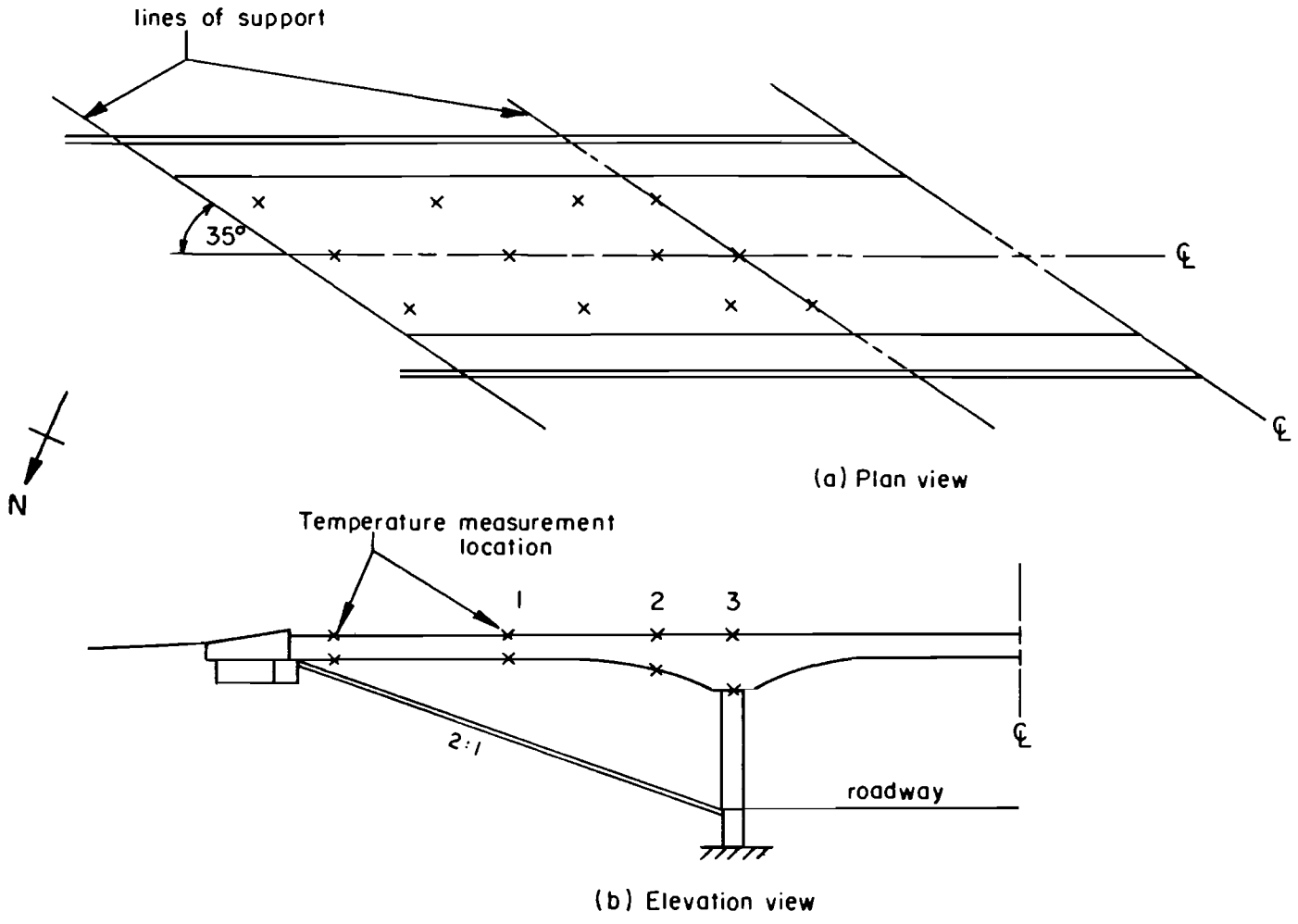

Fig 5.1. Three-span post-tensioned concrete slab bridge.

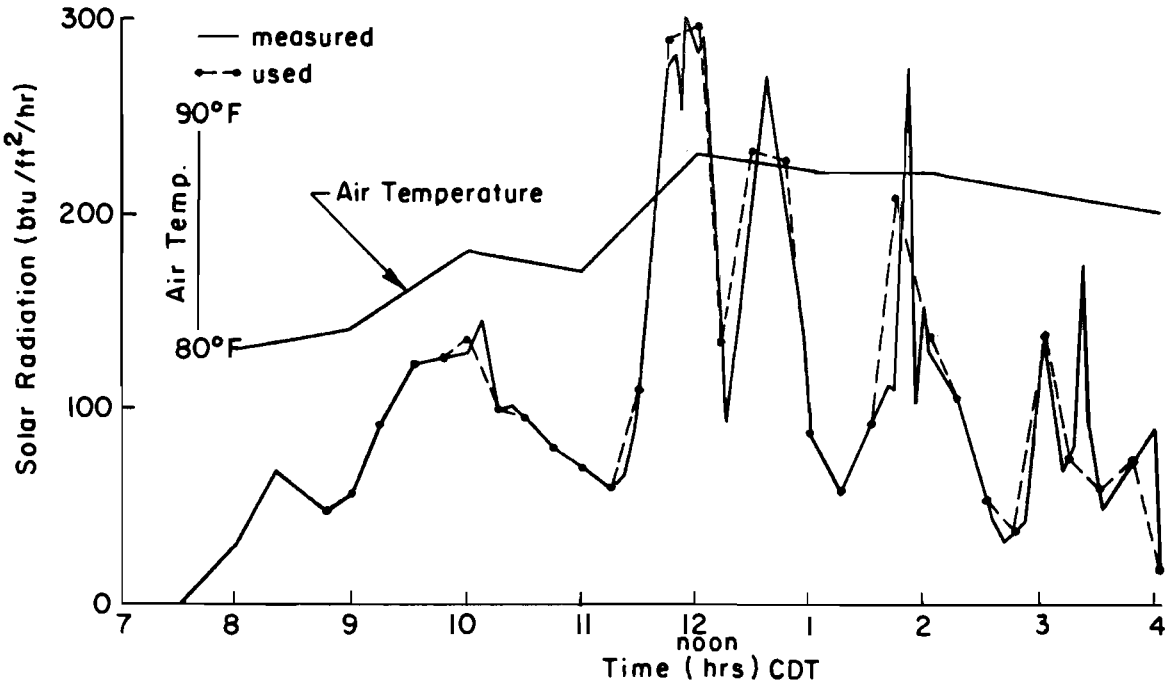

Fig 5.2. Measured air temperature and solar radiation intensity.

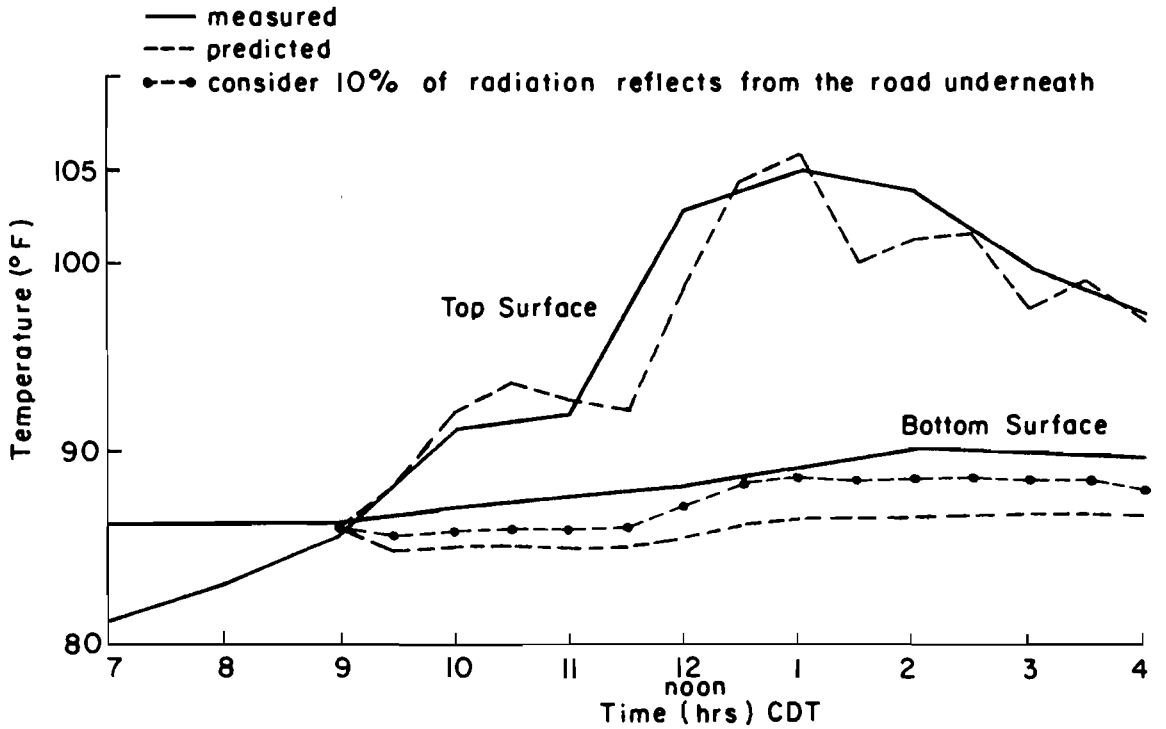

Fig 5.3. Measured and predicted surface temperatures.

Variations of the measured surface temperatures are depicted in Fig 5.3. The average top surface temperature at any particular time was used since the maximum temperature difference measured was approximately 2°F. This was also true at the bottom surface of the bridge.

To predict mathematically the temperature distributions throughout the bridge deck, the starting condition, i.e., the reference time and the initial temperature distribution must be known. As there was no experimental information concerning the temperature variation inside the slab, the reference time was assumed to take place at the time when the top and the bottom surface temperatures reached the same value. Thus, from Fig 5.3, the starting time at 9:00 a.m. was used with the initial uniform temperature distribution 86°F.

In the analysis, a time increment of 15 minutes was selected. Solar radiation intensities at the 15 minute intervals were extracted from the measured values as shown in Fig 5.2 in such a way that the areas under extracted and measured curves were approximately the same. Since no information was available on the thermal properties of the concrete for the test bridge, the material properties were assumed to be at their typical values. Table 5.1 gives the average values of concrete thermal properties and pertinent data used in the analysis.

TABLE 5.1 Average Values of Concrete Thermal Properties and Pertinent Data

Solar radiation intensity	Fig 5.2
Air temperature	Fig 5.2
Wind speed	10 mph
Initial uniform temperature	86 °F
Absorptivity of surface to solar radiation	0.5
Emissivity	0.9
Density	150 lb/ft^3
Thermal conductivity	0.81 btu/ft/hr/°F
Specific heat	0.23 btu/lb/°F

Three different slab thicknesses, i.e., 17 inches, 25.5 inches and 34 inches at sections 1, 2 and 3 respectively, Fig 5.1b, were considered in the analysis. In each case, however, the temperatures computed at the surfaces were identical. The predicted top and bottom surface temperatures are shown in Fig 5.3. The comparison between measured and predicted top surface temperatures was found to be satisfactory. However, there was a greater discrepancy at the bottom surface of the bridge which has been attributed to the fact that the sun's rays reflected from the roadway underneath were neglected in the analysis. Since the orientation of the bridge is not in the east-west direction, the bottom surface receives a portion of the solar radiation intensity thus influencing its temperature. Subsequently an additional analysis was made by assuming that the bottom surface absorbed 10 percent of the measured solar radiation intensity. The results of this analysis are also shown in Fig 5.3. It should be noted that the above assumption, which is felt to be reasonable, results in a better agreement with the measured temperatures.

The above comparison of measured and predicted temperature variations, although limited to the surfaces of the bridge, provide positive evidence that actual bridge temperature distributions over the depth under daily environmental changes can be predicted in a satisfactory way. In the next example, where more extensive data from field measurements were available, comparisons of temperature distributions throughout the depth during a summer day and a winter night will be given. Comparison of vertical thermal deflections during the summer day will also be illustrated.

5.3 Temperature Prediction by the Two-Dimensional Model

The selected bridge was a simply supported structure with a span of 46 feet. Its cross-section consisted of 14 pan-type reinforced concrete beams. A partial cross-section including the edge beam and typical interior beams of the bridge is shown in Fig 5.4. The bridge is located in San Antonio, Texas.

The bridge was field tested under temperature effects by Wah and Kirksey (48). A total of 390 thermocouples was instrumented in the bridge to record

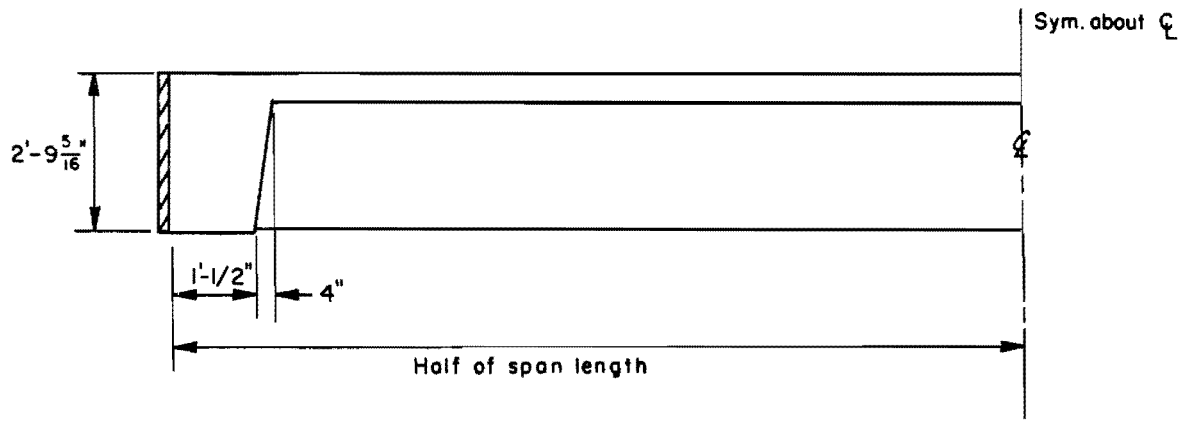

a) Half girder section at center roadway.

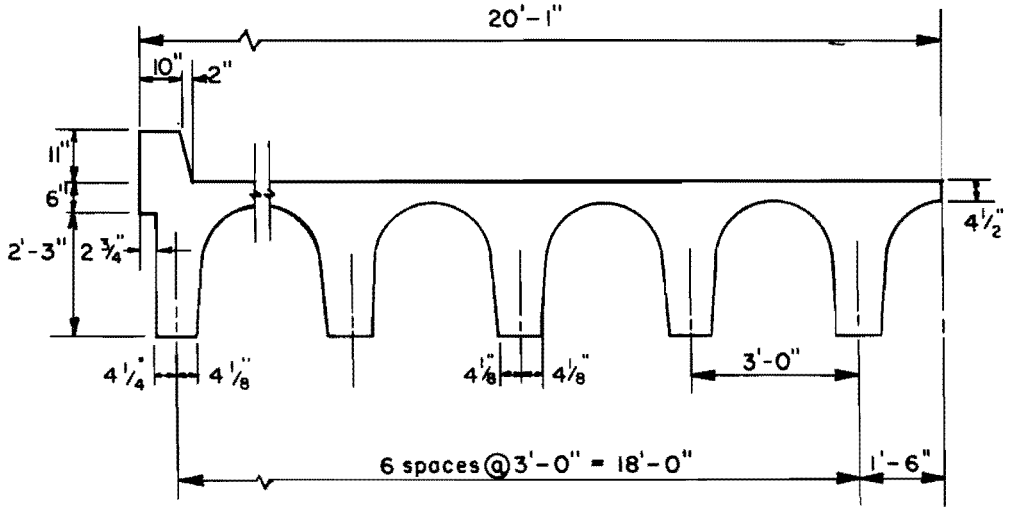

b) Typical transverse section.

Fig 5.4. 40'-0" concrete slab and girder bridge.

temperature. Thirteen thermocouples, six in the slab portion and the remaining seven in the beam portion, were used to measure temperatures over the depth. The location of thermocouples in one typical beam is shown in Fig 5.5a. Tests were made on August 8 and 9, 1967 and on December 11, 1967. Surrounding air temperatures, sky condition and concrete temperatures were recorded at 1-1/2 hour intervals. Details of these field measurements are described in Ref 48.

The finite element mesh of a typical beam section is depicted in Fig 5.5b. Three element layers were used over the slab thickness while two layers were used across the half-width of the beam. Triangular as well as quadrilateral elements were used in this idealization.

5.3.1 Temperature Prediction on August 8, 1967

August is usually considered as the hottest summer month. On August 8, 1967, a field test was performed from 6:00 a.m. to 8:00 p.m. (48). Table 5.2 gives the ambient air temperatures and a brief description of weather conditions during the test period. The solar radiation intensity received on a horizontal surface, on the other hand, was obtained from the U.S. Weather Bureau Reports (14).

From the study of temperature logs given in Ref 48, it was apparent that the bridge temperature distribution was almost uniform at 9:30 a.m. Hence, for simplicity of input data, it was assumed that the starting time is at 9:30 a.m. and the temperature is uniform over the cross section at 89°F, Fig 5.6a. Wind speed, recorded as light wind, was assumed to be constant at 10 mph for every time increment. This amount of wind speed is usually considered as the average value for a normal day. Air temperatures used in the analysis were the average values of the measured top and bottom ambient temperatures given in Table 5.2. Two values of daily total insolation intensity, i.e., 100 and 80 percent of the value obtained from Ref 14 were used in computing the bridge temperatures. The 20 percent reduction was considered to examine the influence of the solar radiation intensity on the temperature variations since no actual information of the insolation intensity was available at the bridge site. The effect of humidity, elevation above sea level and atmospheric contamination in the industrial area is known to lower the solar radiation intensity by about 20 percent (42).

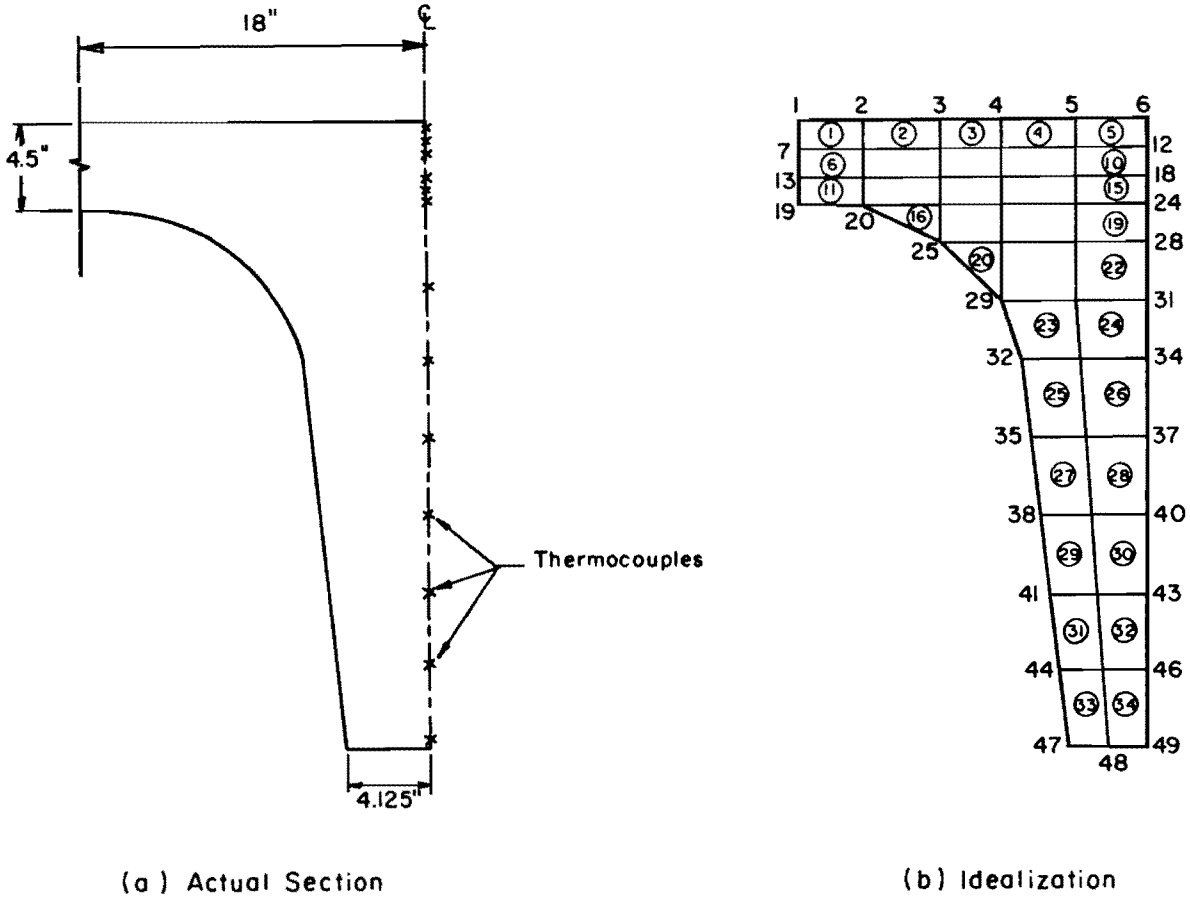

(a) Actual Section

(b) Idealization

Fig 5.5. Bridge section and idealization.

TABLE 5.2 Field Test on August 8, 1967 (Ref 48)

Time	Ambient Temp (B)*	Ambient Temp (T)*	Remarks
0600			Power turned on for instrument warm-up
0630	78°F	78°F	Clear sky - Light wind
0800	79°F	80°F	" "
0930	80°F	82°F	" "
1100	86°F	91°F	" "
1230	90°F	95°F	" "
1400	95°F	100°F	" "
1530	97°F	97°F	" "
1700	99°F	103°F	" "
1830	98°F	104°F	" "
2000	94°F	97°F	" "

*Ambient Temp (B) - Temperature taken with a mercury bulb four inches from the ground in the shade under the bridge.

Ambient Temp (T) - Temperature taken with a thermocouple one inch above the surface of the bridge.

Table 5.3 gives the average concrete thermal properties and relevant data used to perform the analysis.

TABLE 5.3 Relevant Data for Thermal Analysis on August 8, 1967

Daily total solar radiation intensity (100%)	2380 btu/ft^2
Wind speed	10 mph
Initial uniform temperature	89°F
Absorptivity of surface to solar radiation	0.5
Emissivity	0.9
Density	150 lb/ft^3
Thermal conductivity	0.81 btu/ft/hr/°F
Specific heat	0.23 btu/lb/°F
Modulus of elasticity of concrete	3.79×10^6 lb/in^2
Coefficient of thermal expansion	6×10^{-6} in/in/°F
Time increment	1.5 hr

Plots of predicted and measured temperature distributions at 1-1/2 hour intervals are shown in Fig 5.6. Comparisons of temperature distributions are shown to be satisfactory. Good correlations are obtained at all time increments with the use of 80 percent of the solar radiation intensity in the analysis. At 8:00 p.m., however, disagreement was observed which has been attributed to the inaccurate wind speed information and the time of sunset.

It is also of interest at this point to mention the necessity of the two-dimensional heat transfer model. The temperature distribution over the cross section has been found to vary nonlinearly in both vertical and horizontal directions. This is due to the fact that the temperature in the beam is a result of the heat conducting from the top surface and that of the surrounding air temperature exposed to the exterior surfaces of the beam. The distribution of temperature over the depth computed from the one-dimensional heat flow model is depicted in Fig 5.6h for comparison. It can be seen that an erratic magnitude of temperature was calculated when the one-dimensional code was used.

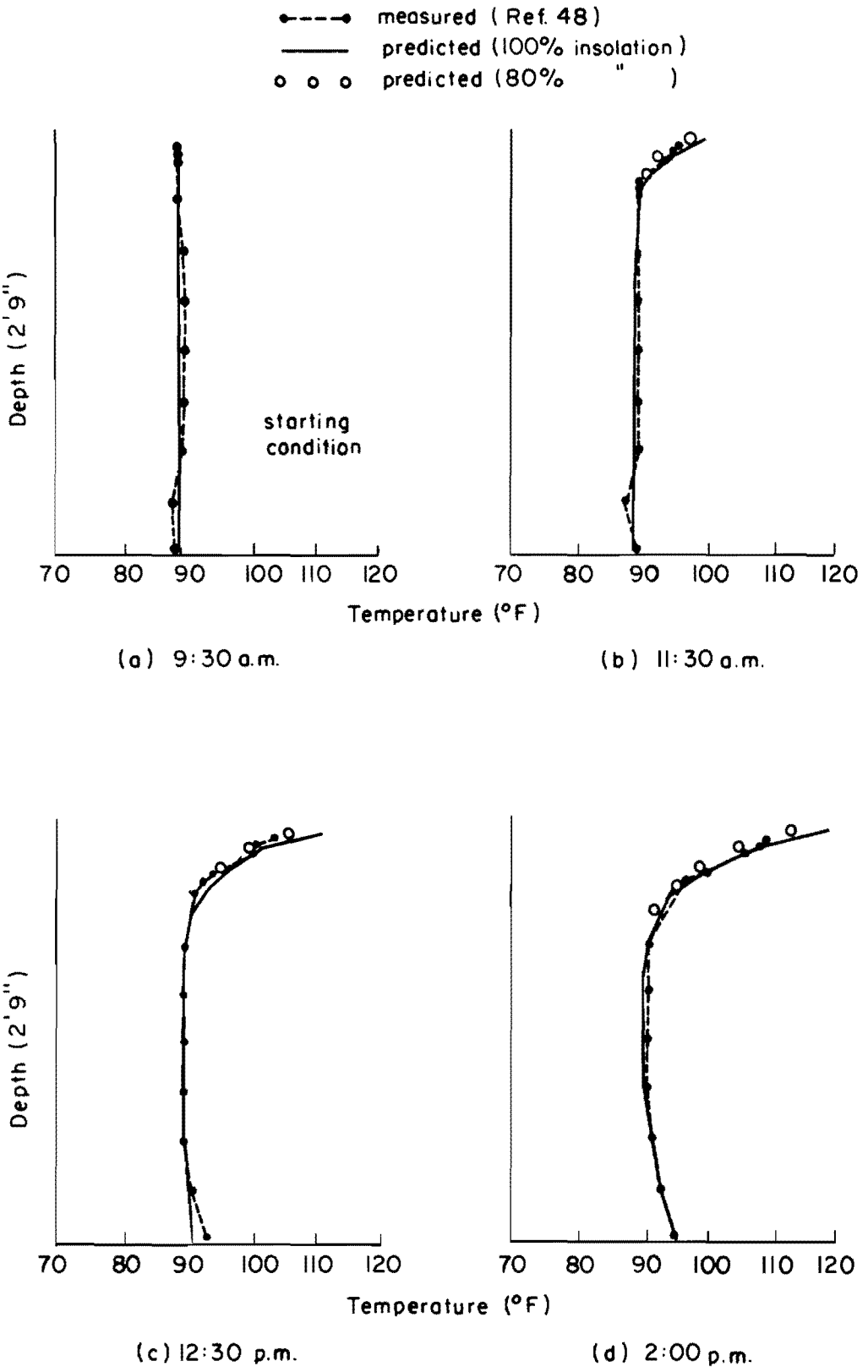

Fig 5.6. Temperature distributions at the center of the section (Aug.8,1967).

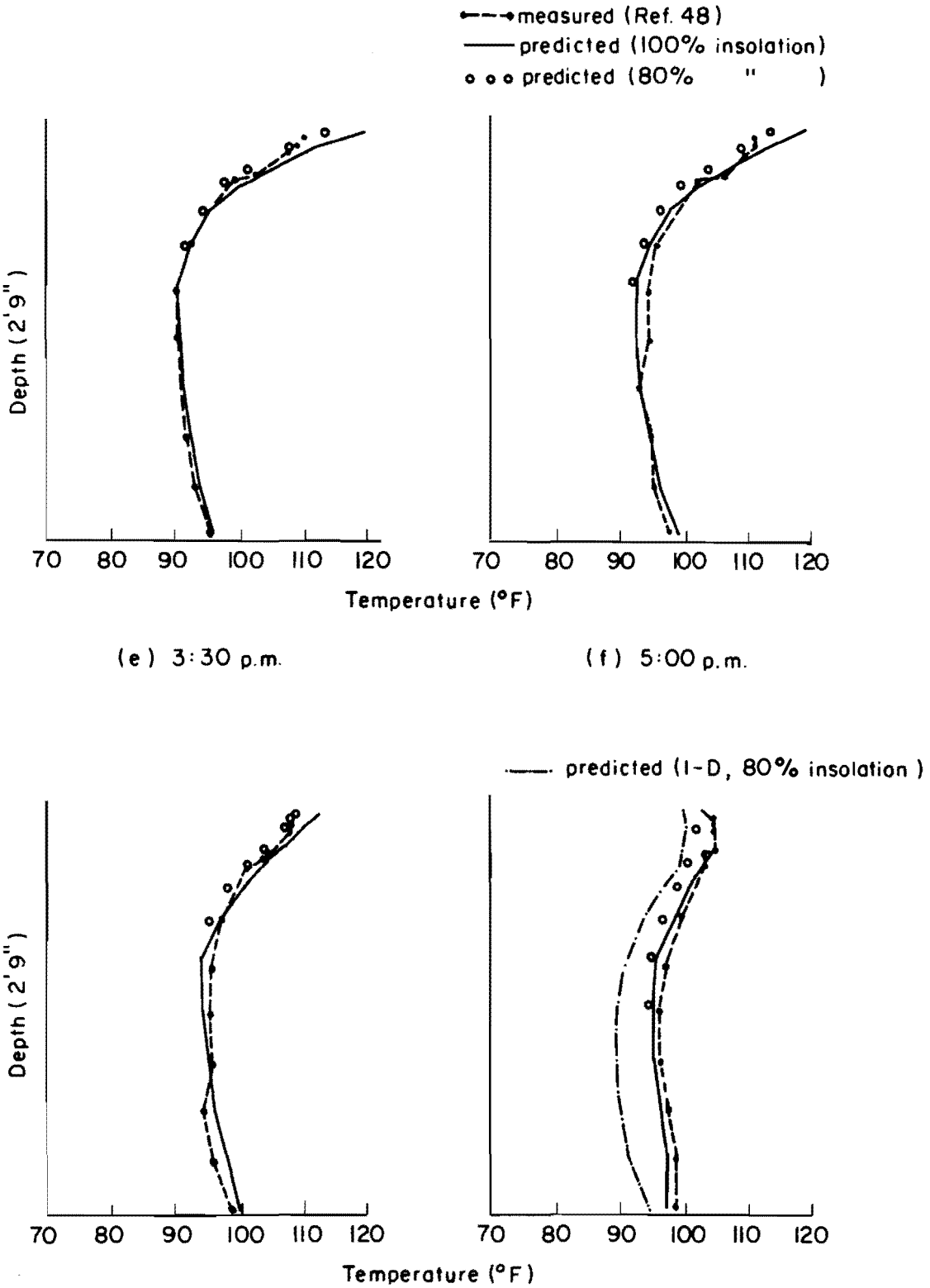

Fig 5.6. Continued.

Deflection at the mid-span of the bridge caused by temperature differentials was also measured at 1-1/2 hour intervals. Predicted deflections were obtained by the method described in Chapter 4. Comparisons between the measured and predicted deflections are depicted in Fig 5.7. No theoretical results from Ref 48 were available for this comparison. The bridge deflects upward because the top surface is warmer than the bottom surface. Although the correlation is not as good as in the temperature distribution case, shapes of deflection have basically the same trend. Both predicted and measured deflection have approximately the same orders of magnitude. It is worth noting that the computed deflections are, theoretically, independent of the modulus of elasticity of the concrete. Thus, the discrepancy of results in Fig 5.7 is believed to be due to the deviation of the actual boundary conditions from the theoretical one and the limited one-dimensional response of the bridge which was assumed in the analysis.

Temperature induced stresses were also computed by the author based on the one-dimensional elastic beam theory, since the bridge under consideration has no complicating factors such as skew or irregularities of beam spacing. Predicted stress distributions over the beam depth are depicted in Fig 5.8a. It should be pointed out that the temperature induced stresses in this case are due only to the nonlinearity of the temperature. Compressive stresses are found at the top and bottom regions while tensile stresses are found in the vicinity of the neutral axis of the beam with a maximum value of 182 psi.

5.3.2 Temperature Prediction on December 11, 1967

During the winter, tests were performed on 10 December 1967 at 5:00 a.m. and continued until 3:00 p.m. of the next day. Table 5.4 gives ambient air temperatures and a brief description of the weather conditions during the field measurements. The initial condition was selected in the same manner as described earlier, thus the starting time at 9:00 p.m. was used with the initial uniform temperature distribution 43°F, Fig 5.9a. Table 5.5 gives the data which was used in the analysis.

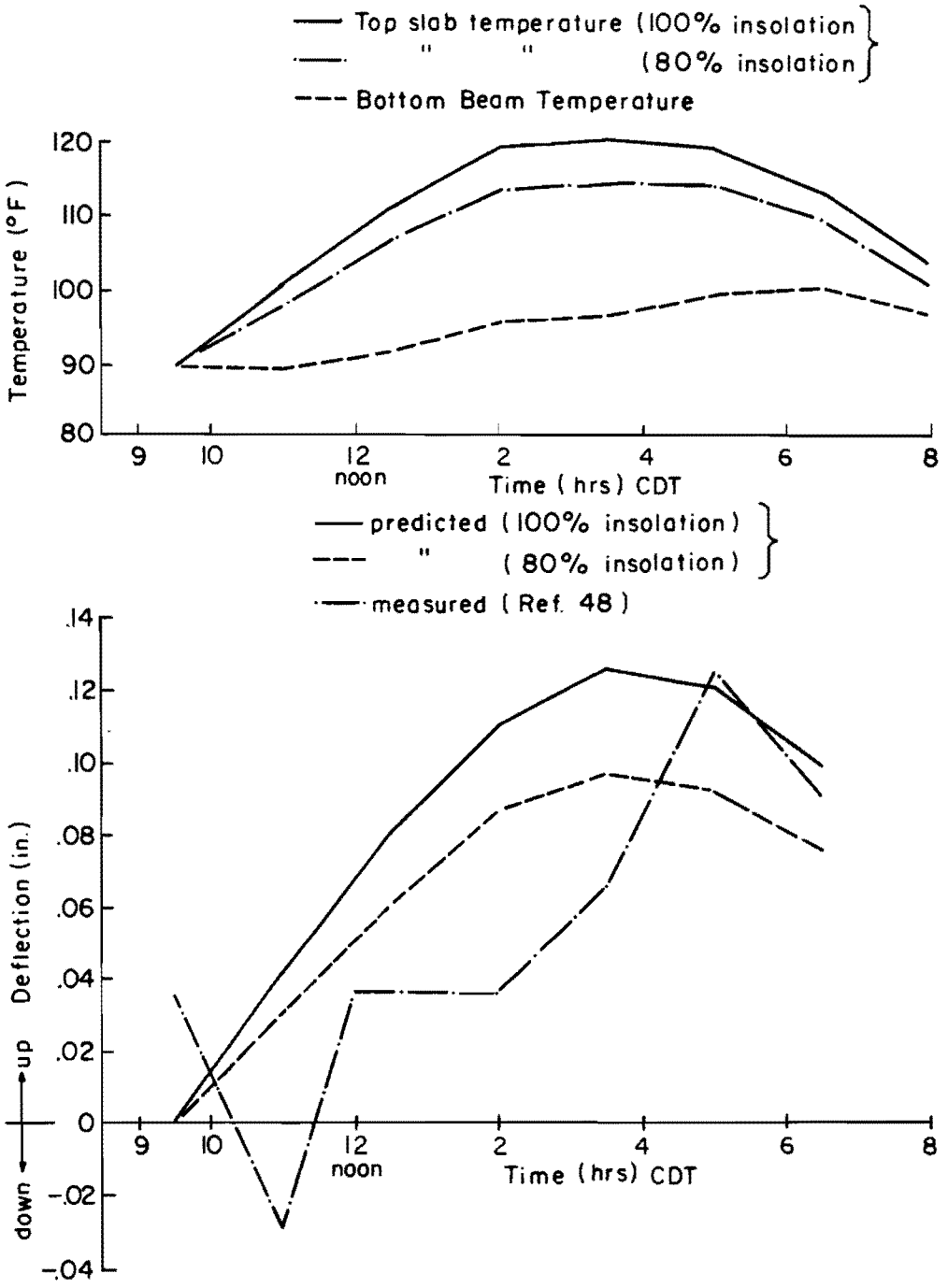

Fig 5.7. Temperatures and vertical deflection vs. time (Aug.8,1967).

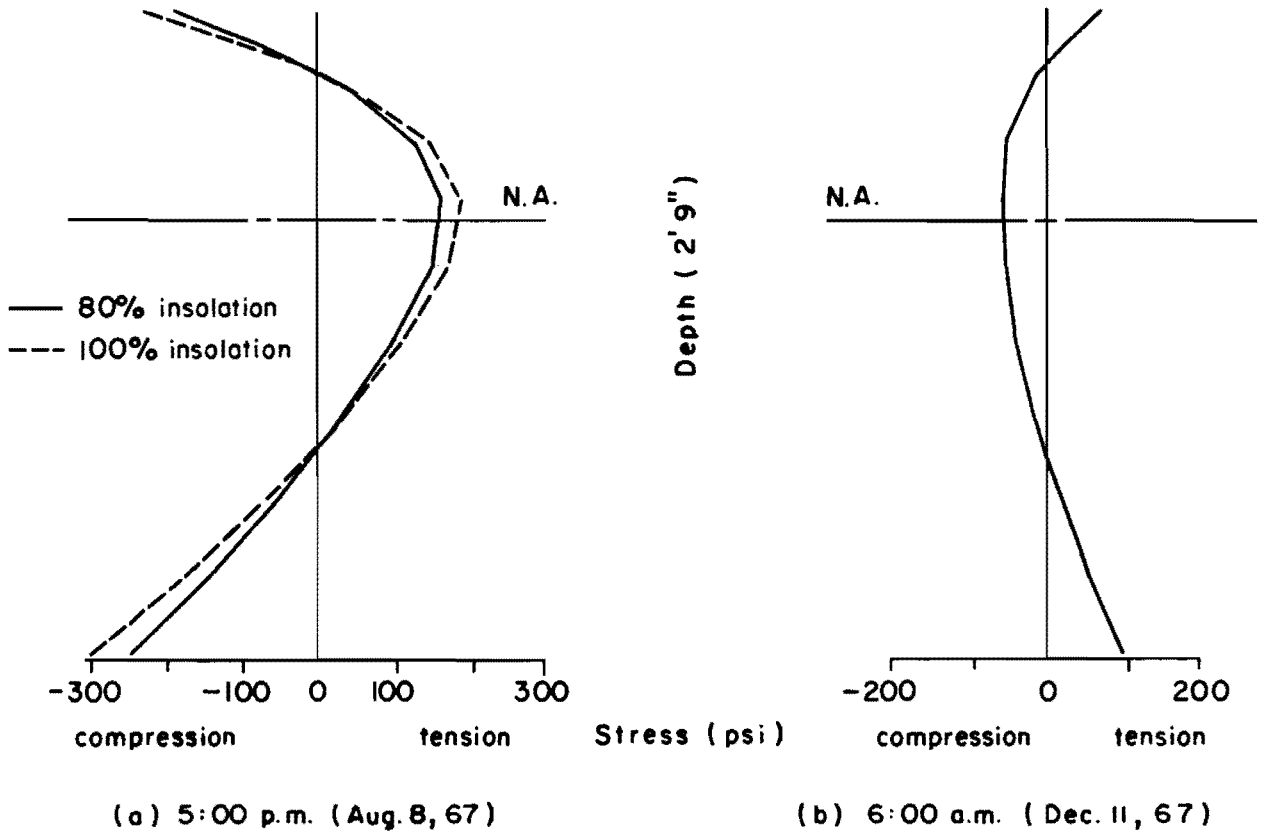

Fig 5.8. Temperature induced stresses.

TABLE 5.4 Field Test on December 10-11, 1967 (Ref 48)

Time	Ambient Temp (B)*	Ambient Temp (T)*	Remarks
1700			Power turned on for instrument warm-up.
1730	41°F	40°F	Overcast - Low Clouds - Light Wind
1900	41°F	40°F	Overcast - Low Clouds - Light Wind - Light Rain
2100	44°F	43°F	Overcast - Low Clouds - Light Wind
2230	41°F	40°F	Clear - Still
2400	39°F	37°F	" "
0130	38°F	36°F	" "
0300	41°F	39°F	Clear - Light Wind
0430	38°F	35°F	" "
0600	36°F	33°F	" "

*See Table 5.2

TABLE 5.5 Data on December 10-11, 1967

Daily total solar radiation intensity (night)	0
Wind speed (still)	0
Initial temperature	43°F
Absorptivity of surface to solar radiation	0.5
Emissivity	0.9
Density	150 lb/ft^3
Thermal conductivity	0.81 btu/ft/hr/°F
Specific heat	0.23 btu/lb/°F
Modulus of elasticity of concrete	3.79×10^6 lb/in^2
Coefficient of thermal expansion	6×10^{-6} in/in/°F
Time increment	1.5 hr

Plots of predicted and measured temperature distributions at 1-1/2 hour intervals are shown in Fig 5.9 and again good correlations are obtained. It should be pointed out that in this analysis the wind speed is not a sensitive parameter since the surface and the surrounding air temperature at all time increments are approximately the same. Predicted vertical deflection at mid-span of the bridge is depicted in Fig 5.10. The bridge deflected downward since the temperature at the top was cooler than the bottom surface. Thermal induced stress distribution at 6:00 a.m. is shown in Fig 5.8b. Maximum tensile stress of 100 psi is observed at the bottom surface of the beam. This stress will, of course, be additive to the dead and live load stresses, thus increasing the magnitude of the final design stress.

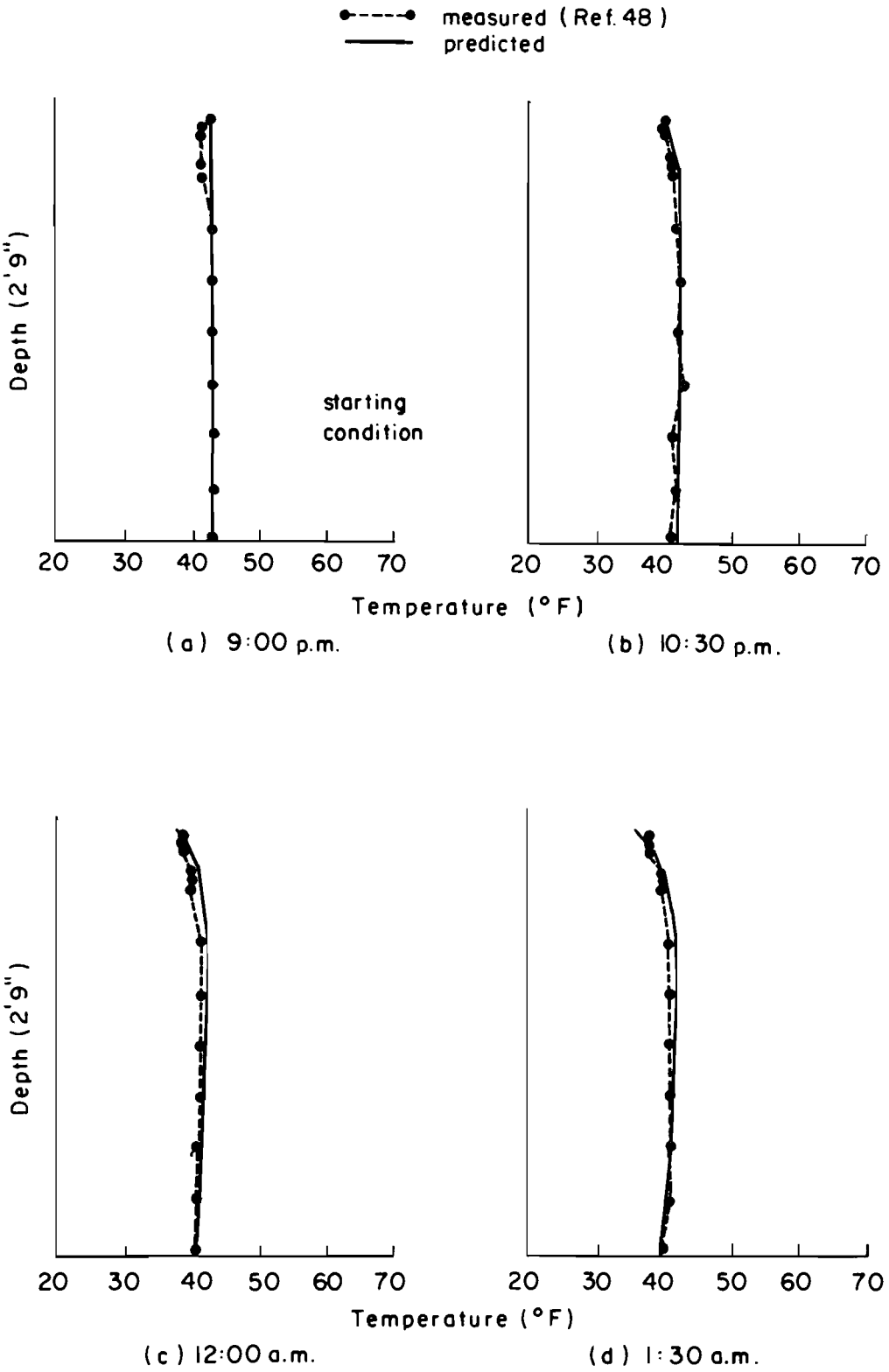

Fig 5.9. Temperature distributions at the center of the section (Dec.11,1967).

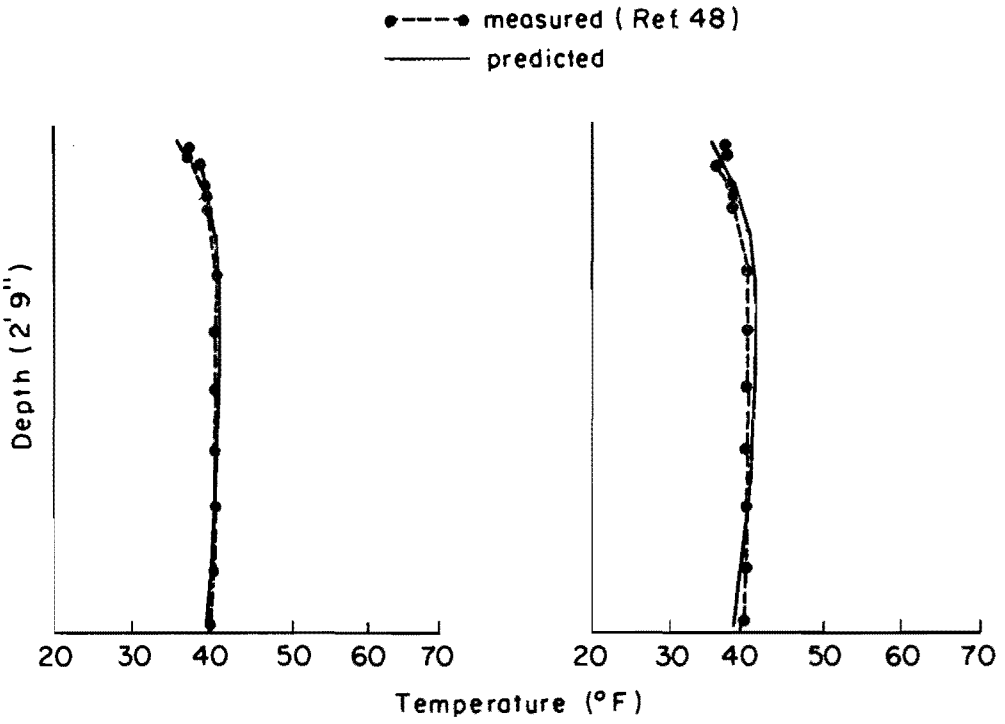

(e) 3:00 a.m. (f) 4:30 a.m.

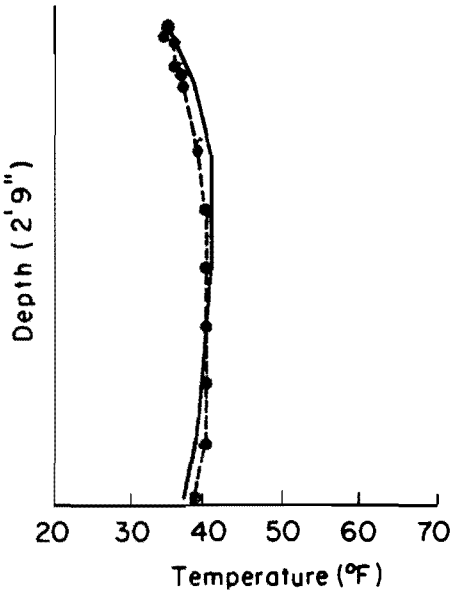

(g) 6:00 a.m.

Fig 5.9. Continued.

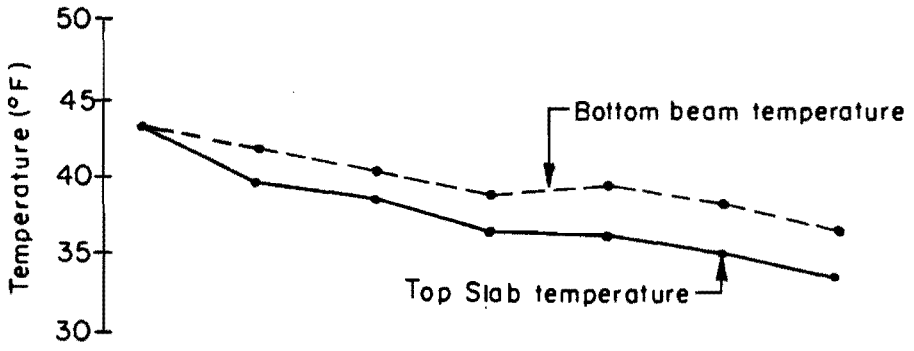

a) Surface temperatures

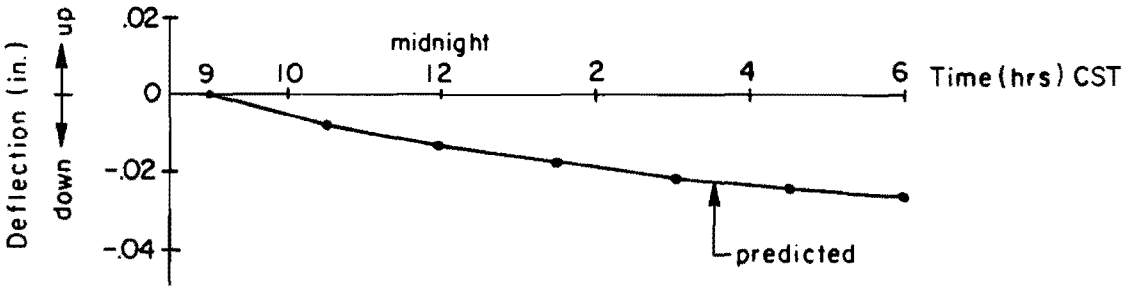

b) Bridge deflection

Fig 5.10. Temperatures and vertical deflection vs. time (Dec.11,1967).

CHAPTER 6. THERMAL EFFECTS IN PRESTRESSED CONCRETE SLAB BRIDGE

6.1 Introduction

In this chapter, the one-dimensional mathematical model developed in Chapter 4 will be used to study temperature effects in a prestressed concrete slab bridge. Temperatures predicted by this model have been shown to compare satisfactorily with experimental results. The following study will be limited to daily climatic variations which are representative of Austin, Texas. The calculations refer specifically to conditions which will give rise to a large temperature gradient and corresponding high thermally induced stresses. These conditions take place on a clear night followed by a clear day with a large range of ambient air temperature. On a clear day, the amount of the solar radiation intensity absorbed by the top surface is a maximum, thereby causing a large temperature gradient over the bridge depth. Maximum outgoing radiation, on the other hand, takes place during a clear night, thus producing a large reverse temperature gradient.

Studies are performed for both summer and winter conditions. Parameters affecting bridge thermal behaviors such as material thermal properties, depth, indeterminacy of the structure, span ratio and variable thickness are also considered. The solar radiation intensities and the air temperature were obtained from the U.S. Weather Bureau records (14) and newspapers.

6.2 Temperature Effects in a Prismatic Concrete Slab Bridge

Although the geometry of the bridge under investigation is as shown in Fig 6.1, it is of interest at the present time to consider the bridge to have a uniform thickness of 17 inches. The effect of the prestressing steel on temperature induced stresses is also neglected. However, these parameters will be included in the study in the next section. In view of the bridge cross section which is depicted in Fig 6.1b, it is evident that the temperature will be practically uniform across the width of the bridge

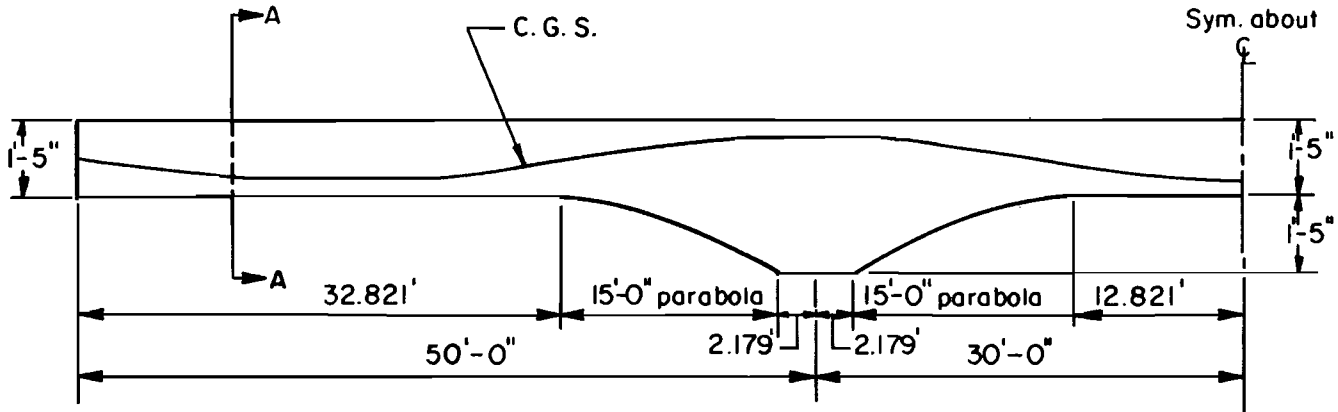

(a) Half slab deck section

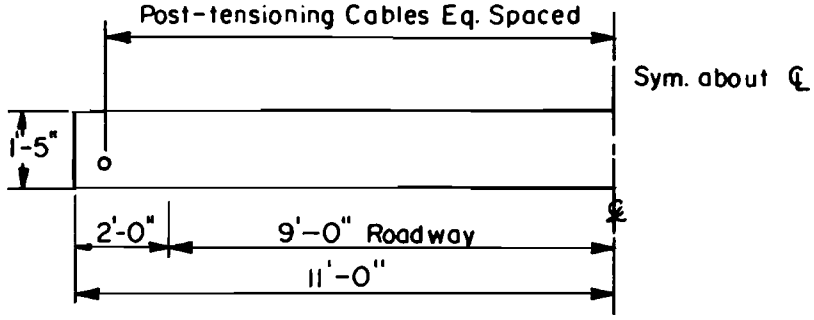

(b) Section A–A

Fig 6.1. 160'-0" continuous concrete slab bridge.

except for the regions near the ends. Consequently, the bridge was analyzed by assuming the temperature to vary one-dimensionally over the depth. Also the bridge was assumed to have orthogonal supports.

6.2.1 Sensitivity Analysis of the Model

The purpose of this study was to detect the significant factors that affect the bridge thermal behaviors subjected to daily environmental changes. In doing so, eight variables were considered: daily total insolation intensity, surface absorptivity, thermal conductivity, specific heat, unit weight, wind speed, thickness and the range of daily air temperature. Weather variables which are representative of August were used. Material thermal properties selected are typical for a normal weight concrete. These values are listed in Table 6.1 for future references.

In the analysis a starting time at 7:00 a.m., which is approximately one hour after sunrise, was used. This selection was made due to past experiences which indicated that temperatures in a bridge would be relatively uniform at or a few hours after sunrise with a value equaling the air temperature at that time. Consequently, an initial uniform temperature distribution of 78°F was used. The analysis was performed for a complete 24 hour period with a time increment of 15 minutes.

Temperature distributions and stresses were calculated, using the data given in Table 6.1. The predicted results are also listed in Table 6.1. By keeping the rest of the variables at their average values, one variable at a time was increased by 10 percent and the temperatures and stresses were computed. A summary of comparisons of the maximum surface temperature and the maximum temperature gradient, etc., is given in Table 6.2. It can be seen that the most significant factor with respect to the material thermal properties is the absorptivity of the surface to the solar radiation. Also of importance is the coefficient of thermal expansion and contraction, since the thermal induced stresses vary linearly with this variable. However, an increase in the thermal conductivity, specific heat and density reduces the temperature gradient and thus decreases the induced stresses.

With respect to the environmental variables, an increase in the solar radiation intensity and the daily air temperature range amplifies the predicted temperature gradient and the temperature induced stresses. An

TABLE 6.1 SELECTED AVERAGE VALUES FOR THE SENSITIVITY ANALYSIS (AUGUST)

Average total insolation intensity	2380	btu/ft^2
Air temperature distribution	Fig 3.2a	
Wind speed	10	mph
Absorptivity of surface to solar radiation	0.5	
Emissivity	0.9	
Thermal conductivity	0.81	btu/ft/hr/°F
Specific heat	0.23	btu/lb/°F
Unit weight	150	lb/ft^3
Depth	17	inches
Modulus of elasticity of concrete	4.25×10^6	lb/in^2
Coefficient of thermal expansion	6.0×10^{-6}	in/in/°F

PREDICTIVE RESULTS (3-equal-span-bridge)

Maximum top surface temperature	120	°F
Maximum temperature gradient	30	°F
Maximum reverse temperature gradient	7	°F
Maximum tensile stress (bottom half)	239	psi
Maximum tensile stress (top)	318	psi
Maximum compressive stress (top)	818	psi
Maximum vertical deflection (downward)	0.125	inch
Maximum mean bridge temperature	35	°F

increase in the wind speed, on the other hand, decreases the computed results. Consequently , the extreme climatic condition is believed to take place on a still day with a maximum value of the solar radiation and a maximum range of daily ambient air temperature.

Comparisons of predicted results using different variations of solar intensity are also given in Table 6.2. By keeping the total insolation in

TABLE 6.2 THE EFFECTS OF A 10% INCREASE IN ONE VARIABLE AT A TIME ON TEMPERATURES AND STRESSES IN A THREE EQUAL SPAN CONCRETE SLAB BRIDGE (AUGUST)

	Temp. (top)	Temp. gradient	Tensile stress	Comp. stress	Reverse gradient	Tensile stress(top)	Vertical deflection	Mean bridge temp.
Average	0%	0%	0%	0%	0%	0%	0%	0%
Insolation	2.5	10	9.2	8.1	0	1.6	9.6	2.9
Absorptivity	2.5	10	9.2	8.1	0	1.6	9.6	2.9
Conductivity	-0.8	-3.3	-0.8	-3.3	0	-2.5	-0.8	0
Specific heat	-0.8	-3.3	-2.9	-0.1	0	-2.5	-2.4	-2.9
Density	-0.8	-3.3	-2.9	-0.1	0	-2.5	-2.4	-2.9
Wind speed	-0.8	-3.3	-2.1	-1.5	0	0	-2.4	0
Thickness	0	0	-0.8	3.3	0	-0.3	-11.2	-5.7
Range of air temperature	1.7	0	2.1	3.1	14.3	4.7	0.8	2.9
Insolation (Eq 3.1)	3.3	13.3	9.2	11.4	0	0.3	10.4	-0.3

a day the same, Eq 3.1, instead of Eq 3.2, was used in the analysis. Two distributions of solar intensity computed from these two equations have been shown in Fig 3.1. It can be seen, from Table 6.2, that larger temperature stresses were predicted when Eq 3.1 was used.

6.2.2 A Study on Initial Conditions

Before the bridge temperature distributions can be predicted the initial condition must be specified. This condition includes the reference time and the initial temperature distribution. A study of a typical daily solar radiation and air temperature variation indicates that the temperature in a bridge will be relatively uniform early in the morning. At about this time, the sun's radiation is small and the air temperature has just passed the minimum value. It should be pointed out that bridges subjected to daily atmospheric variations may not have an exact thermal equilibrium condition, thus it was the purpose of this study to investigate the response of the temperature distributions and stresses caused by different initial conditions.

Computed temperature and stress distributions using different reference times and different initial temperature variation are depicted in Fig 6.2. The initial temperature distribution was assumed to be uniform and equal to the surrounding air temperature at the selected reference time. The analyses were made at 15 minute intervals using the data contained in Table 6.1. It is found that maximum interior tensile stresses occurred at 3:00 p.m. while maximum reverse stresses occurred at 5:00 a.m. From Fig 6.2, it is evident that different starting conditions do not have significant effects on the temperature induced stresses. According to the assumed initial conditions at 7:00 a.m., the following results were observed. At 3:00 p.m., a maximum tensile stress of 239 psi is located at three-fourth's of the bridge depth. At the bottom surface, the tensile stress is much smaller, i.e., 97 psi. A maximum temperature gradient took place at 2:00 p.m. and the corresponding maximum compressive stress is 818 psi at the top fiber of the bridge. At 5:00 a.m., on the other hand, a maximum reverse temperature gradient was calculated with a maximum tensile stress of 318 psi at the top surface, Fig 6.2b.

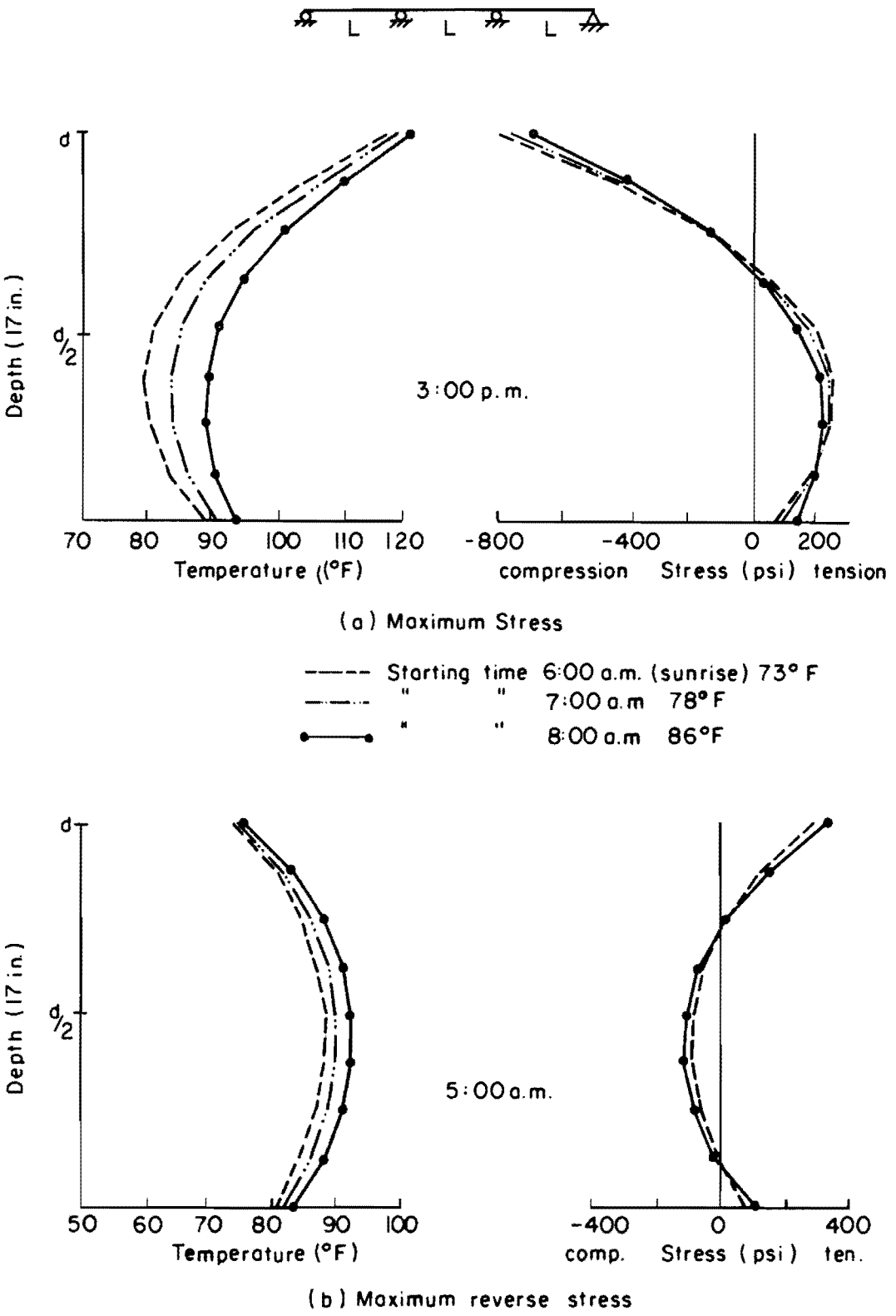

Fig 6.2. Effect of starting conditions on temperature and stress distributions (August).

The above stresses were computed at the center of the middle span. However, it should be pointed out that, in this three-span case, the temperature induced stresses are constant longitudinally in the middle span. In the exterior spans, the stresses reduce linearly such that zero stress is computed at the exterior ends.

The determination of temperature and stresses caused by the same environmental conditions which are repeated over a period of several days is also of interest. In this study, the daily climatic changes as recorded in August and January were considered. Figure 6.3a depicts temperature and stress distributions at 3:00 p.m. in August. On the first day, the thermal equilibrium was assumed to take place at 7:00 a.m. and calculations proceeded for three consecutive days. It can be seen from Fig 6.3a that during the first day additional heat is stored within the bridge, thus decreasing the nonlinearity of the temperature distribution. This gain of heat, however, reduces considerably during the second day and a isothermal condition is observed on the third day. The changes of stress distribution, on the other hand, are found to be relatively small. Stresses computed at the center of the middle span are also shown in Fig 6.3a. According to the above analyses, it is evident that the system will stabilize itself at 8:00 a.m., i.e., if a starting condition at 8:00 a.m. is used the bridge will reach an equilibrium condition with the environment at this time on the next day. This conclusion is clearly illustrated by comparing plots in Fig 6.2a and Fig 6.3a.

Temperature and stress distributions at 7:00 a.m. in January are depicted in Fig 6.3b. The plots shown are those giving the maximum reverse temperature differential and the maximum stresses. The distribution of air temperature used in the analysis is shown in Fig 3.2b. The initial condition was assumed to occur at 8:00 p.m. with a uniform temperature of 65°F. This time was selected since experimental data (20,48) have shown that during the winter period the temperature distribution over the depth is relatively uniform at about this time. It can be seen in Fig 6.3 that changes of temperature between the first and the second day are small and that computed stresses are almost identical. The maximum reverse gradient of 9°F was calculated and a maximum tensile stress of 352 psi was predicted at the top surface.

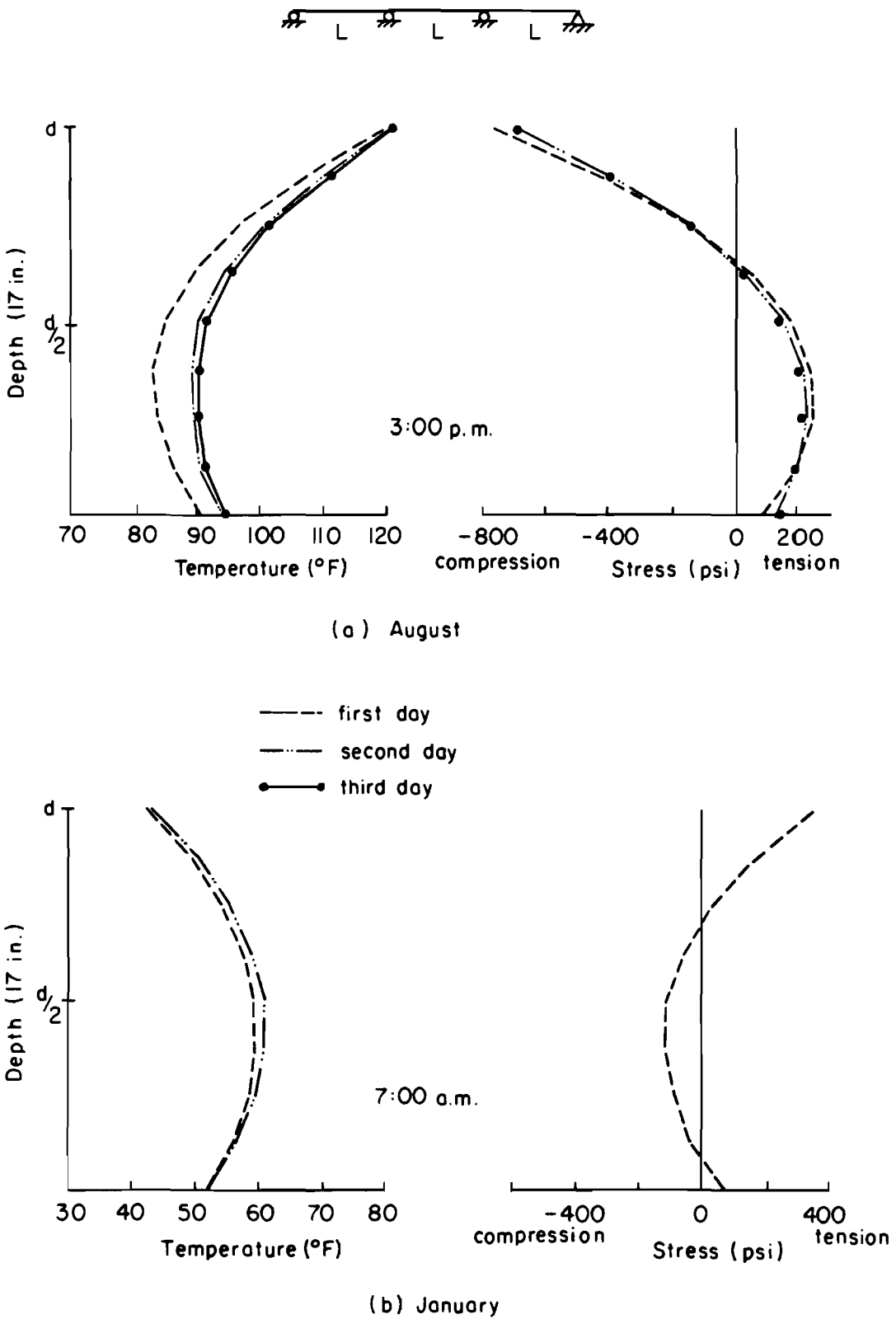

Fig 6.3. Effect of the environmental repetition on temperature and stress distributions.

The above study thus indicates that different starting times have little influence on the induced stresses. In the following investigation the starting time at 7:00 a.m. and 8:00 p.m. will be used for the summer and winter condition respectively.

6.2.3 A Study on Summer Conditions

It has been shown in Section 6.2.1 that large temperature gradients occur during a day with high solar radiation, large air temperature range and no wind. However, although the range of air temperature is found to be maximum in August, Fig 3.2a, a maximum solar radiation intensity is recorded in June, Table 3.1. Therefore, in order to study the bridge thermal behaviors associated with summer daytime conditions, daily climatic changes in June, July and August needed to be investigated.

Temperature and stress distributions calculated at 4:00 p.m. and 5:00 a.m. are depicted in Fig 6.4. The analyses were performed using the starting condition at 7:00 a.m. In addition, a wind speed of 5 mph was used. The stresses were computed at the center of the middle span. It can be seen that the changes of the stress distribution are small. A maximum tensile stress of 270 psi is located at three-fourth's of the depth, Fig 6.4a. At 2:00 p.m., a maximum compressive stress was calculated at the top surface and is 890 psi. Figure 6.4b shows the predicted maximum reverse gradients and the stresses. A maximum tensile stress of approximately 310 psi is found at the top surface.

Therefore, it is evident from this study that the daily environmental variations in August are the extreme summer conditions in Austin, Texas. Plots of predicted top and bottom surface temperatures versus time in August are depicted in Fig 6.5a. A maximum difference of 35°F is found between the top and the bottom temperature at 2:00 p.m. At this time, the top surface is approximately 20°F warmer than the air temperature.

6.2.4 A Study on Winter Conditions

In contrast to the summer conditions, large reverse temperature gradients occur during a still night with a maximum amount of outgoing radiation and a large range of air temperature. In view of these factors,

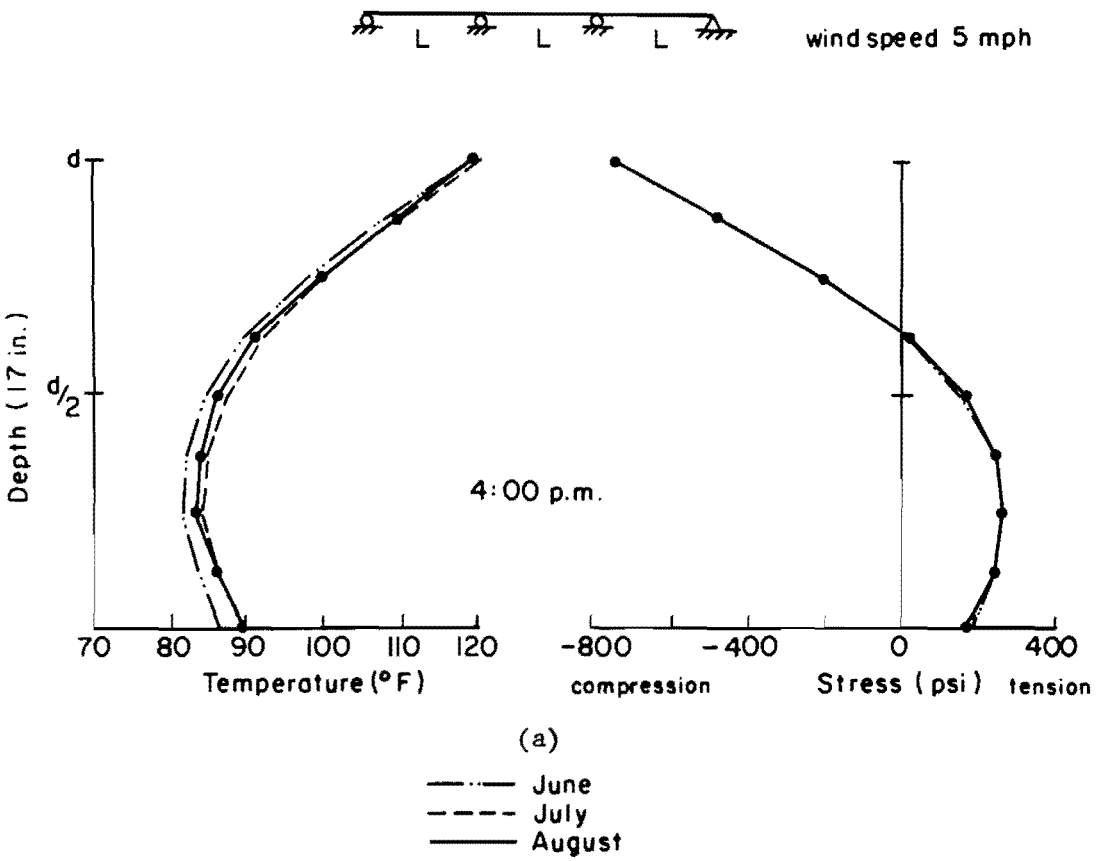

Fig 6.4. Temperature and stress distributions (summer conditions).

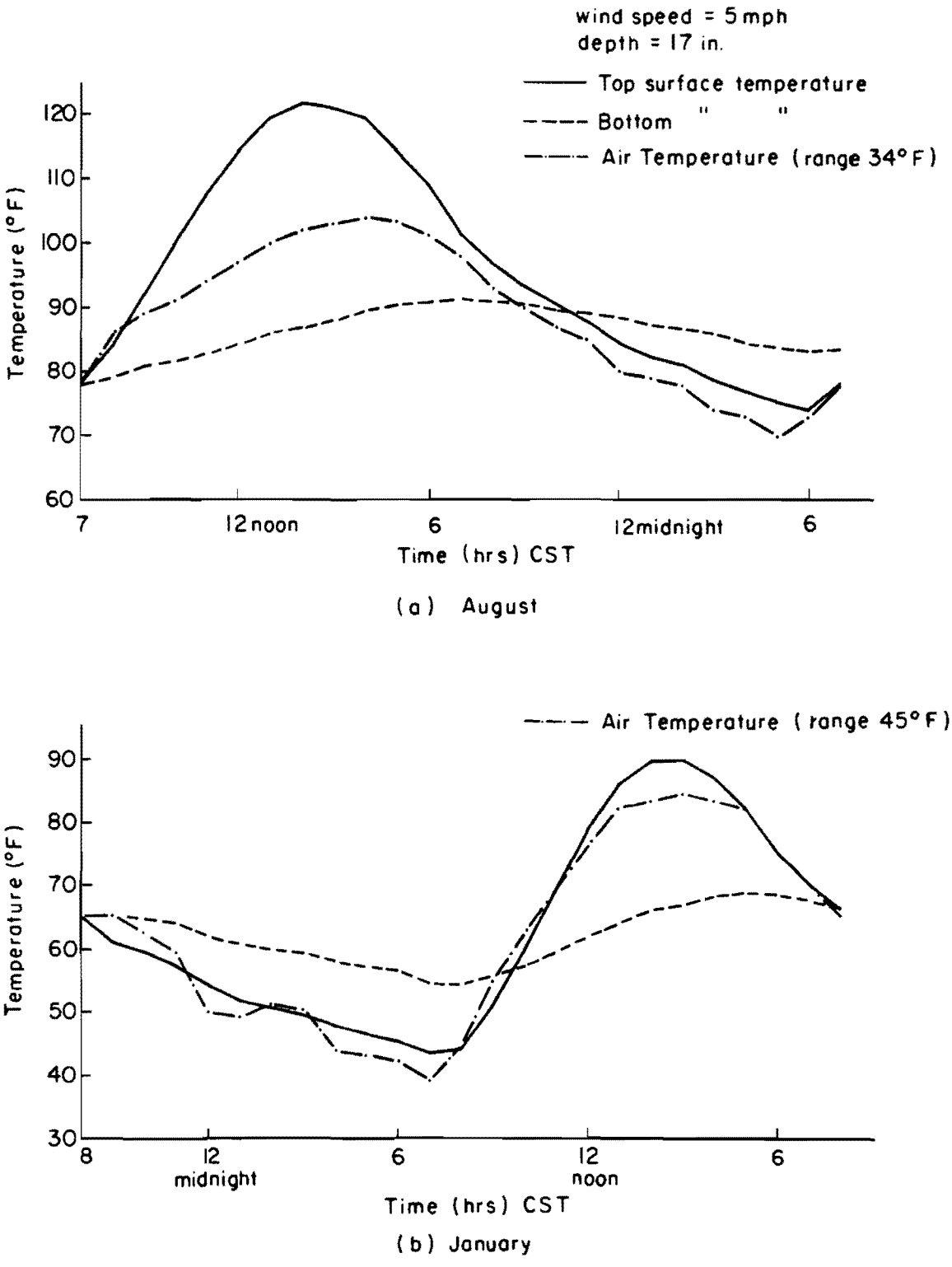

Fig 6.5. Plots of temperatures for a clear day and night.

the daily atmospheric variations in December, January and February are used for this study. The hourly distribution of air temperatures for each of these months are depicted in Fig 3.2b. The solar radiation intensities, on the other hand, are listed in Table 3.1.

Temperature and stress distributions calculated at 7:00 a.m. and 3:00 p.m. are shown in Fig 6.6. The starting condition was assumed to take place at 8:00 p.m. Again, the induced stresses were computed at the center of the middle span. Figure 6.6a indicates that a maximum tensile stress of 352 psi at the top surface occurs in January. Figure 6.6b, on the other hand, shows that a maximum tensile stress located at three-fourth's of the depth occurs in February. This is due to the fact that the solar radiation intensity in February is higher than that in January, thus producing larger temperature gradients and consequently higher induced stresses during the daytime. These stresses, however, are less than those induced under the summer conditions.

It is, therefore, concluded that the daily climatic changes in January are the extreme winter conditions in Austin, Texas. Plots of predicted top and bottom surface temperatures versus time in this month are shown in Fig 6.5b. A maximum difference of 9°F is found between the top and bottom temperature at 7:00 a.m. During daytime, the top surface temperature increases at a somewhat faster rate than the air temperature, but the maximum difference of only 6°F is observed between the two temperatures and takes place at 2:00 p.m.

6.2.5 Effects of Interior Supports on Temperature Induced Stresses

The indeterminacy of the structure has been known to be one of the significant sources of thermal induced stresses. The temperature stresses in a simply supported bridge are due only to the nonlinear temperature while a continuous bridge share this same stress plus flexural stresses since the interior supports offer vertical restraint which would take place due to a temperature differential over the bridge depth.

Temperature induced stresses for a single span statically determinate bridge and statically indeterminate structures with two and three spans are shown in Fig 6.7. The stresses were computed at the section of symmetry of

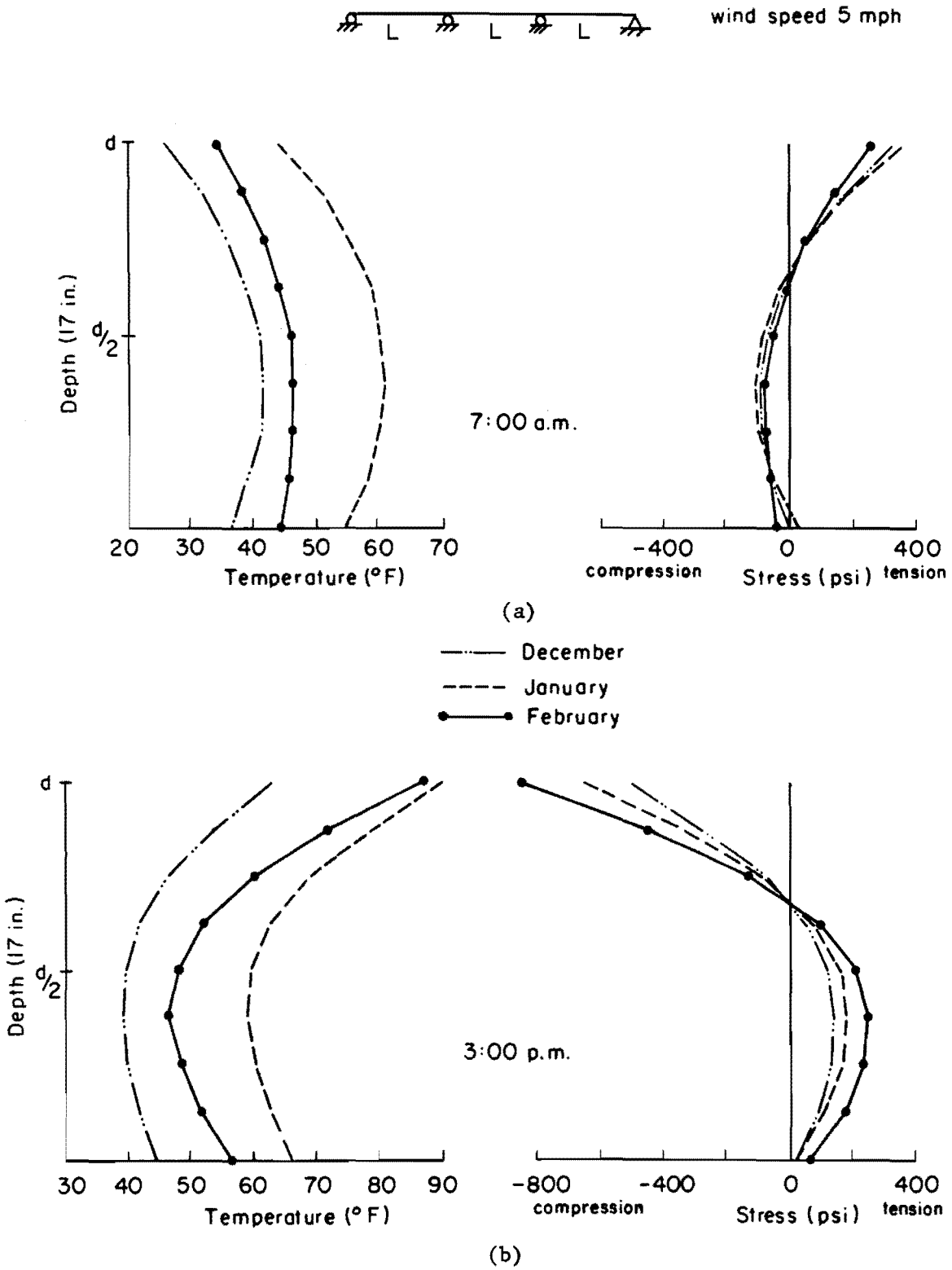

Fig 6.6. Temperature and stress distributions (winter conditions).

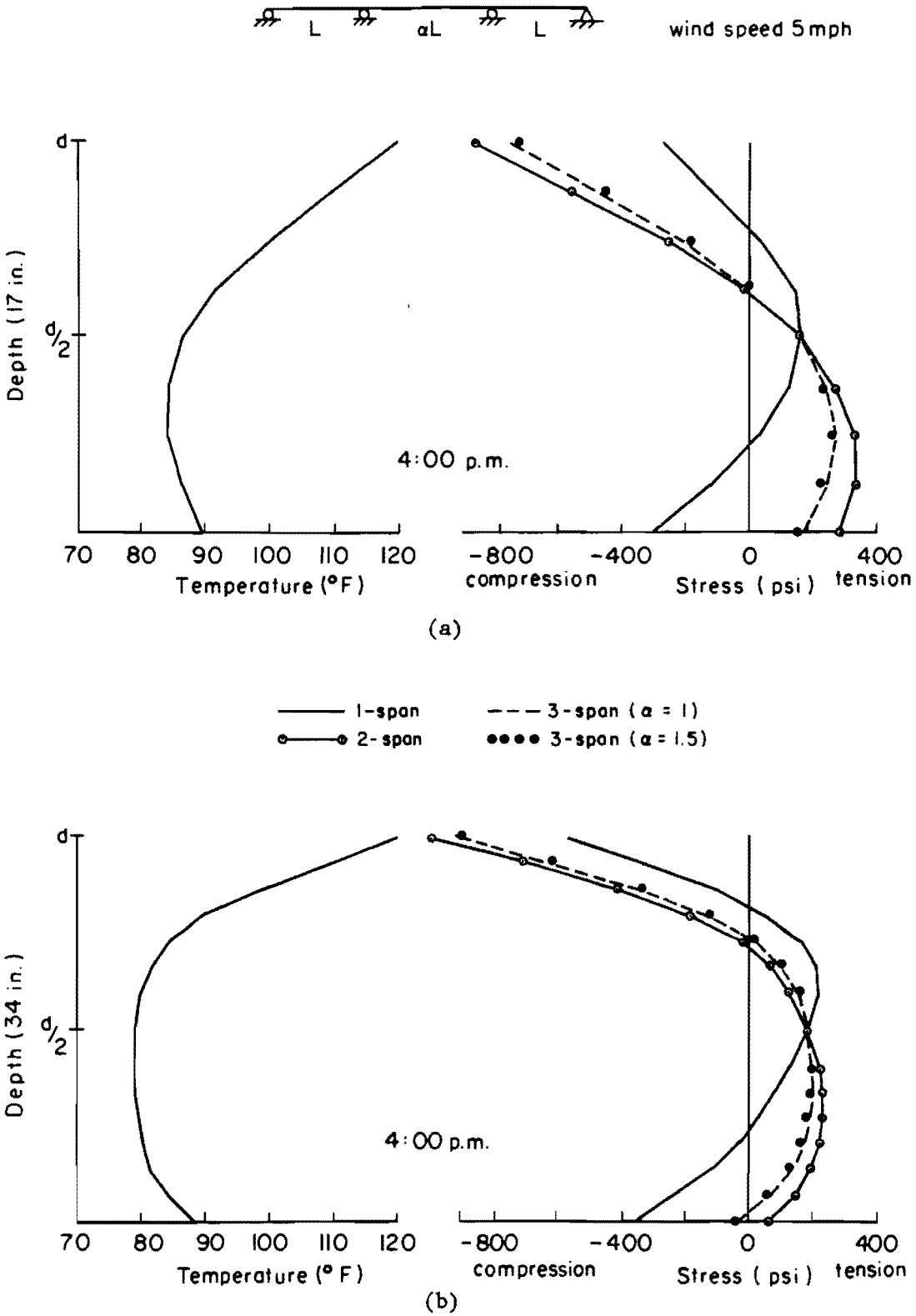

Fig 6.7. Temperature induced stresses for a one-, two-, and three-span bridge (August).

the bridge and the summer conditions were used. Figure 6.7a depicts the thermal stress distributions in a concrete slab bridge with a thickness of 17 inches. For the one-span case, compressive stresses predominate at the top as well as at the bottom surface with a maximum value of 460 psi at 1:00 p.m. A maximum tensile stress of approximately 180 psi, however, is predicted at the neutral surface of the section at 2:00 p.m. For the two- and three-span case, all sections below the neutral axis are subjected to tension with a maximum value of 330 psi located near the bottom surface at 4:00 p.m. At the top surface, on the other hand, a maximum compressive stress of 1000 psi was observed at 2:00 p.m. The length effect of the center span in the three-span case was also studied. It has been found, however, that this parameter contributes insignificant changes of stress, Fig 6.7a. It is also of interest to note that all stress distributions coincide at mid depth, i.e., the neutral surface of the section. This is due to the fact that the intermediate supports prevent vertical movement of the bridge, thus affecting only the bending stress component.

Temperature and temperature induced stress distributions in a 34 inch concrete slab at 4:00 p.m. are shown in Fig 6.7b. Although a lower magnitude of tensile stress is computed below the neutral axis, i.e., 230 psi, a higher compressive stress is predicted at the top surface with the maximum value of 1100 psi at 2:00 p.m.

Figure 6.8, on the other hand, depicts the maximum reverse gradients and the associated stresses computed under the winter conditions. Temperature and stress distributions over the depth of 17 inches are shown in Fig 6.8a. A maximum tensile stress of 180 psi is found at the bottom surface in the one-span structure. At the top surface, however, the two-span case yields higher tensile stress with a maximum value of 400 psi. Similar forms of stress distribution are found in a deeper section, Fig 6.8b. Higher tensile stresses, nevertheless, are predicted at the exterior surfaces, i.e., 490 and 250 psi at the top and the bottom surface respectively.

The above study also indicates that the temperature induced stresses in any statically indeterminate bridge will be bounded by the stresses computed from a one- and two-span case.

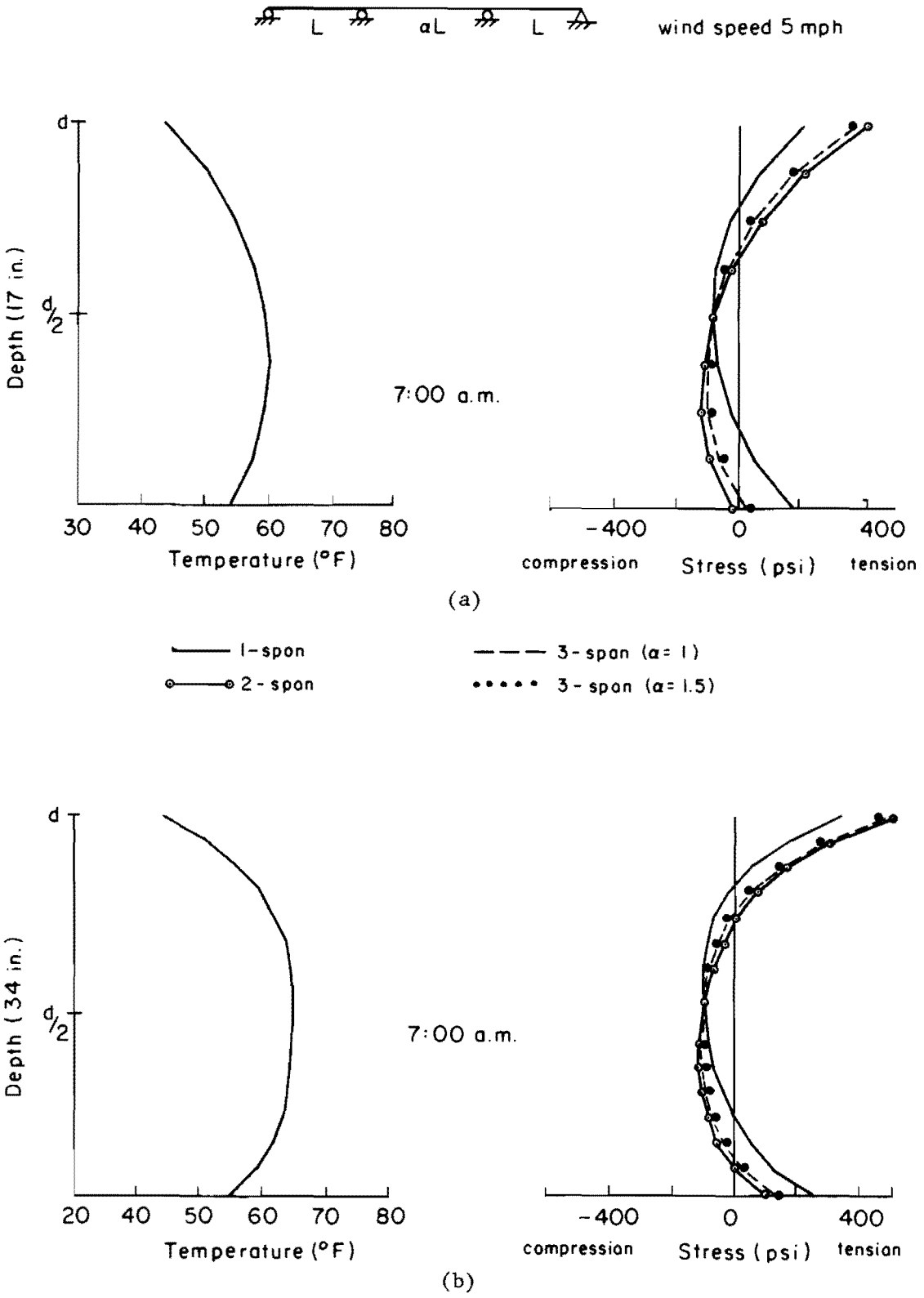

Fig 6.8. Temperature induced stresses for a one-, two-, and three-span bridge (January).

6.2.6 Effects of Longitudinal Restraining Forces on Temperature Induced Stresses

In the preceding studies, the stresses were calculated based on the assumption that the bridge was unrestrained longitudinally. In general, as a thermal movement occurs, restraining forces are developed at the supports, thus yielding another set of stresses. For a friction bearing, the translational force will be transmitted directly to the support until the magnitude of thermal force equals μR, where μ is the coefficient of friction which normally depends on the type of the bearing, corrosion of the bearing, etc. The reaction R must also include the additional reaction change caused by a temperature differential in the bridge.

Consider a simply supported concrete slab bridge 60 ft long and 17 inches deep. If the bridge temperature is raised uniformly 1°F above the temperature representative of the thermal equilibrium condition, the amount of force which is required to prevent the longitudinal movement will be 5200 lb. The friction force at the support, on the other hand, is only 1280 lb with μ equal to 0.2. Since the thermal force is greater than the friction force, movement occurs. According to the author's analyses, the stresses caused by this restraining force have been found to be insignificant because the computed maximum stress is only 8 percent of the maximum unrestrained temperature induced stress.

6.2.7 A Study on Polynomial Interpolation

The study was made in order to select a mathematical function which can represent the shapes of the temperature distribution as well as the shapes of the temperature induced stress in the concrete structure. In doing so, two types of polynomial interpolation were investigated. They are second- and fourth-order polynomials. Comparisons of results are given in Fig 6.9. It can be seen that the quartic function has superior representation compared to the quadratic function in fitting the predicted temperature and the stress distribution. Although the quadratic function gives good results for the depth of 17 inches, Fig 6.9a, poor results, however, are observed for the depth of 34 inches, Fig 6.9b.

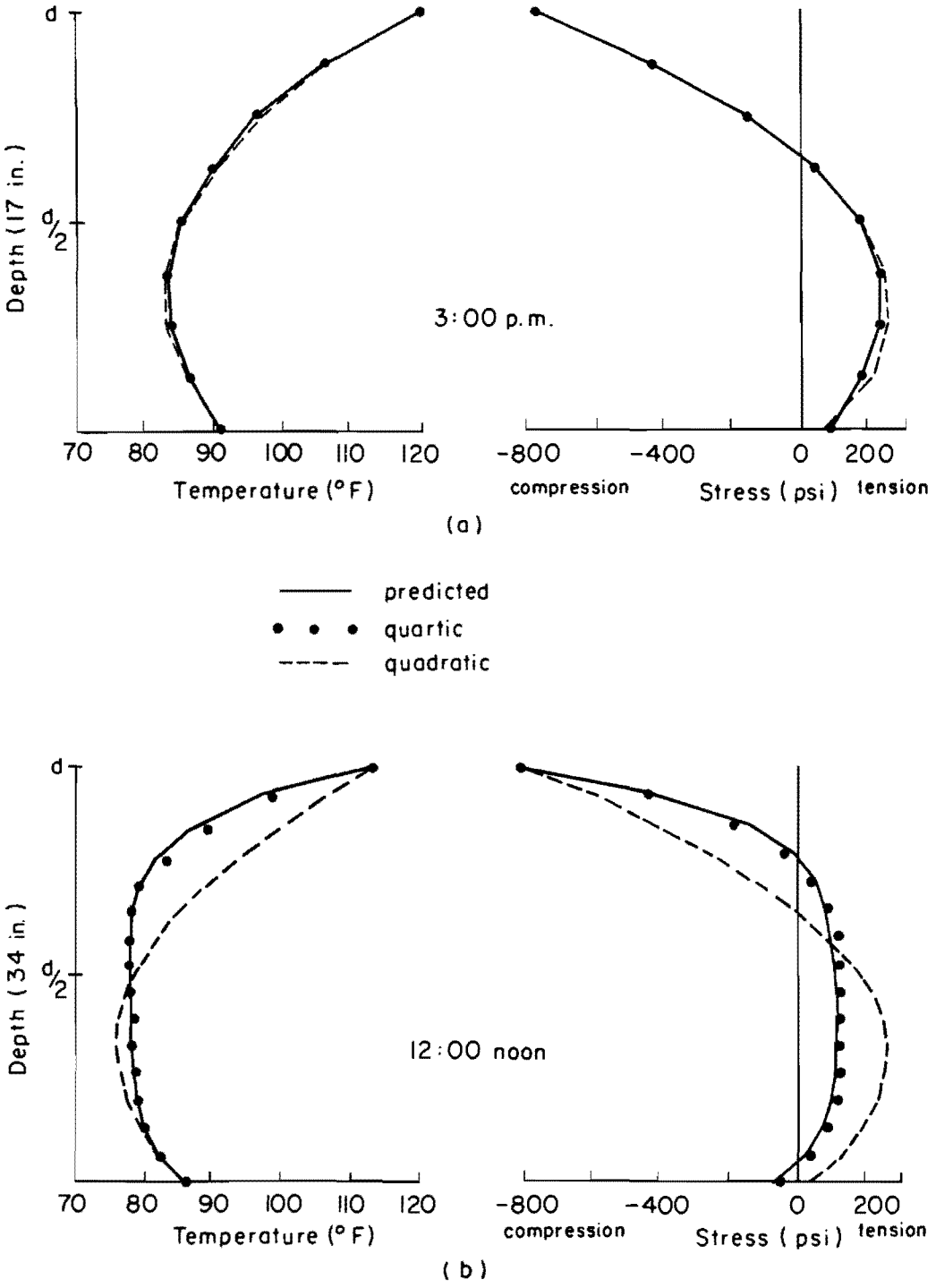

Fig 6.9. Representative polynomial interpolations for temperature distributions.

It has been shown, therefore, that the bridge temperature distribution at any time can be reproduced by knowing the temperature at 5 locations over the depth. An in depth study of the temperature induced stresses can now be made. Figure 6.10 depicts the decomposition of a given temperature distribution into each component of the fourth-order polynomial interpolation. Stresses at exterior surfaces computed from each component of temperature gradient are also shown in Fig 6.10. It can be seen that the linear and the cubic stress components depend on the span ratio, thus affecting the flexural stress. The linear stress component, however, will vanish if a one-span bridge is being considered while the cubic stress component will yield a certain amount of induced stresses. The quadratic and the quartic stress components, on the other hand, are independent of the span ratio, thus affecting only the axial stress. It should be noted that these two stress components always exist even for the statically determinate bridge. The method presented herein can then be easily used in estimating the temperature induced stresses.

6.3 Temperature Effects in a Non-Prismatic Concrete Slab Bridge

Temperature effects in the concrete slab bridge, as shown in Fig 6.1, studied so far assumed that the bridge had a uniform thickness throughout its length. To take into account the varying section, an approximate analysis is employed herein. In this method the bridge is divided into a number of beam elements. Each element has a constant depth as shown in Fig 6.11. If the prestressing steel effect is neglected, the equivalent end forces of each beam element due to changes of temperature can be computed by the method discussed earlier. Since these beam elements are connected at nodal points, net forces will be left over at points where adjacent elements have different thicknesses. Stresses caused by these forces can then be calculated by using the stiffness method. To obtain the temperature induced stresses, stresses computed from the clamped condition are superimposed upon the above stresses. Comparisons of results are given in tabular form in Fig 6.12a. It can be seen that a change of approximately 15 percent is observed for the maximum tensile stress.

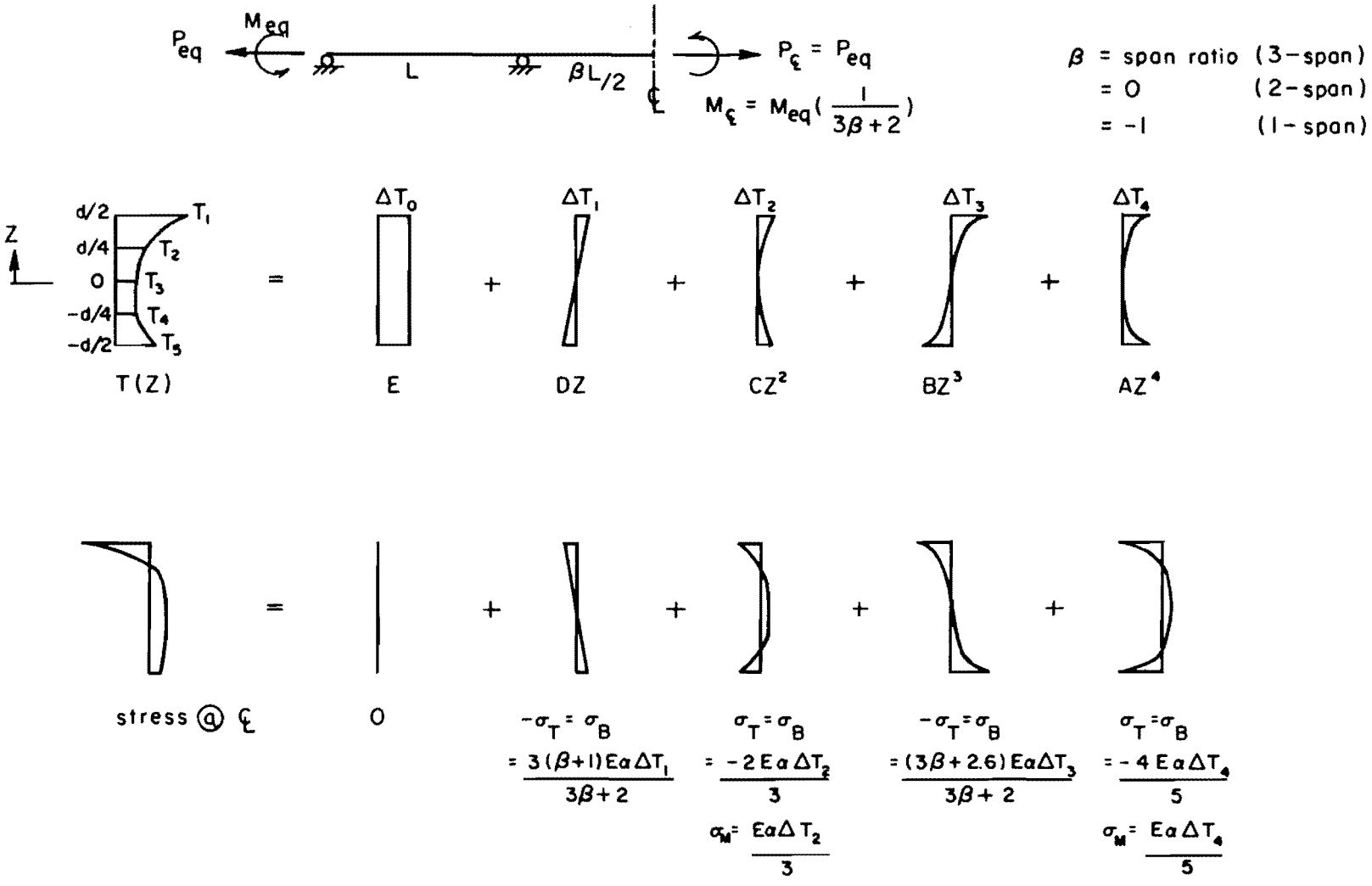

Fig 6.10. Fourth order polynomial components representing temperature and stress distributions.

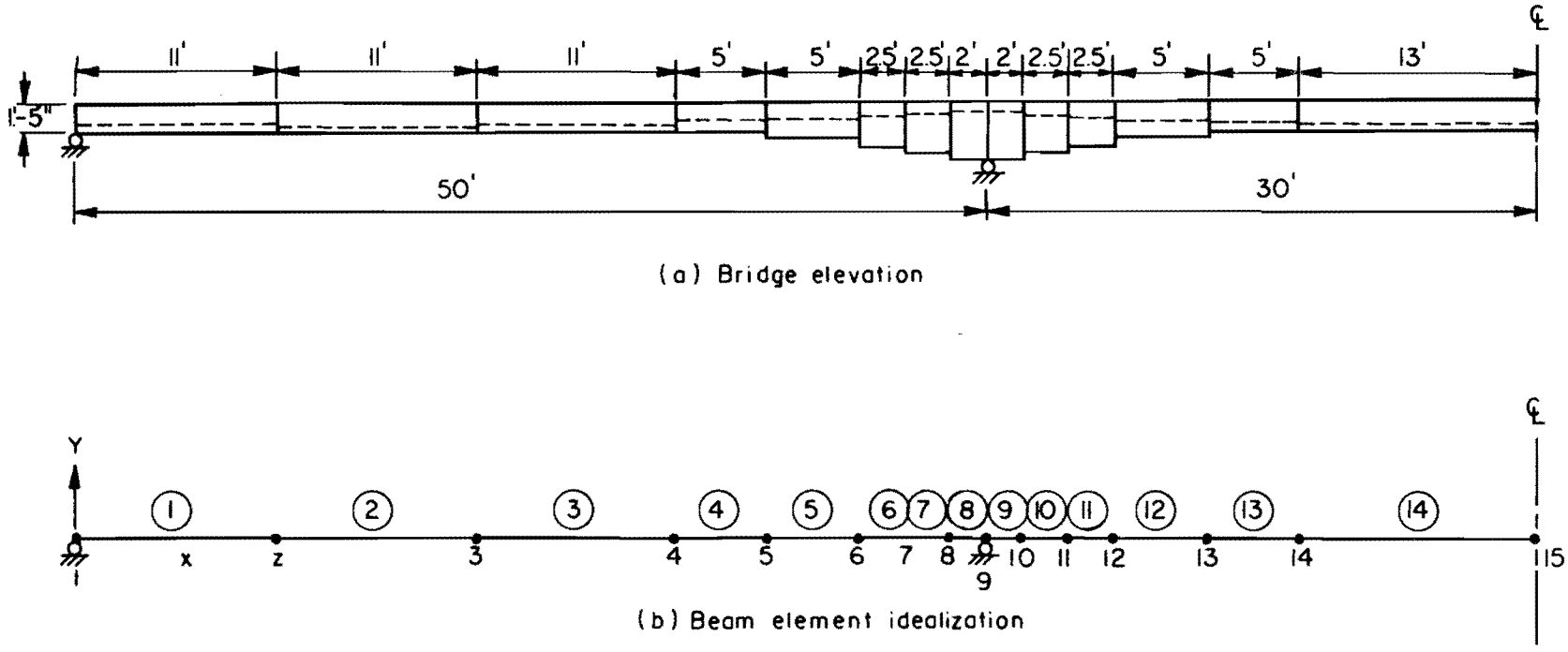

Fig 6.11. Prestressed non-prismatic concrete slab bridge and the idealization.

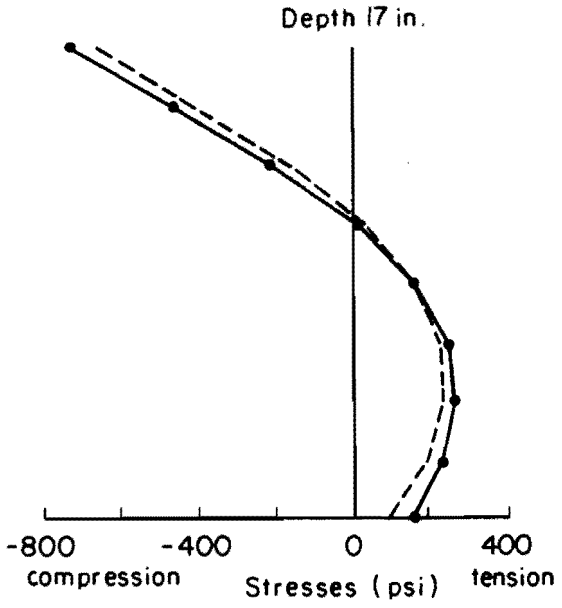

Stresses (psi)		
Constant section	Vary section	Vary Sec. with P/S
-669	-731	-734
-420	-469	-472
-169	-206	-209
31	13	10
162	166	163
228	250	247
235	268	264
190	240	236
97	164	160

(a) At section of symmetry (August)

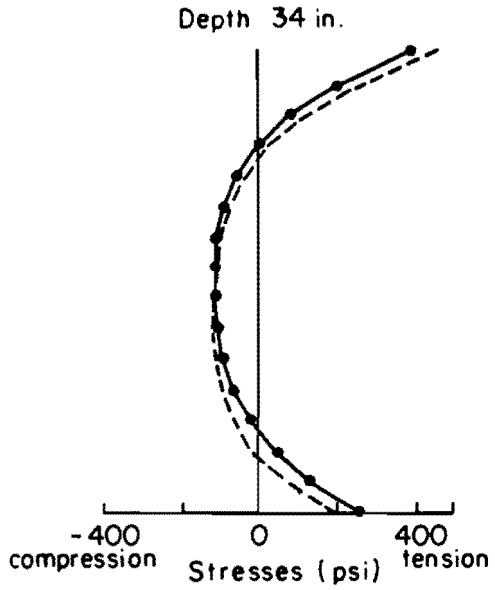

vary section with P/S

constant section

$E_c = 4.25 \times 10^6$ psi

$E_s = 30 \times 10^6$ psi

$f_{se} = 125$ ksi

$A_s = 0.1$ in.^{2} / in.

(b) At section over interior support (January)

Fig 6.12. Temperature induced stresses.

If the steel tendon is considered in the stress analysis, an additional restraining force at the location of the steel must be taken into account. This force is induced due to the strain compatibility requirement since concrete and steel have a different coefficient of thermal expansion and contraction. In computing this restraining force, it is assumed that the temperature in the tendon is the same as the temperature of the surrounding concrete. The derivation of this force can be found in Appendix D. The temperature induced stresses are then obtained by the same procedure mentioned above. Comparisons of stresses are shown in Fig 6.12a and b. Also, in the table of Fig 6.12a, the effect of the prestressing steel on temperature induced stresses is found to be very small. This is due to the fact that the difference of the coefficient of thermal expansion between steel and concrete is small.

6.4 Summary

It can be seen from the foregoing studies that the daily climatic changes introduce nonlinear temperature distributions in concrete structures. These temperature variations over the depth can be approximately represented by a fourth-order polynomial interpolation. During a hot summer day, a maximum temperature differential between the top and the bottom surface of 35°F is possible. At this time, the top surface will be about 20°F warmer than the air temperature. On a cool winter morning, however, a maximum reverse temperature gradient is only 9°F.

With regard to longitudinal movements of the bridge, the calculated maximum and minimum mean bridge temperatures are approximately 35°F and 40°F respectively. These values were computed by assuming the bridge temperature at the time of erection was 60°F. Consequently, on a cool winter morning, a thermal strain of 240 millionths is predicted. This compares with a shrinkage strain of 200 millionths suggested in the AASHO Specifications. The specifications, however, suggest the maximum and the minimum mean bridge temperatures to be 30°F and 40°F respectively.

The computed thermal deflections are small. The thermal induced stresses, on the other hand, appear to be significant. Analyses of

temperature stresses in a typical continuous concrete slab bridge indicate that on a typical hot summer afternoon the top surface may experience compressive stresses close to 1000 psi. These stresses, therefore, represent about 50 percent of the allowable compressive stress for concrete. Also, interior tensile stresses of approximately 330 psi are predicted at locations below the neutral surface of the section, thus accounting for about 60 percent of the modulus of rupture for concrete. On a typical cool winter morning, however, top surface tensile stresses of about 400 psi are possible.

CHAPTER 7. THERMAL EFFECTS IN COMPOSITE BRIDGES

7.1 Introduction

The problem of thermal effects in composite structures has been studied by many researchers. In the past, due to the lack of the mathematical nature of temperature distribution within the composite bridges, temperature induced stresses were computed based on assumed temperature variations over the bridge section. Temperature distributions such as a uniform, linear and parabola (4,35,57) were commonly assumed. Stress results thus obtained can then be either too high or too low. Field measurements of temperature in existing composite steel bridges are, therefore, being undertaken in many places to determine actual bridge temperature distributions. Obviously, this involves a lot of time and labor. Another means of obtaining bridge temperature distributions is by an analytical approach.

In Chapter 4, a two-dimensional mathematical model was developed for predicting bridge temperature distributions. The application and the validity of the model has been verified in Chapter 5. Based on good correlations between the predicted and the measured bridge temperatures in a typical pan-type reinforced concrete bridge, it is felt that temperature variations in various types of highway bridges can be estimated in a systematic way. In this chapter, investigations of temperature effects will be performed for two types of composite bridges, i.e., a precast pretensioned concrete beam-reinforced concrete slab and a steel beam-reinforced concrete slab bridge. Daily environmental conditions recorded in the city of Austin, Texas will be used in these studies.

In addition, the study of temperature effects in a narrow bridge structure is also included in this chapter. This type of bridge was selected since it inherits the complexities due to side heating of the girders and shading of the slab by the parapet. The bridge was analyzed under thermal loading using measured surface temperatures. The study was intended to compare the measured effects with the results computed from theoretical considerations employing the one-dimensional beam behavior.

7.2 Composite Precast Pretensioned Bridge

A typical interior girder, Texas standard type-B, of a composite precast pretensioned bridge is shown in Fig 7.1. The bridge is made continuous for live load by placing reinforcing steel in the slab over the piers. The beam spacing is 8 ft center to center with a cast-in-place concrete slab of 6.5 inches thick. The finite element mesh has a total number of 90 elements with 117 nodal points. Triangular as well as rectangular elements are used to represent the true I-shape of the beam cross section. The effect of prestressing steel on thermal induced stresses is not considered as it has been shown in the previous chapter that this effect on final stresses is small. The concrete thermal properties which were used are given in Table 6.1. The compressive strength of the concrete slab and beam are 3000 and 6000 psi respectively.

7.2.1 Temperature Effects on a Warm Sunny Day

Temperature distribution at 3:00 p.m. on a warm sunny day, in the month of August, is depicted in Fig 7.2a. August was selected since it has been shown in Chapter 6 that daily environment during this month induces maximum temperature stresses. Only a portion of the slab is included in Fig 7.2a because the temperature is found to be uniform over the rest of the slab. The top surface temperature at this time is about 20°F warmer than the surrounding air temperature. The temperature at the bottom surface of the slab is found to be warmer than the surface temperature along the side of the beam. This is as expected since additional heat energy is gained by conduction at the bottom slab surface while along the side of the beam heat exchange is taking place only by convection and radiation. At the center of the cross section, the temperature distribution over the depth shows changes in curvature, see Fig 7.3a. This is due to the varying thickness of the precast beam. A thinner section will, of course, have higher temperature than a thicker section thus explaining the increase of temperature at the middle portion of the beam. A temperature difference as high as 9°F occurs between the exterior and the interior face at the bottom portion of the beam. Fig 7.2a also shows that although temperature distribution in the slab varies constantly in the transverse direction, temperature distribution in the beam,

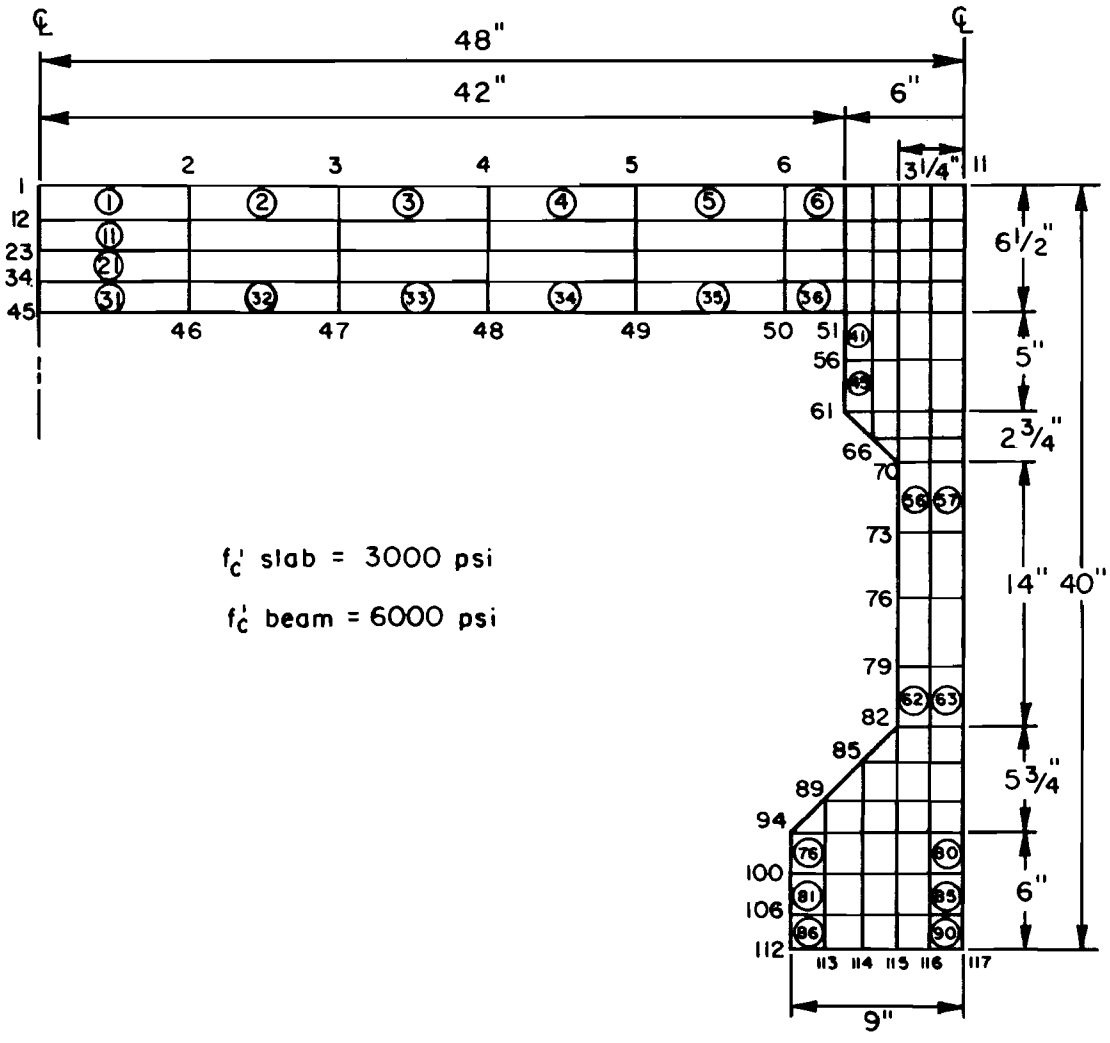

Fig 7.1. Typical interior girder idealization of a composite precast pretensioned bridge (Texas standard type B-beam).

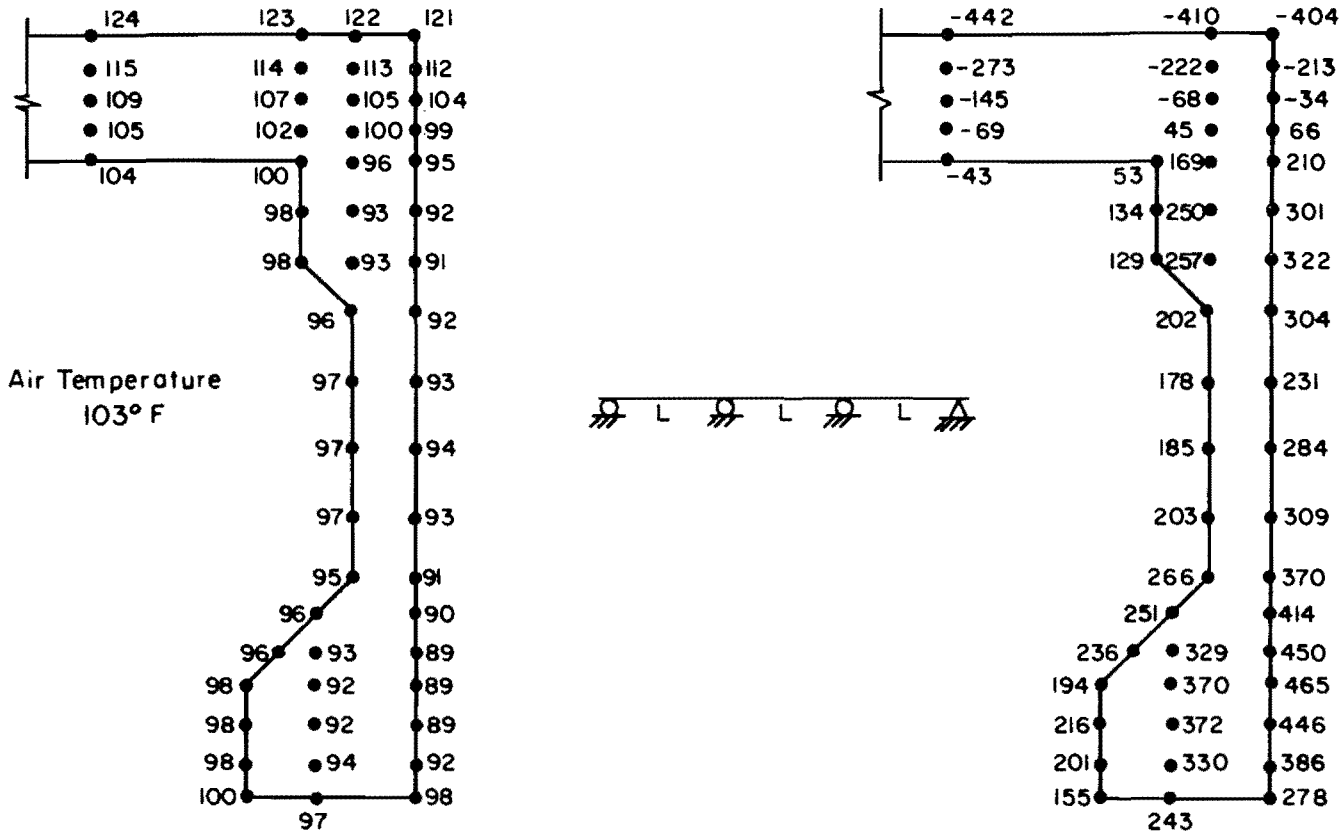

Fig 7.2. Temperature and stress distributions (August).

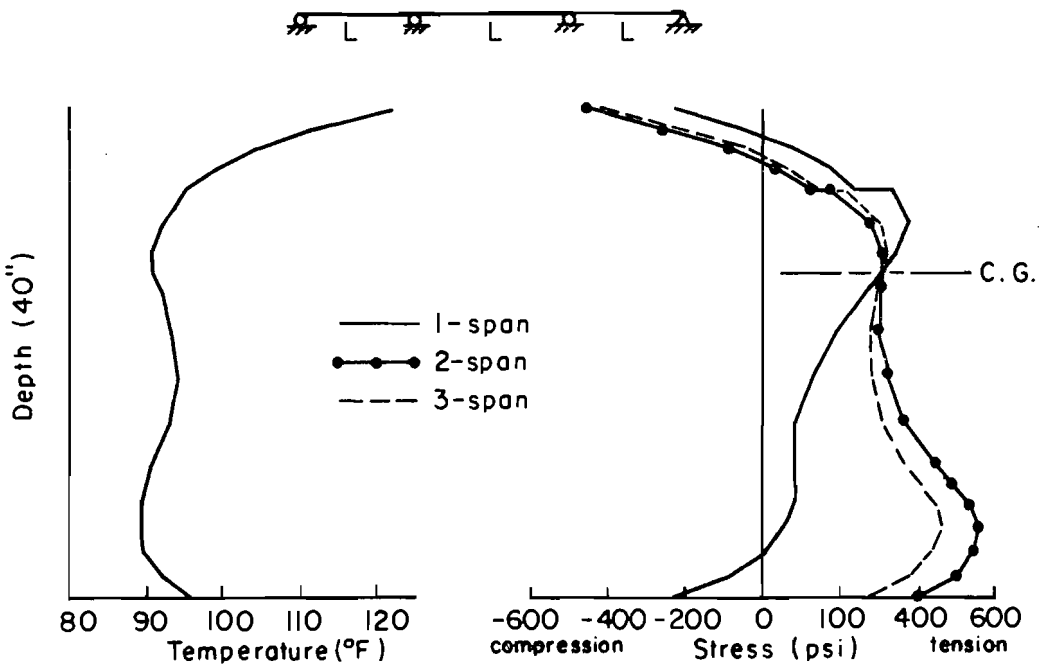

(a) August

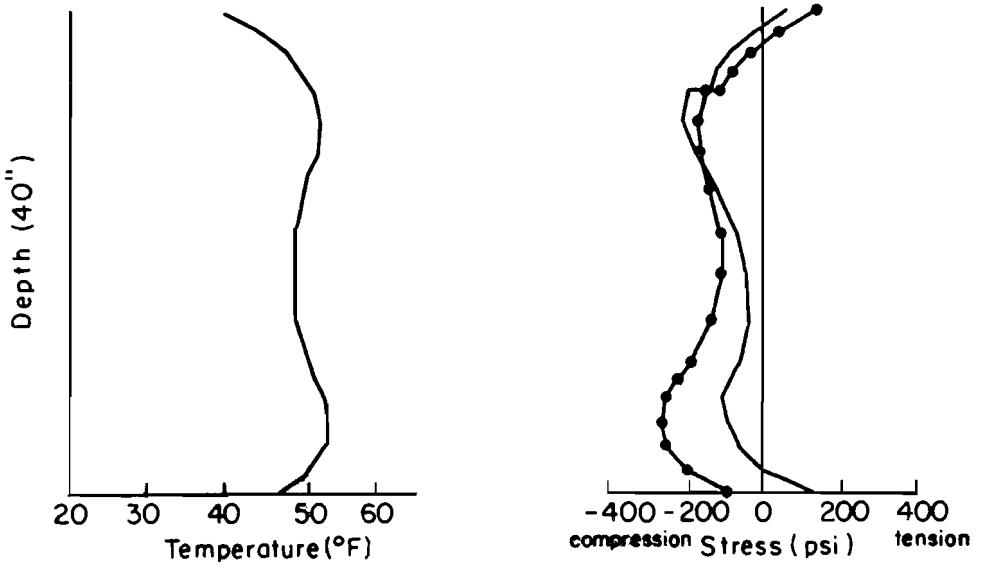

(b) January

Fig 7.3. Temperature and stress distributions at the section of symmetry.

on the other hand, varies nonlinearly in both the vertical and transverse directions. The predicted maximum temperature gradient is 27°F and takes place at 2:00 p.m.

At 3:00 p.m., the longitudinal thermal induced stresses calculated at the center of the middle span of the three span bridge are shown in Fig 7.2b. The stress distribution varies considerably over the cross section. High tensile stresses are found near the bottom portion of the beam with a maximum value of 465 psi at six inches above the bottom surface of the beam. At the same level on the exterior face, a tensile stress of only 194 psi is given. Maximum compressive stress of 477 psi, however, takes place at 2:00 p.m. and is found at the top surface of the slab. Fig 7.3a depicts temperature stresses induced in a one-, two- and three-span bridge. In each case the individual spans have the same length. The difference in stress distribution, caused by the indeterminacy of the bridge is noteworthy. For the one-span case, a maximum tensile stress of 380 psi is calculated at a location close to the neutral surface of the section. Compressive stress predominates at the top as well as at the bottom surface. Large tensile stresses, on the other hand, are found near the bottom portion of the beam in the two- and three-span cases. These high stresses were anticipated since the neutral surface of the composite section is located high in the upper portion of the beam causing thermal bending stresses to be large in the bottom region.

7.2.2 Temperature Effects on a Cold Sunny Day

Temperature distribution at 7:00 a.m. on a cold sunny day, in the month of January, is shown in Fig 7.4a. January is selected since it has been shown in Chapter 6 that daily environment during this month yields the maximum reverse temperature gradient. Again, a temperature difference as high as 9°F is observed between the exterior and the interior face at the bottom portion of the beam. The maximum temperature gradient is found to be 7°F. The temperature induced stresses in a simply supported bridge is shown in Fig 7.4b. Tensile stress of 239 psi is found at the bottom surface of the beam on the exterior face. Fig 7.3b depicts temperature and stress distributions over the depth of the composite section. Tensile stress of 148 psi is found at the top surface at section over interior support in the two-span case.

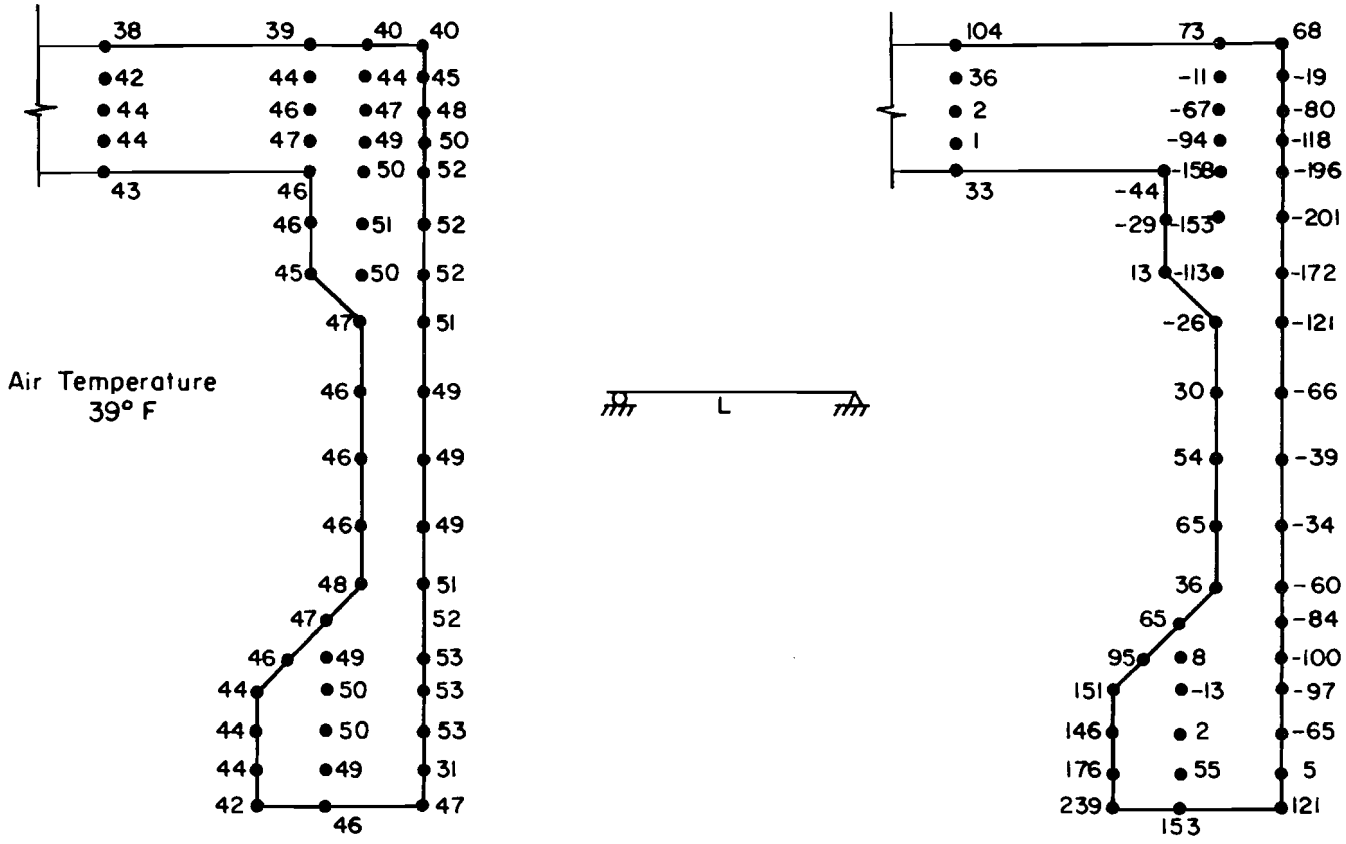

Fig 7.4. Temperature and stress distributions (January).

7.2.3 General Remarks

It has been shown that temperature distribution through the depth of a prestressed composite bridge subjected to daily environmental conditions is nonlinear, and that it cannot be represented by a parabolic distribution as was assumed by some pioneer researchers. This can be seen from Fig 7.3b which indicates that distributions of temperature stresses, in general, follow the shape of the temperature. Hence, an arbitrary temperature distribution should not be used in computing the stresses. For the weather conditions considered, the maximum tensile stress in the three span bridge is 465 psi. This stress is approximately 80 percent of the cracking stress, $7.5\sqrt{f'_c}$ where f'_c is the compressive strength of concrete at 28 days, given by the AASHO Specifications, section 1.6.7B. Of more importance is the fact that this stress is additive to the design stresses caused by combinations of dead load and live loads. For winter conditions, the stresses show a sign change and have a magnitude of approximately 40 to 50 percent of the summer values.

With regard to longitudinal movements, it is found that the range of the rise and fall of bridge temperature from an assumed temperature, 60°F, at the time of erection are 45°F. For comparison, the AASHO Specifications recommend temperature rise and fall to be 30°F and 40°F respectively, section 1.2.15. Studies have also shown that vertical deflections are generally small. However, the development of theoretical large interface shear force and moment should be noted. These interface forces are induced by the temperature difference between the concrete slab and steel beam. Effects of these forces at the bridge interface will be discussed in section 7.4.

7.3 Composite Steel Bridge

This type of highway bridge has gained popularity due to its relatively low cost, increased stiffness and increased overload capacity. The thermal behavior of this bridge type has been a major concern to many research engineers for years. Actual bridge temperature measurements were carried out over a two year period by Zuk (58). Extensive field data has been recorded and plots of daily temperature distribution over the depth presented for both cold and warm sunny days. Results obtained from that work will be used as spot checks in these theoretical studies.

Figure 7.5 depicts the idealization of a typical interior composite steel beam. A total number of 46 rectangular elements with 71 nodal points were used. The compressive strength of the concrete slab was assumed to be 3000 psi. Its average thermal properties are listed in Table 6.1. The modulus of elasticity of the steel girder was taken to be 29×10^6 psi with a density of 490 lb/ft^3 . The average thermal properties of structural steel are

coefficient of thermal expansion	6.5×10^{-6}	in/in/°F
thermal conductivity	26.6	btu/ft/hr/°F
specific heat	0.11	btu/lb/°F

7.3.1 Temperature Effects on a Warm Sunny Day

Figure 7.6a shows predicted surface temperature distributions on a warm sunny day in August. It is found that the maximum temperature differential through the depth of the bridge occurs at 2:00 p.m. and is 22°F. In addition, the top surface temperature is about 21°F warmer than the surrounding air temperature. Reference 58 reported this value to be 20°F to 30°F depending on the color of the concrete surface. The bottom flange temperature is very close to the air temperature. This is due to the steel's high conductivity. It is observed that in the late afternoon and during the night, the bottom flange temperature is warmer than the air temperature. This same phenomenon was also experimentally observed by Zuk (58).

Although a maximum temperature gradient occurs at 2:00 p.m., the maximum tensile stress in the steel beam is found to take place a few hours later. Consequently, it is the shape of the temperature distribution over the cross section and not necessarily the highest thermal differential between the top and bottom surface that induces the highest internal thermal stress. Temperature distribution at 6:00 p.m. is shown in Fig 7.6b. As is anticipated, bottom slab temperature affects the temperature at the top of the steel beam. Temperature distribution in the concrete slab is nonlinear, while a uniform gradient is found over a large portion of the steel beam. Stress distributions at the section of symmetry in a one-, two- and three-span bridge are also presented in Fig 7.6b. For the three-span case, maximum induced tensile stress in the beam is about 1000 psi. Maximum compressive

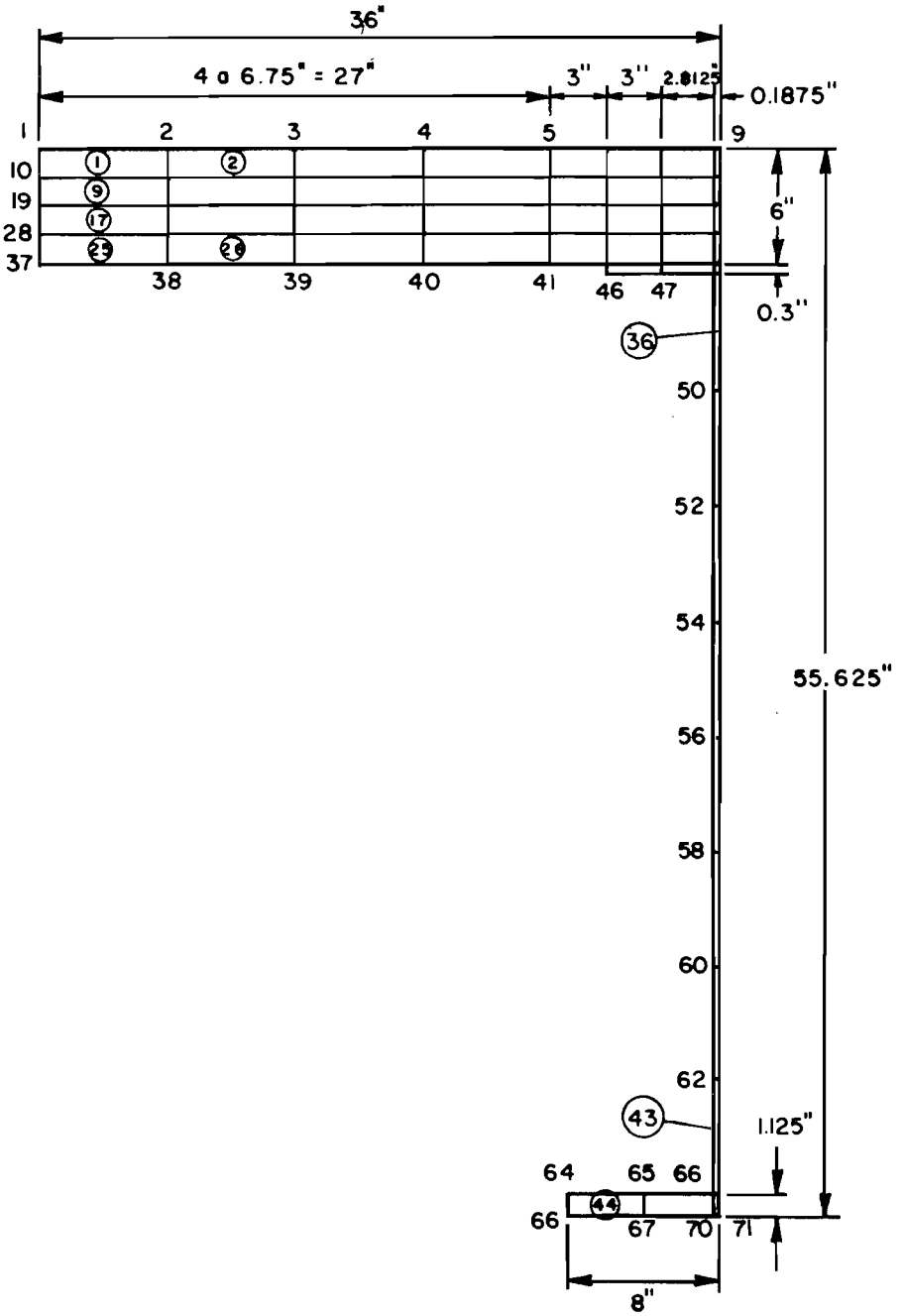

Fig 7.5. Typical interior girder idealization of a composite steel bridge.

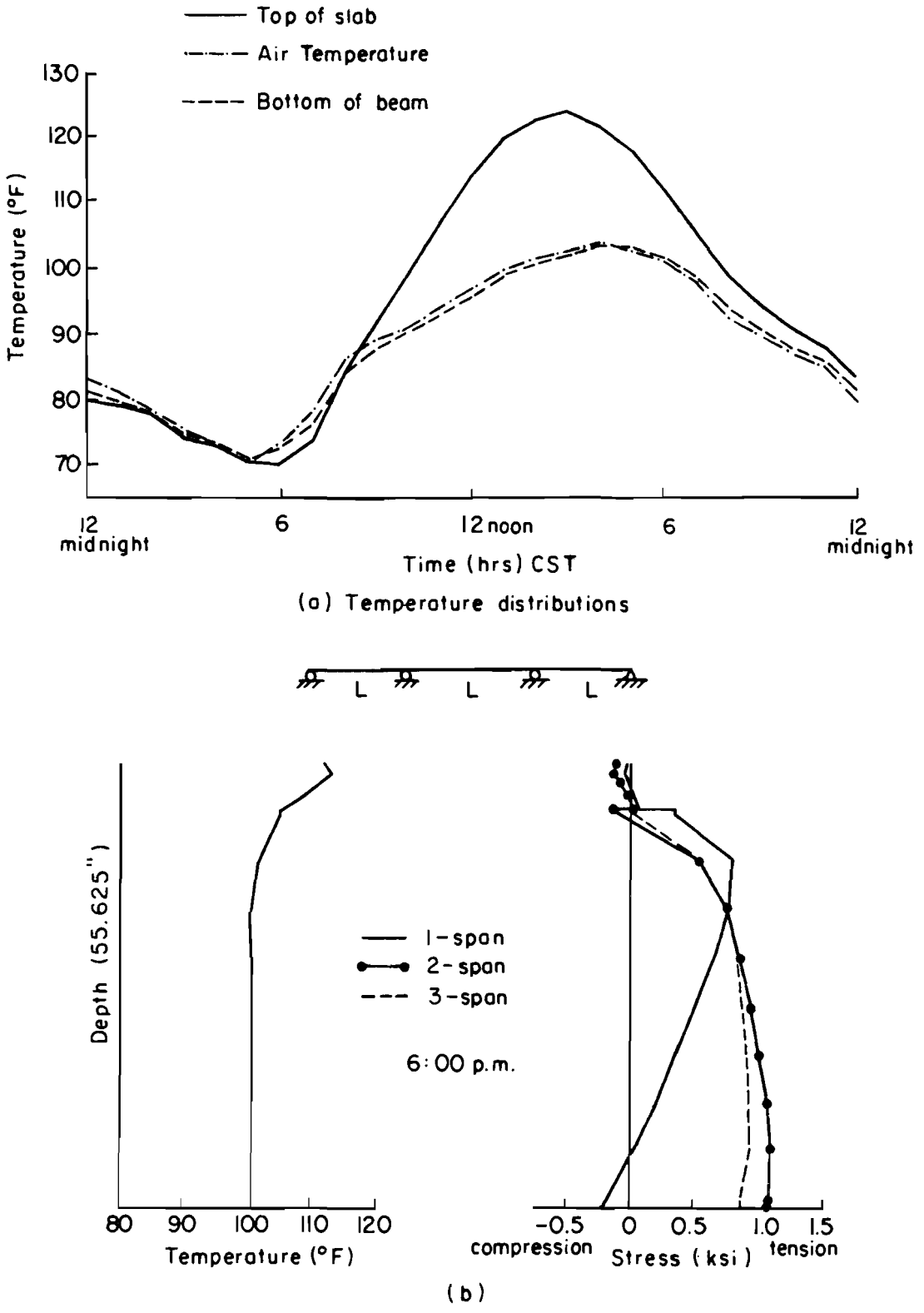

Fig 7.6. Temperature and stress distributions at the section of symmetry (August).

stress, however, is 330 psi at the top of the concrete slab and occurs at 2:00 p.m.

Because of the steel's high conductivity which is approximately 30 times that of concrete, the steel beam will have rapid responses to air temperature. The critical environmental conditions would, therefore, take place during a hot sunny afternoon followed by a quick drop of air temperature. Figure 7.7a depicts two kinds of daily air temperature distribution. Curve A represents a normal increase and decrease of air temperature. Curve B represents a normal increase up to the maximum value and a sudden decrease of air temperature of 10°F during the next hour. Temperature and stress distributions throughout the depth are shown in Fig 7.7b. It can be seen that thermal induced stresses in case B is about twice as much as stresses induced in case A. Maximum tensile stress of 1910 psi is found at the bottom portion of the steel beam. For a A36 steel beam, stress induced by temperature will be about 10 percent of the allowable stress. This temperature stress is, however, less than the AASHO allowable 25 percent overstress for group loadings, section 1.2.22.

7.3.2 Temperature Effects on a Cold Sunny Day

Surface temperature distributions of a typical interior beam during a cold sunny day in January are shown in Fig 7.8a. In contrast to the hot sunny afternoon, the top slab temperature is only 10°F warmer than the air temperature. This is due to the lower value of solar radiation intensity in winter than in summer. Temperature variation at the bottom flange of the beam again follows the same trend as that of air temperature. The maximum reverse temperature gradient is found to be 5°F and takes place at 9:00 a.m.

Temperature and stress distribution at 11:00 a.m. are shown in Fig 7.8b. This is the time at which the maximum compressive stress is induced in the beam. For a two-span bridge, a compressive stress of 1750 psi is found at the bottom portion of the steel beam at the section over the interior support.

With regard to longitudinal movements, it is found that the range of the rise and fall of the bridge temperature from an assumed temperature, 60°F,

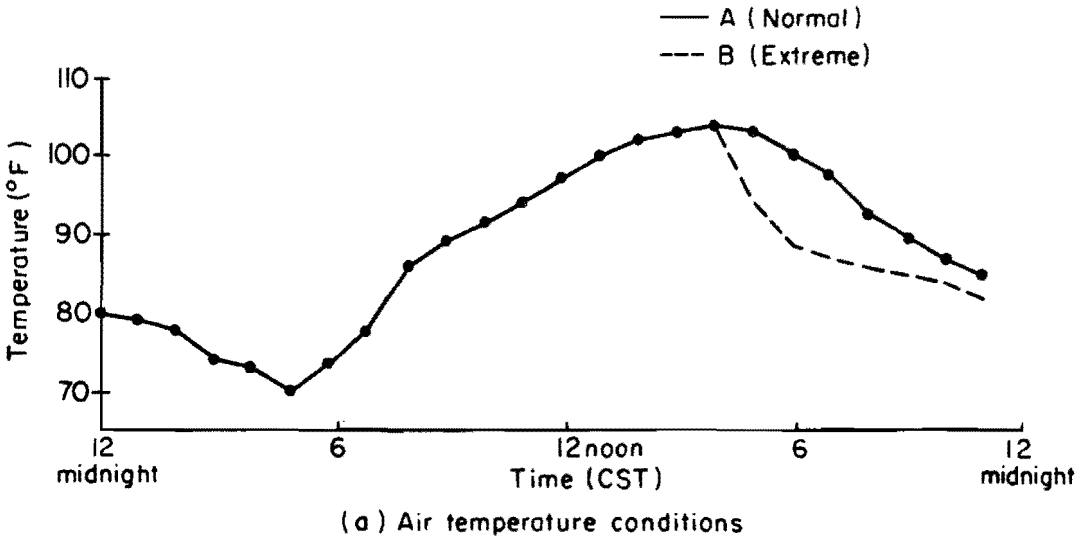

(a) Air temperature conditions

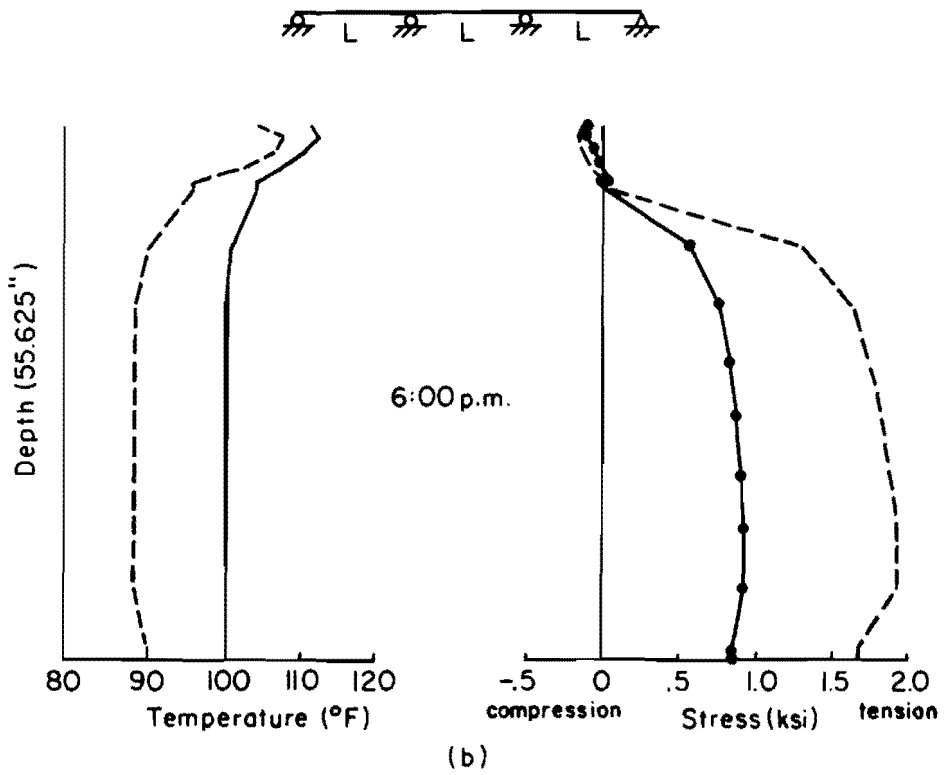

(b)

Fig 7.7. Temperature and stress distributions at the section of symmetry (August).

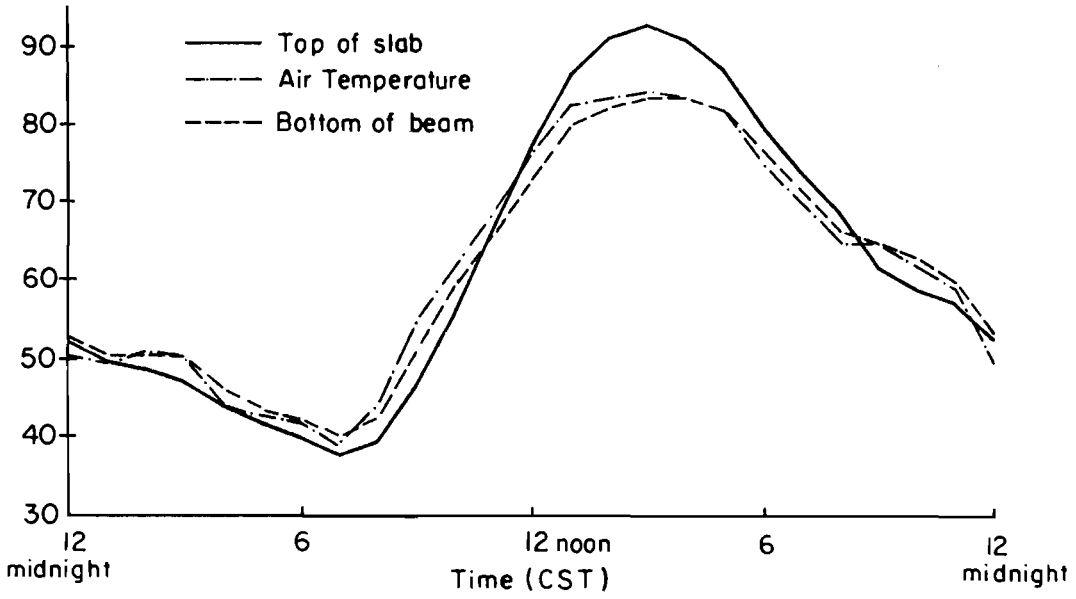

(a) Temperature distributions

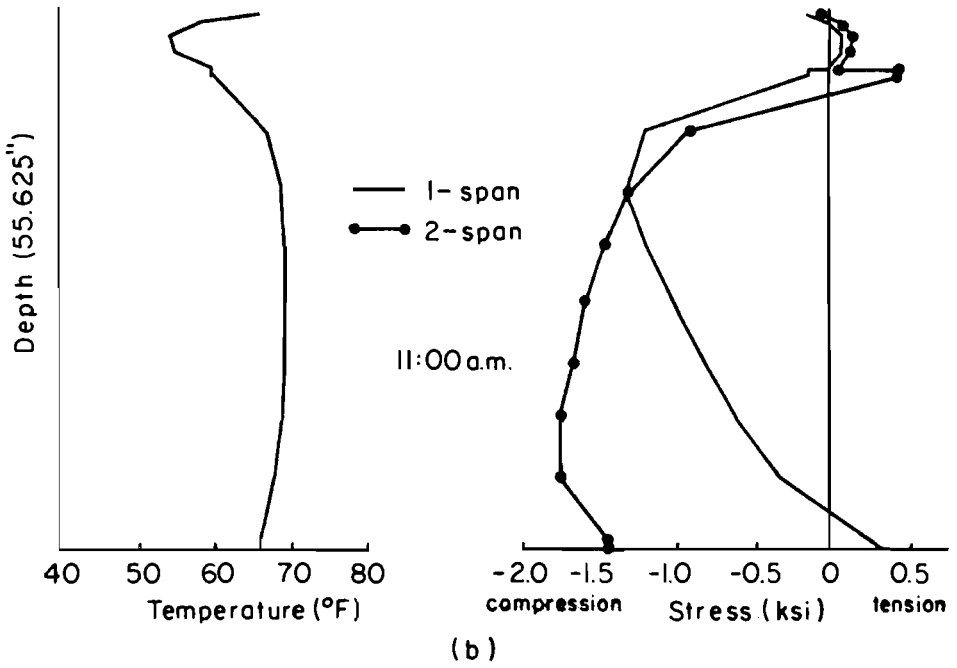

(b)

Fig 7.8. Temperature and stress distributions at the section of symmetry (January).

at the time of erection are 45°F. This is the same range of mean bridge temperature found in the prestressed composite bridge discussed earlier.

7.4 Interface Forces

The function of mechanical shear connectors in composite construction is to transfer forces across the surface between the concrete slab and the beam, so that the bridge can deform effectively as a single unit in resisting external loads. In design practice, shear connectors are normally designed only for the forces caused by the dead load carried by the composite section and the live load including impact (46). No consideration is made to account for additional interface forces induced by temperature differential between the slab and the beam. While observing actual bridge behavior under temperature changes, Zuk (58) found that there was considerable interface slip between the steel and the concrete.

With regard to the effects of these interface forces, experiments by Graf (24) has shown that the ends of a composite steel beam are subjected to special shear forces due to temperature difference between the slab and the beam. He found that these shear forces are concentrated at the ends and their magnitude varies according to the type of shear connectors employed. The magnitude is a maximum for fully rigid connectors and is a minimum for very flexible connectors. Results of such experiments are shown in Fig 7.9. These test results perhaps explain why the German Specifications require special heavy end anchorages tying the slab and beam together at their interfaces. In addition, shear forces due to temperature difference may be considered to be distributed as a triangular shear force diagram at the ends of the girder with a length equal to the effective slab width, Fig 7.10a. These shear forces are then assumed to be taken by shear connectors located over this length. Such requirements, however, are never found in the AASHO Specifications. Although the slip behavior was observed at the interface by Zuk (3), it does not significantly affect the overall safety of the bridge. This is perhaps due to the use of flexible shear connectors, such as stud and channel connectors, which when slip occurs will experience redistribution of force and distribute interface forces over a greater region.

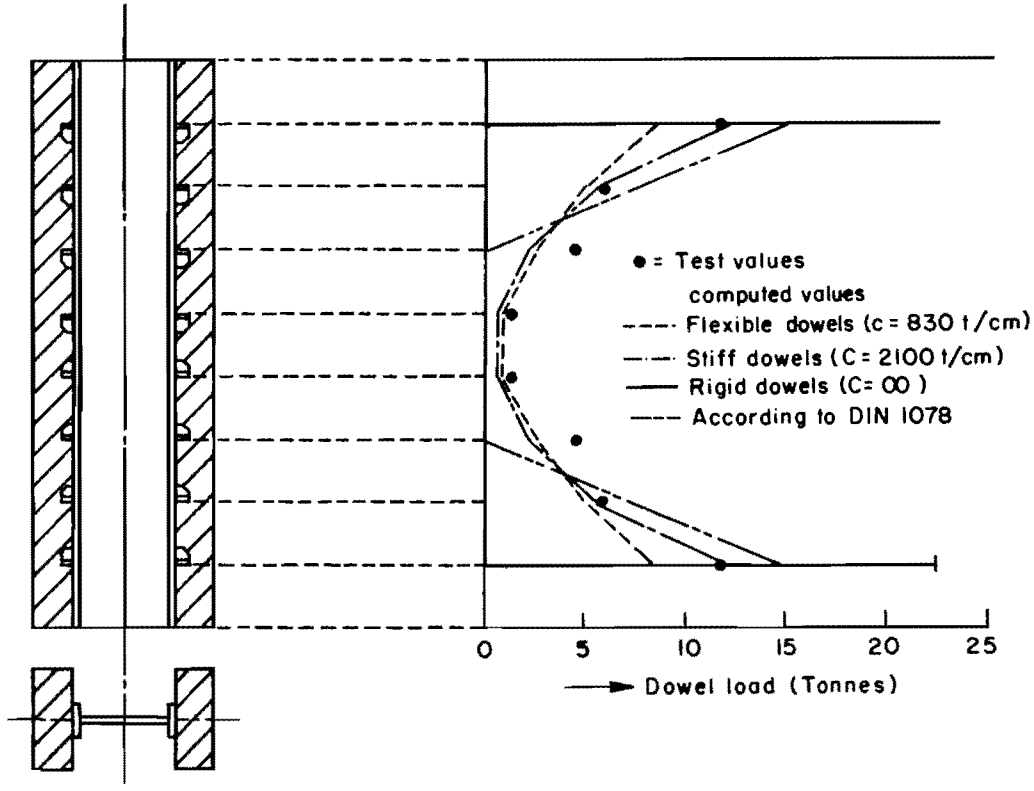

Fig 7.9. Variation of shear at the ends of a composite beam for a temperature difference of 21.5 F (11.9 C) between the slab and beam (Ref 5).

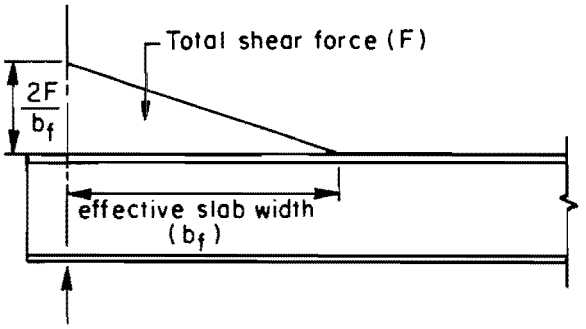

a) Triangular shear force diagram in accordance with the German code.

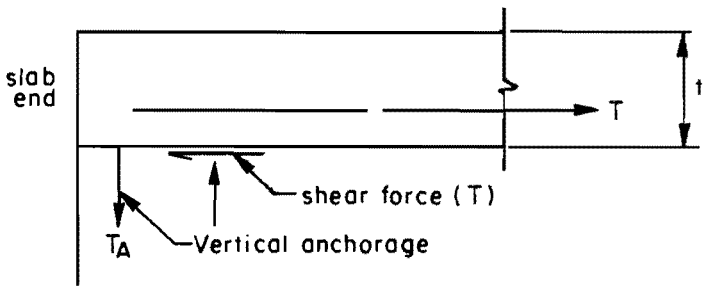

b) Temperature forces near slab end.

Fig 7.10. Interface forces near the slab end caused by a temperature differential.

Since interface forces result from the strain compatibility requirements, their magnitudes are, therefore, independent of the presence of interior supports. Shear force is then computed by integrating temperature stresses over the slab cross section in the single span case. According to the author's analysis, the resultant shear force in the prestressed composite bridge, Fig 7.1, is found to be 22400 lb. If no interface slip is allowed, this force will be transmitted by shear across the interface near the ends. Following the German code, this force will require additional shear connectors of approximately 50 percent of that required by the design load over the length of the effective width of the slab. This transfer, of course, results in a moment which is computed to be 185000 lb in. This moment is transferred by creating a vertical holding down force with a balancing compressive force across the interface, Fig 7.10b. Therefore, vertical end anchorages are required to prevent curling of the interface. For the composite steel bridge, Fig 7.5, the interface shear and moment are found to be 6000 lb and 96000 lb in., respectively. From the German code, this force will again require additional shear connectors of approximately 50 percent of that required by the dead and live loads at the ends of the steel beam.

7.5 Pedestrian Overpass (Narrow Structure)

A pedestrian overpass located in Austin, Texas was field tested on 14 March 1975. This test was performed as part of this research project and will be further discussed in the next project report. The bridge is a two-span composite prestressed structure with perpendicular supports. Its transverse section including parapets, slab deck and girders are shown in Fig 7.11b. Although the structure was designed as a pedestrian overpass, the slab thickness, the size of the girder and the spacing between the center-to-center of the two girders are commonly found in highway bridges of this type. Consequently, the bridge is considered as a narrow structure in which the thermal response is of interest for study.

Due to the fact that this structure has only two I-beams and is oriented at an angle to the sun's path, the temperature distributions will be complex due to side heating of the girders and shading of the slab by the parapets.

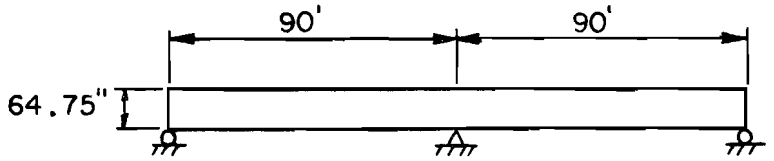

(a) Elevation view

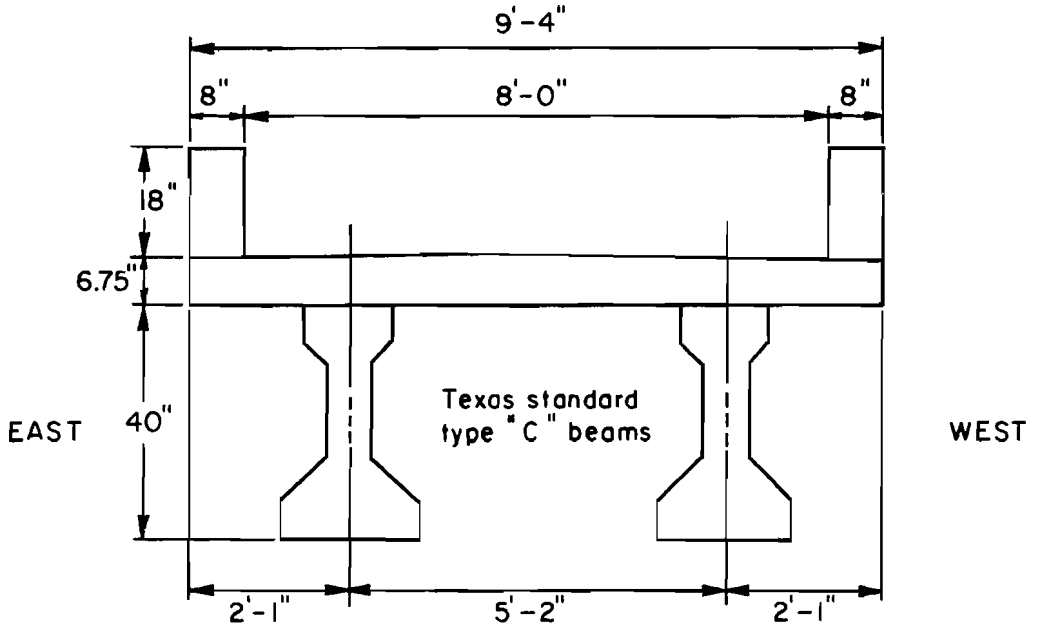

(b) Transverse section

Fig 7.11. Pedestrian overpass (Austin,Texas).

Since the developed two-dimensional temperature model does not have the capability of predicting surface temperatures under such conditions, the bridge was analyzed using measured surface temperatures. The temperature, therefore, was measured at 56 locations over the surface of the cross section in order to predict a representative temperature distribution within the bridge. These locations consisted of 11 stations on the top of the bridge and 45 stations along the side and bottom. Slope changes at the center of the slab over the end support were also measured continuously from 10:00 a.m. to 7:00 p.m. Details of this field test can be found in the next project report.

Figure 7.12 depicts the observed temperature variations with time. Originally, temperatures on the top were lower than those on the bottom surface. The two surfaces, however, attained the same temperature at approximately 9:30 a.m., Figs 7.12b and c. At the left girder, Fig 7.12a on the other hand, the two surfaces did not reach the same temperature until about noon which has been attributed to the side heating of the girder. The maximum difference in temperature between the top of the slab and the bottom of the right girder was recorded to be 19°F and occurred at 1:30 p.m. The maximum surface temperature, however, was 75°F at 3:30 p.m. and took place at the top surface of the slab.

In order to define accurately the temperature distribution over the bridge cross section, a finite element idealization consisting of 256 elements with 311 nodal points was used in the analysis. Four layers of rectangular element were utilized across the thickness of both the parapets and the slab. For each girder, ten layers were used over the depth while six, four and eight layers were used across the web at the top, middle and bottom portion respectively. The concrete thermal properties used in this temperature prediction are listed in Table 6.1. The compressive strength of the concrete slab and parapets were assumed to be 3000 psi while 6000 psi was assumed for the precast beams.

From a study of the recorded surface temperatures at all 56 locations, it was deduced that temperature variations within the bridge would be relatively small at approximately 8:30 a.m. Thus it was assumed that the bridge had a thermal equilibrium condition at this time with a uniform temperature of 41°F.

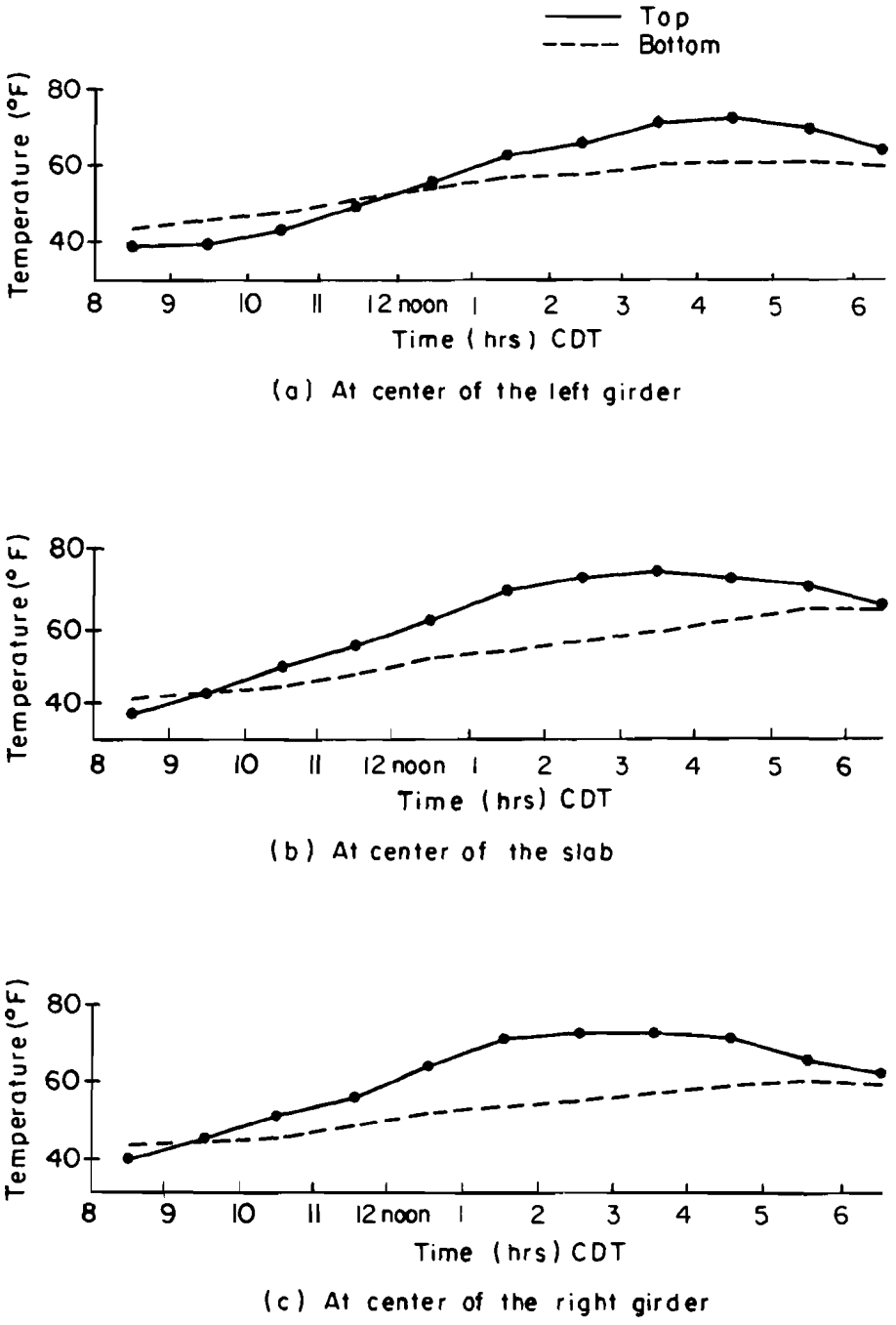

Fig 7.12. Temperature variations with time on March 14,1975.

Comparisons of measured and predicted longitudinal slope changes at the center of the slab over the end support are depicted in Fig 7.13. It can be seen that the predicted results underestimate the measured values. The maximum predicted value, however, is about 85 percent of that obtained from field measurements. The discrepancy of the results can be attributed to the fact that local behaviors caused by temperature differences cannot be accounted for in the one-dimensional model. See Table 6.1, p 77. The presented method, of course, predicts the result as an average value. In view of these factors, the comparison between measured and predicted slope change is considered to be favorable.

Plots of temperature induced stresses versus time at the section over the interior support are shown in Fig 7.14. It should be pointed out that although these longitudinal stresses were computed from a conventional beam theory, an arbitrary two-dimensional temperature distribution can be simulated by this procedure. From Figs 7.14b and c, it can be seen that beam B experienced more severe temperature induced stresses. A maximum tensile stress of 360 psi was observed at 7 inches above the bottom surface and occurred at 4:30 p.m. This tensile stress, however, reduced sharply such that only 65 psi was computed at the bottom surface of the beam. A maximum compressive stress of 383 psi, on the other hand, was found at the top surface of the slab and took place at 1:30 p.m.

With regard to the discrepancy between the measured and predicted movements of the overpass, it should also be pointed out that the concrete thermal properties used in the analysis were assumed to be the same as the values which gave satisfactory correlations for the Pasadena bridge. It is possible that the actual concrete thermal properties of this overpass were slightly different than those used in the analysis.

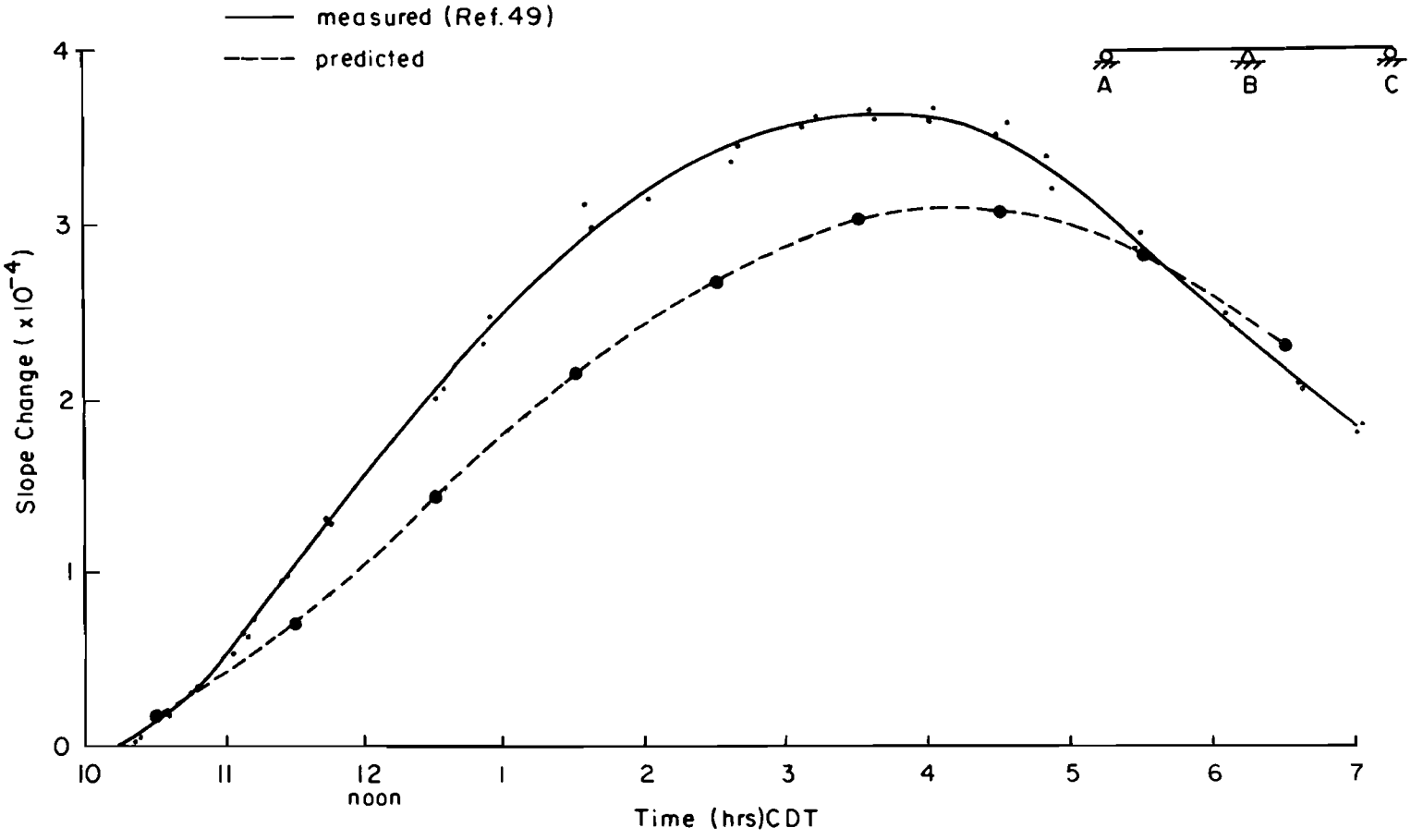

Fig 7.13. Comparisons of measured and predicted slope change vs. time for the pedestrian overpass.

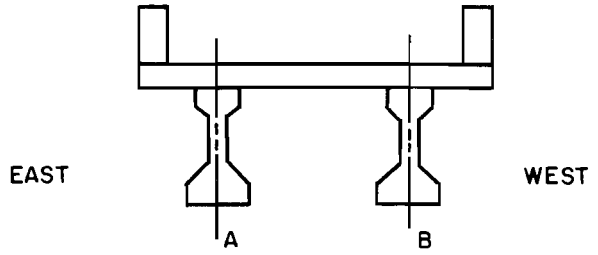

(a) Bridge section

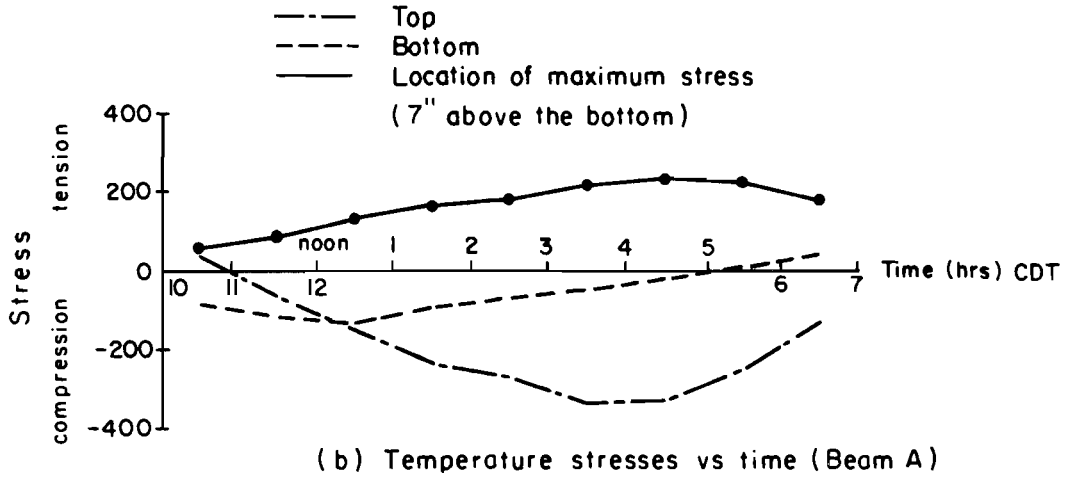

(b) Temperature stresses vs time (Beam A)

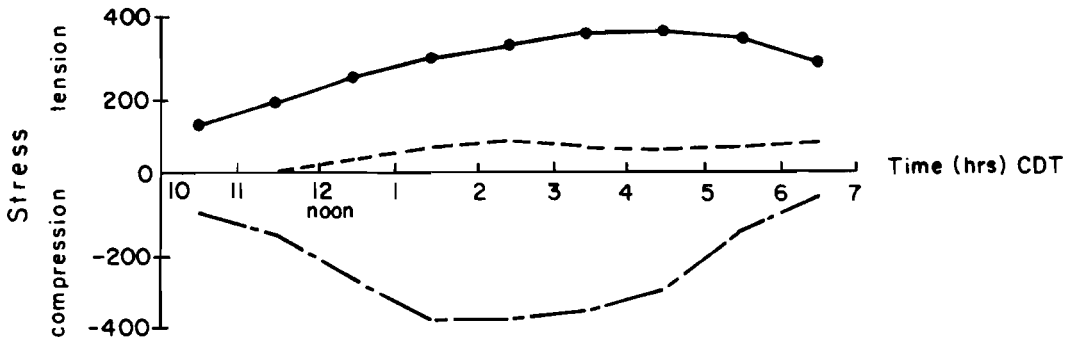

(c) Temperature stresses vs time (Beam B)

Fig 7.14. Longitudinal temperature induced stresses vs. time at the center section over the interior support.

CHAPTER 8. SUMMARY, CONCLUSIONS AND RECOMMENDATIONS

8.1 Summary

The computational procedures for the prediction of the transient bridge temperature distribution and the resulting structural response have been developed. The purpose of which is to assess the significance of the thermal effects in three types of highway bridges. They are 1) a post-tensioned concrete slab bridge, 2) a composite precast pretensioned bridge, and 3) a composite steel bridge. Particular attention is given to the study of bridge behaviors under the extreme environmental conditions that have existed in Austin, Texas.

Numerical procedures as applied to the heat transfer analysis can represent both the one-dimensional and two-dimensional heat flow. Boundary conditions at the exterior surfaces of the bridge are those of solar radiation intensity, ambient air temperature and wind speed. The one-dimensional heat equation is written in finite difference form and temperatures over the bridge cross section are determined by an incremental process. The finite element method, however, is used in determining the distribution of temperature over the bridge cross section where the flow of heat varies two-dimensionally. The temperature distribution along the length of the bridge, on the other hand, is assumed to be constant.

The structural response under temperature changes is assumed to be in the elastic range. Structural stiffness is computed based on the uncracked section. Temperature induced stresses and deformations are calculated based on the one-dimensional beam theory. Hence, the method is limited to straight bridges with supports perpendicular to the longitudinal direction of the bridge. Temperature effects in both simple span and continuous span bridges were studied.

All of these computations are included in a computer program to form a complete system for predicting temperature behaviors of highway bridges exposed to atmospheric conditions. Documentations of this computer program, TSAP (Temperature and Stress Analysis Program), will be in a later project report.

The input data required to use the program is easy to obtain. Environmental data can be obtained from regular Weather Bureau Reports and material thermal properties can be obtained from handbooks or Table 3.3.

8.2 Conclusions

The study demonstrates the feasibility and validity of analytically predicting the structural response of a bridge structure subjected to daily atmospheric variations. The method presented has been shown to be quite general in that it can be used to treat various conditions of the environment, types of highway bridge cross section as well as the indeterminacy of the structure. Although the study focused on the climatic conditions that have existed in Austin, Texas, other locations can also be studied if the relevant weather conditions are input.

It is found that the important weather parameters influencing the bridge temperature distributions are radiation, ambient air temperature and wind speed. Incoming solar radiation is the primary source that increases the top surface temperature during the day. Outgoing radiation, on the other hand, results in decreasing bridge temperature during the night. The important material thermal properties are the absorptivity, emissivity and thermal conductivity. Shape, size and thickness of the structure also affects the temperature variations over the bridge cross section.

The extreme environmental conditions have been found to take place on a clear night followed by a clear day with a large range of air temperature. In general, on a clear sunny day, the maximum incoming solar radiation intensity occurs at about noon, the peak ambient air temperature occurs at 4:00 p.m., and yet the top surface temperature is found to be maximum at 2:00 p.m. The maximum temperature gradient over the bridge depth also occurs at this time. On a clear night, the minimum surface temperature and the maximum reverse gradient are normally found to take place one hour before sunrise. The presence of wind at these times will reduce the maximun values of the temperature gradient.

Thermal deflections are found to be small. The range of the longitudinal movement of the studied bridges is found to be somewhat greater than the value suggested by the AASHO Specifications, section 1.2.15.

Temperature induced stresses appear to be significant. The magnitude of these stresses is found to be a function of the temperature distribution over the depth of the bridge cross section whether the bridge is statically determinate or indeterminate. It is also a function of the modulus of elasticity and the coefficient of thermal expansion and contraction of the material. For the weather conditions considered, the temperature induced tensile stresses in a post-tensioned concrete slab bridge and a composite precast pretensioned bridge are found to be in the order of 60 and 80 percent respectively of the cracking stress of concrete recommended by the AASHO, section 1.6.7B. On the other hand, stresses induced by temperature are approximately 10 percent of the design dead and live load stresses in a composite steel bridge. However, this magnitude of stress is less than AASHO's allowable 25 percent overstress for group loadings, section 1.2.22. Therefore, in the composite steel bridge, the temperature induced stresses are generally within tolerable design limits.

In general, highway bridges will be subjected to cyclic temperature induced stress at 30 cycles per month (365 cycles per year), and the frequency of one cycle in 24 hours. Furthermore, the fluctuations of stresses are not at their maximum values. Therefore, it is believed that this cyclic character should not be compared with behaviors observed from a fatigue test in which several hundred cycles per minute are normally applied.

It is also found that the interface shear force caused by the temperature difference between the slab and the beam is of considerable magnitude. Consequently, temperature effects may cause slip to take place earlier.

8.3 Recommendations

The method presented has made it possible to study computationally the temperature effects in highway bridges subjected to various conditions of the environment. With this capability it is suggested that further investigation be made on different types of highway bridge cross sections, for example, a box girder bridge. Weather conditions at different locations and different latitudes can also be included in the study.

Although it would be a major undertaking, it is a possibility to incorporate the effect of the sun's rays which fall along the side of the bridge in the computer program.

Another topic of practical interest is the use of the computer program TSAP, developed in this work to serve as a design tool to determine the maximum temperature induced stresses in the bridge under investigation. After these stresses have been defined, they can then be superimposed with the dead load and live load stresses in order to obtain the final design stresses.

APPENDIX A

COEFFICIENTS OF MATRICES FOR

A PLANE TRIANGULAR ELEMENT

APPENDIX A. COEFFICIENTS OF MATRICES FOR A PLANE TRIANGULAR ELEMENT

A typical triangular element is shown in Fig A.1. Temperature distribution within the element is assumed to be linear, i.e.,

$$U(x,y) = \underset{\sim}{\phi}(x,y)\,\underset{\sim}{\alpha} \tag{A.1}$$

and

$$\dot{U}(x,y) = \underset{\sim}{\phi}(x,y)\,\underset{\sim}{\beta} \tag{A.2}$$

where

$$\underset{\sim}{\phi}(x,y) = [\,1 \;\; x \;\; y\,] \tag{A.3}$$

$$\underset{\sim}{\alpha} = \begin{bmatrix} \alpha_1 \\ \alpha_2 \\ \alpha_3 \end{bmatrix}, \text{ and } \underset{\sim}{\beta} = \begin{bmatrix} \beta_1 \\ \beta_2 \\ \beta_3 \end{bmatrix} \tag{A.4}$$

Equation A.1 is evaluated at three vertices of the triangle and the three equations are solved simultaneously, finally we have

$$\underset{\sim}{\alpha} = \underset{\approx}{A}\,\underset{\sim}{u}, \qquad \underset{\sim}{\beta} = \underset{\approx}{A}\,\dot{u} \tag{A.5}$$

where

$$\underset{\approx}{A} = \frac{1}{\lambda}\begin{bmatrix} \lambda & \cdot & \cdot \\ b_j - b_k & b_k & -b_j \\ a_k - a_j & -a_k & a_j \end{bmatrix} \tag{A.6}$$

$$\lambda = a_j b_k - a_k b_j, \quad \underset{\sim}{u} = \begin{bmatrix} u_i \\ u_j \\ u_k \end{bmatrix}, \text{ and } \dot{\underset{\sim}{u}} = \begin{bmatrix} \dot{u}_i \\ \dot{u}_j \\ \dot{u}_k \end{bmatrix} \tag{A.7}$$

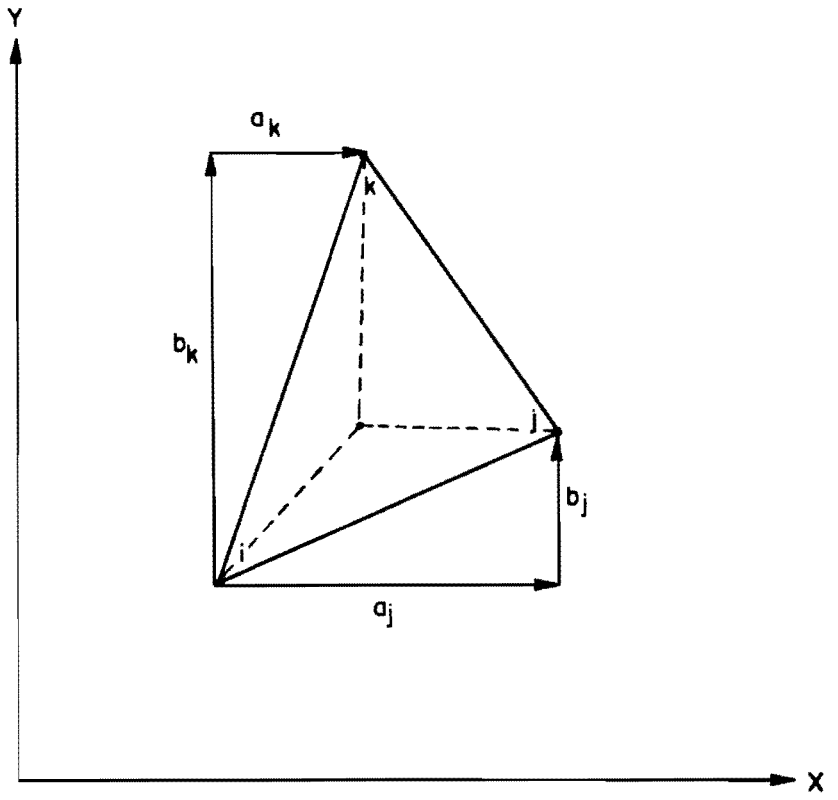

Fig A.1. A typical triangular element.

Rewritten equations A.1 and A.2

$$U(x,y) = \underset{\sim}{\phi}(x,y)\,\underset{\approx}{A}\,\underset{\sim}{u} = \underset{\approx}{N}\,\underset{\sim}{u} \tag{A.8}$$

$$\dot{U}(x,y) = \underset{\sim}{\phi}(x,y)\,\underset{\approx}{A}\,\dot{\underset{\sim}{u}} = \underset{\approx}{N}\,\dot{\underset{\sim}{u}} \tag{A.9}$$

$$\underset{\sim}{\nabla}\,U(x,y) = \underset{\sim}{\nabla}\,\underset{\sim}{\phi}(x,y)\,\underset{\approx}{A}\,\underset{\sim}{u} = \underset{\approx}{D}\,\underset{\sim}{u} \tag{A.10}$$

where $$\underset{\approx}{D} = \begin{bmatrix} \frac{\partial}{\partial x} \\ \frac{\partial}{\partial x} \end{bmatrix} [\,1 \;\; x \;\; y\,]\,\underset{\approx}{A}$$

or $$\underset{\approx}{D} = \frac{1}{\lambda}\begin{bmatrix} b_j - b_k & b_k & -b_j \\ a_k - a_j & -a_k & a_j \end{bmatrix} \tag{A.11}$$

For an isotropic triangular element with constant thickness, t , the conductivity matrix is

$$\underset{\approx}{B} = \frac{kt}{2\lambda}\begin{bmatrix} e^2+d^2 & b_k e - a_k d & b_j e + a_j d \\ b_k e - a_k d & b_k^2 + a_k^2 & b_j a_k - a_j a_k \\ b_j e + a_j d & b_j a_k - a_j a_k & b_j^2 + a_j^2 \end{bmatrix} \tag{A.12}$$

where $$d = a_k - a_j \tag{A.13}$$

and $$e = b_j - b_k \tag{A.14}$$

For the heat capacity matrix, the lumped method is used instead of Eq 4.26. The heat capacity is lumped at exterior nodes. Therefore, the diagonal coefficients are, Fig A.1,

$$c_{11} = \frac{\rho c t}{2}\,(A_1 + A_3)$$

$$c_{22} = \frac{\rho c t}{2} (A_1 + A_2) \tag{A.15}$$

$$c_{33} = \frac{\rho c t}{2} (A_2 + A_3)$$

If both convection and radiation take place only on the i-j face with the constant film coefficient, the matrix $\underset{\approx}{H}$ is then

$$H_{ii} = H_{jj} = \frac{h_c \ell_{ij}}{3}$$

$$\text{and} \qquad H_{ij} = \frac{h_c \ell_{ij}}{6} \tag{A.16}$$

The vector $\underset{\sim}{h^*}$ is also given by

$$\underset{\sim}{h^*} = \frac{h_c \ell U_a}{2} \begin{bmatrix} 1 \\ 1 \\ 0 \end{bmatrix} \tag{A.17}$$

The heat vector $\underset{\sim}{q^*}$ is

$$\underset{\sim}{q^*} = \frac{Q_r \ell}{2} \begin{bmatrix} 1 \\ 1 \\ 0 \end{bmatrix} \tag{A.18}$$

APPENDIX B

EFFECT OF PRESTRESSING STEEL ON END FORCES

APPENDIX B. EFFECT OF PRESTRESSING STEEL ON END FORCES

To take into account the effect of the steel tendon, concrete and steel are first considered separately. Under temperature rise, concrete and steel will expand unequally due to the difference in the coefficient of thermal expansion. Additional end forces thus required to maintain the strain compatibility condition at the location of the steel.

Without the steel tendon, the concrete strain at any point caused by the change of temperature is, Fig 4.5e,

$$\varepsilon_{ci} = \frac{P}{E_c A_c} + \frac{M y}{E_c I_x} \tag{B.1}$$

where ε_{ci} = concrete strain

A_c = gross area of the concrete section

I_x = moment of inertia about x-axis

y = distance from the centroid in y-direction

$$P = \int_{-d/2}^{d/2} b E_c \alpha_c T(y)\, dy \tag{B.2}$$

and

$$M = \int_{-d/2}^{d/2} b E_c \alpha_c T(y)\, y\, dy \tag{B.3}$$

Therefore, at the location of the steel, i.e., at the distance e below the centroid of the section, the concrete strain is

$$\varepsilon_{ci} = \frac{P}{E_c A_c} - \frac{M e}{E_c I_x} \tag{B.4}$$

The strain of the steel, under free expansion, is

$$\epsilon_{si} = \alpha_s T_{d'} \tag{B.5}$$

Let F_s be the end force, compression in the steel and tension in the concrete, which acts at the location of the tendon. The final concrete strain is, therefore,

$$\epsilon_c = \epsilon_{ci} + \frac{F_s}{E_c A_c} + \frac{F_s e^2}{E_c I_x} \tag{B.6}$$

Similarly, the final steel strain is

$$\epsilon_s = \epsilon_{si} - \frac{F_s}{E_s A_s} \tag{B.7}$$

Since $\epsilon_c = \epsilon_s$, from Eqs B.6 and B.7 we have

$$F_s = \frac{\epsilon_{si} - \epsilon_{ci}}{\left(\frac{1}{E_c A_c} + \frac{1}{E_s A_s} + \frac{e^2}{E_c I_x}\right)} \tag{B.8}$$

Consequently, thermal induced stresses are given by

$$\sigma_c = \frac{P'}{A_c} + \frac{M'y}{I_x} - E_c \alpha_c T(y) \tag{B.9}$$

where $P' = P + F_s$ (B.10)

and $M' = M - F_s e$ (B.11)

BIBLIOGRAPHY

1. Barber, E. S., "Calculation of Maximum Pavement Temperatures from Weather Reports," Highway Research Board Bulletin 168, pp. 1-8, 1957.

2. Becker, E. B., and Parr, C. H., "Application of the Finite Element Method to Heat Conduction in Solids," Technical Report S-117, U.S. Army Missile Command, Redstone Arsenal, Alabama, November 1968.

3. Berks, C. J., "New Mechanical Bridge Joint System," Civil Engineering, Vol. 68, No. 741, London, April 1968, pp. 439-440.

4. Berwanger, C., "Thermal Stresses in Composite Bridges," The Journal of the Institute of Structural Engineers, April 1974.

5. Billington, N. S., Thermal Properties of Buildings, Cleaver-Hume Press, LTD., 1952.

6. Boley, B. A., and Weiner, J. H., Theory of Thermal Stress, John Wiley & Sons, Inc., 1960.

7. Boresi, A. P., Elasticity in Engineering Mechanics, Prentice-Hall, Inc., Englewood Cliffs, New Jersey, 1965.

8. Brisbane, J. J., Heat Conduction and Stress Analysis of Anisotropic Bodies, Vol. 1, Rohm and Haas Company, Redstone Research Laboratories, Huntsville, Alabama, October 1969.

9. Brisbane, J. J., Becker, E. B., and Parr, C. H., "The Application of the Finite Element Method to the Solution of Stress and Diffusion Problems of Continua," Journal of the Alabama Academy of Science, Vol. 39, No. 2, April 1968.

10. Capps, M. W. R., "The Thermal Behavior of the Beachley Viaduct/Wye Bridge," RRL Report, LR 234, Road Research Laboratory, Ministry of Transport, London, England, 1968.

11. Carslaw, H. S., and Jaeger, J. C., Conduction of Heat in Solids, Oxford University Press, 2nd Edition, London, 1959.

12. Chapman, A. J., Heat Transfer, The Macmillan Company, 2nd Edition, 1960.

13. Climates of the States, Vol. II, Western Series, U.S. Department of Commerce, 1974.

14. "Climatological Data," The U.S. Weather Bureau Reports, National Summary, Environmental Science Services Administration, Environmental Data Service.

15. Crandall, S. H., and Dahl, N. C., An Introduction to Mechanics of Solids, McGraw-Hill 1959.

16. Desai, C. S., and Abel, J. F., Introduction to the Finite Element Method, Van Nostrand Reinhold Company, 1972.

17. Ekberg, C. E., Jr., and Emanuel, J. H., "Current Design Practice for Bridge Bearing and Expansion Devices," Final Report, Project 547-9, Engineering Research Institute, Iowa State University, Ames, Iowa, August, 1967.

18. Emanuel, J. H., and Eckberg, C. E., Jr., "Problems of Bridge Supporting and Expansion Devices and an Experimental Comparison of the Dynamic Behavior of Rigid and Elastomeric Bearings," Special Report, Iowa State University, Iowa Engineering Experiment Station, September, 1965.

19. Emanuel, J. H., Best, J. L., Hulsey, J. L., Senne, J. H., and Thompson, L. E., "An Investigation of Design Criteria for Stresses Induced by Semi-Integral End Bents," Phase I-Feasibility Study, Civil Engineering Department, University of Missouri-Rolla, Rolla, Missouri, Study 72-1.

20. Emerson, M., "The Calculation of the Distribution of Temperature in Bridges," TRRL Report LR 561, Transport and Road Research Laboratory, Department of the Environment, Crowthorne, 1973.

21. Gaumer, G. R., "Stability of Three Finite Difference Methods of Solving for Transient Temperatures," Journal of American Rocket Society, Vol. 32, No. 10., 1962, pp. 1595-1596.

22. Gloyne, R. W., "The Diurnal Variation of Global Radiation on a Horizontal Surface - with Special Reference to Aberdeen," Meteorological Magazine 101, 1972, pp. 44-48.

23. Gortz, W., Agnew, F. S., and Palmer, M. F., "Bridge Deck Expansion Joints," Consulting Engineer, Vol. 31, No. 5, London, May, 1967, pp. 76-78, 81.

24. Graf, O., "Uber Versuche mit Verbundtragen," Der Bauingenieur, January, 1950, Heft 8.

25. Griffiths, E., and Davis, A. H., "Transmission of Heat by Radiation and Convection," Food Investigation Board, Special Report 9, 1922.

26. Gurtin, M. E., "Variational Principles for Linear Initial Value Problems," Quarterly Applied Mathematics, Vol. 23, 1964.

27. "Heating, Ventilating, Air Conditioning Guide," American Society of Heating and Air Conditioning Engineers, Vol. 37, 1959, p. 52.

28. Hendry, A. W., and Page, J. K., "Thermal Movements and Stresses in Concrete Slabs in Relation to Tropical Conditions," Rilem Symposium II 1960, International Symposium of Concrete and Reinforced Concrete in Hot Countries.

29. Hudson, F. M., "Investigation of a Full-Size Continuous Concrete Highway Bridge, Parts I and II," Final Report, HPR Report No. 24, Alabama Highway Research, Alabama Highway Department, June, 1967.

30. Hudson, F. M., "Simulation of Settlement of Supports of a Full Scale Continuous Concrete Bridge," Final Report, HPR Report No. 49, Alabama Highway Research, Alabama Highway Department, June, 1970.

31. Johns, D. J., Thermal Stress Analyses, Pergamon Press, 1965.

32. Johnson, C. P., and Matlock, H., "Temperature Induced Stresses in Highway Bridges by Finite Element Analysis and Field Tests," Proposal submitted for Research Project 3-5-74-23, Center for Highway Research, The University of Texas at Austin, May, 1970.

33. Kreith, F., Principles of Heat Transfers, International Text Book Company, 2nd Edition, 1965.

34. Krishanamurthy, N., "Temperature Effects on Continuous Reinforced Concrete Bridge," HPR Report No. 58, Research Project 930-047, State of Alabama Highway Department, July, 1971.

35. Liu, Y. N., Zuk, W., "Thermoelastic Effects in Prestressed Flexural Members," Journal of Prestressed Concrete Institute, Vol. 8, No. 3, June, 1963, pp. 64-85.

36. Maher, D. R. H., "The Effects of Differential Temperature on Continuous Prestressed Concrete Bridges," Civil Engineering Transactions, Institute of Engineering, Vol. CE12, No. 1, paper 2793, April, 1970, pp. 29-32.

37. Matlock, H., Panak, J. J., Vora, M. R., and Chan, J. H. C., "Field Investigation of a Skewed, Post-stressed Continuous Slab Structure Structure," Interim Study Report, Center for Highway Research, Research Project 3-5-63-56, The University of Texas at Austin, Texas, May 1970.

38. Meenan, A. R., "Parking Garages for New Orleans Superdome," Journal of Prestressed Concrete Institute, Vol. 19, No. 2, March-April, 1974, pp. 98-111.

39. Monteith, J. L., "Light Distribution and Photosynthesis in Field Corps," Ann. Bot., London 29, 1965, pp. 17-37.

40. Narouka, M., Hirai, I., and Yamaguti, T., "Measurement of the Temperature of the Interior of the Reinforced Concrete Slab of the Shigita Bridge and Presumption of Thermal Stress," Proceedings, Symposium of the Stress Measurements for Bridge and Structures, Japanese Society for the Promotion of Science, Tokyo, Japan, 1957, pp. 106-115.

41. "Standard Specifications for Highway Bridges," Association of State Highway Officials, Washington, D.C., 1973.

42. Strock, C., and Koral, R. L., Handbook of Air Conditioning Heating and Ventilating, Industrial Press, Inc., 2nd Edition, 1965.

43. Swinbank, W. C., "Long-Wave Radiation from Clear Skies," Quarterly Journal of Royal Metorological Society, Vol. 89., 1963, pp. 339-348.

44. Timoshenko, S. P., Theory of Elasticity, McGraw-Hill, 3rd Edition, 1970, pp. 439-441.

45. Van Wyk, H. F., "Aspects of Thermal Stresses in Reinforced Concrete Structures Subjected to Differential Temperature Change," Rilem Symposium, International Symposium of Concrete and Reinforced Concrete in Hot Countries, 1960.

46. Viest, I. M., Fountain, R. S., and Singleton, R. C., Composite Construction in Steel and Concrete, McGraw-Hill, 1958.

47. Visser, W., "A Finite Element Method for the Determination of Non-Stationary Temperature Distribution and Thermal Deformations," Proceedings, Second Conference on Matrix Methods in Structural Mechanics, Wright-Patterson Air Force Base, Ohio, November, 1966.

48. Wah, T., and Kirksey, R. E., "Thermal Characteristics of Highway Bridges," Final Report, No. HR 12-4, Southwest Research Institute, July, 1969.

49. Will, Kenneth M., Johnson, C. Philip, and Matlock, Hudson, "Analytical and Experimental Investigation of the Thermal Response of Highway Bridges," Research Report No. 23-2, Center for Highway Research, The University of Texas at Austin, February 1977.

50. Willems, N., "Experimental Strain Analysis of Continuous Skew Slab Bridge Decks," CRES Project No. 2070, Final Report, University of Kansas, October, 1973.

51. Williamson, P. J., "The Estimation of Heat Outputs for Road Heating Installations," Road Research Laboratory, LR Report 77, Ministry of Transport, 1967.

52. Wilson, E. L., "The Determination of Temperatures within Mass Concrete Structures," Structural Engineering Laboratory Report 68-17, University of California, Berkeley, California, December, 1968.

53. Wilson, E. L., and Nickell, R. E., "Application of the Finite Element Method to Heat Conduction Analysis," Nuclear Engineering and Design, Vol. 4, 1966, pp. 276-286.

54. Yan, H. T., Composite Construction Steel and Concrete, Orient Longmans, 1965.

55. Zienkiewicz, O. C., The Finite Element Method in Engineering Science, McGraw-Hill, 1971.

56. Zienkiewicz, O. C., and Parekh, C. J., "Transient Field Problems - Two and Three Dimensional Analysis of Isoparametric Finite Elements," International Journal for Numerical Methods in Engineering, Vol. 2, Wiley-Interscience, London, 1970.

57. Zuk, W., "Thermal and Shrinkage Stresses in Composite Beams," Journal of American Concrete Institute, Vol. 58, No. 3, September, 1961, pp. 327-340.

58. Zuk, W., "Thermal Behavior of Composite Bridges Insulates and Uninsulated," Highway Research Record, No. 76, 1965, pp. 231-253.

59. Zuk, W., "Simplified Design Check of Thermal Stresses in Composite Highway Bridges," Highway Research Record, No. 103, 1965, pp. 10-13.

60. Zuk, W., "End Movement Studies of Various Type Highway Bridges," Highway Research Record, No. 295, 1969.